

**PRESSURE DEPENDENCE OF HYDROGENOLYSIS OF  
PROPANE OVER SUPPORTED RUTHENIUM**

**By .**

**PO KIANG TSJENG, B.Sc., Eng.**

**A Thesis**

**Submitted to the Faculty of Graduate Studies  
in Partial Fulfilment of the Requirements  
for the Degree  
Master of Engineering**

**McMaster University**

**March, 1973**



### ACKNOWLEDGEMENTS

The author wishes to express his appreciation to his supervisor, Professor R. B. Anderson, who proposed and guided this project. The many helpful suggestions concerning the experimental technique, the analysis of the experimental data and the preparation of the thesis will always be remembered.

The author is very grateful to T. Wong who did most of the typing of the thesis.

Lastly, the author wishes to acknowledge the contribution of Dr. R. Hemrajani who assisted in the determination of the surface area of the catalyst by porosimeter.

## TABLE OF CONTENTS

	<u>PAGE</u>	
<b>Chapter 1</b>	<b>Introduction</b>	<b>1</b>
1.1	General	1
1.2	Hydrogenolysis of hydrocarbon	2
1.3	The Reactor	7
1.4	Analysis of Reaction Networks	11
<b>Chapter 2</b>	<b>Experimental Equipment</b>	<b>15</b>
2.1	Materials	15
2.2	Equipment	19
2.3	Operating Procedure	28
<b>Chapter 3</b>	<b>Hydrogenolysis of Propane</b>	<b>30</b>
3.1	General	30
3.2	Experimental Results	34
3.3	Discussion and Summary	55
<b>Chapter 4</b>	<b>Product Distribution</b>	<b>61</b>
4.1	Introduction	61
4.2	Experimental Results	66
4.3	Discussion and Summary	101
<b>Chapter 5</b>	<b>Conclusion</b>	<b>107</b>
	<b>References</b>	<b>109</b>

PAGE

Appendix A	Measurement of Pore Size Distribution and Specific Area by Mercury Porosimeter	112
Appendix B	Various Possible Mechanisms for the Hydrogenolysis of Propane	115
Appendix C	Product Distribution Network	119
Appendix D	Tables of Experimental Data	126

## LIST OF FIGURES

<u>FIGURE</u>		<u>PAGE</u>
1.1	Butane Hydrogenolysis Mechanism	8
1.2	Carberry Fixed Bed Stirred Reactor	10
2.1	Ruthenium Concentration Gradient	16
2.2	Pore Size Distribution	18
2.3	Equipment Flow Diagram	20
2.4	The Reactor	25
2.5	Paddle Basket Assembly	26
3.1	Mechanism for Hydrogenolysis of Propane	33
3.2	Comparison of Experimental & Calculated Rates	36
3.3	Propane Hydrogenolysis Kinetics at 15 psig.	37
3.4	Propane Hydrogenolysis Kinetics at 20 psig.	38
3.5	Propane Hydrogenolysis Kinetics at 40 psig.	39
3.6	Propane Hydrogenolysis Kinetics at 60 psig.	40
3.7	Propane Hydrogenolysis Kinetics at 80 psig.	41
3.8	Arrhenius Plots for Rate Constants at Various Pressures ( Equation 3.2 )	45
3.9	Plots of $\log k_H$ and $\log k_{C_3}$ as a Function of $1/T$	48
3.10	Arrhenius Plot of Hydrogenolysis Rate Constant ( Equation 3.10 )	49
3.11	Comparison of Experimental & Calculated Rates	50

FIGUREPAGE

3.12	Dependence of Reaction Rates on Pressures	51
3.13	Dependence of Propane Conversion on Pressures	53
3.14	Dependence of Rates on Total Pressures	54
3.15	Arrhenius Plot for Equation (3.15)	59
3.16	The Ranges of a and b	60
4.1	Propane Hydrogenolysis Mechanism	63
4.1a	Propane Hydrogenolysis Mechanism	65
4.2	Product Distribution at 120°C and 2 psig.	68
4.3	Product Distribution at 130°C and 30 psig.	69
4.4	Product Distribution at 150°C and 80 psig.	70
4.5	Product Distribution Analysis at 120°C and 2 psig.	71
4.6	Product Distribution Analysis at 130°C and 30 psig.	72
4.7	Product Distribution Analysis at 150°C and 80 psig.	72
4.8	Product Distribution at 40 psig.	76
4.9	Product Distribution at 50 psig.	77
4.10	Product Distribution at 60 psig.	78
4.11	Product Distribution at Zero Conversion at Several Pressures	79
4.12	Product Distribution Analysis at 30 psig.	80
4.13	Product Distribution Analysis at 40 psig.	81
4.14	Product Distribution Analysis at 50 psig.	82
4.15	Product Distribution Analysis at 60 psig.	83
4.16	Arrhenius Plot for $k_2''/k_3''$	85
4.17	Arrhenius Plot for $k_2^*/k_2'$	86
4.18	Product Distribution at 128°C	88

<u>FIGURE</u>		<u>PAGE</u>
4.19	Product Distribution at 139°C	89
4.20	Product Distribution at 148°C	90
4.21	Product Distribution Analysis at 128°C	91
4.22	Product Distribution Analysis at 139°C	92
4.23	Product Distribution Analysis at 148°C	93
4.24	Product Distribution at Zero Conversion at Several Temperatures	97
4.25	Pressure Dependence of $k_2''/k_3''$	98
4.26	Arrhenius Plots for $h_2^*/h_2'$ and $h_3^*/h_3'$	100
4.27	Comparison of Experimental and Calculated Selectivity of Ethane	103
A1	Penetration Volume vs External Pressure Plot	114
C1	Propane Hydrogenolysis Mechanism	122
C2	Propane Hydrogenolysis Mechanism	125

LIST OF TABLES

<u>TABLE</u>		<u>PAGE</u>
1.1	Hydrogenolysis Data ( 0.5 Weight % Ruthenium on $\gamma$ -Alumina )	6
2.1	Summary of Catalyst Properties Determined From Nitrogen Adsorption Isotherm and Porosimeter	17
2.2	Gas Chromatographic & Integrator Operating Conditions	23
2.3	Component Retention Times & Calibration Factors	23
3.1	Parameters of Equation ( 3.2 )	35
3.2	Rate Constant Obtained from Plots of $r$ vs $P_{C3}^a P_{H2}^b$	44
3.3	Summary of Parameters from the Analysis of Equations ( 3.2 ) and ( 3.3 )	46
3.4	Analysis of Rate Data Using Equation ( 3.10 )	47
3.5	Activation Energies and Heat of Adsorption Obtained from Equation ( 3.10 )	52
4.1	Product Distribution Analysis ( Equation 4.3 )	73
4.2	Product Distribution Analysis ( Equation 4.3 )	84
4.3	Pre-exponential Factors and Activation Energies for $k_2''/k_3''$	87
4.4	Pre-exponential Factors and Activation Energies for $k_2^*/k_2^0$	87
4.5	Product Distribution Analysis ( Equation 4.3 )	94
4.6	Product Distribution Analysis ( Equation 4.6 )	99
4.7	Ratio of Cracking Rate to Desorption	102

TABLEPAGE

A1	Hydrogenolysis Data at 2psig. and 120°C	126
A2	Hydrogenolysis Data at 15psig. and 114.5°C	127
A3	Hydrogenolysis Data at 20psig. and 126°C	128
A4	Hydrogenolysis Data at 40psig. and 144.5°C	129
A5	Hydrogenolysis Data at 60psig. and 147.5°C	130
A6	Hydrogenolysis Data at 80psig. and 150°C	131
A7	Hydrogenolysis Data at 20psig.	132
A8	Hydrogenolysis Data at 40psig.	133
A9	Hydrogenolysis Data at 60psig.	135
A10	Hydrogenolysis Data at 80psig.	137
B1	Hydrogenolysis Data at 128°C	138
B2	Hydrogenolysis Data at 139°C	140
B3	Hydrogenolysis Data at 143.5°C	142
B4	Hydrogenolysis Data at 148°C	143
B5	Data for Pressure Dependence of Rate	145
C1	Product Distribution Data at 2psig. and 120°C	146
C2	Product Distribution Data at 30psig. and 130°C	147
C3	Product Distribution Data at 80psig. and 150°C	148
C4	Product Distribution Data at 40psig.	149
C5	Product Distribution at 30 and 50psig.	151
C6	Product Distribution Data at 60psig.	153
C7	Product Distribution Data at 128°C	155
C8	Product Distribution Data at 139°C	156

<u>TABLE</u>		<u>PAGE</u>
C9	Product Distribution at 143°C	157
C10	Product Distribution Data at 148°C	158
D1	Data Obtained from Mercury Porosimeter	159

CHAPTER ONE  
INTRODUCTION

1.1 General

Many studies have been made on the hydrogenolysis of small paraffinic hydrocarbons over supported ruthenium at atmospheric pressure, and the rate was found to be inversely proportional to hydrogen pressure. As pointed out by Kempling (1), the rate of hydrogenolysis decreased as total pressure increased, and a single power rate equation failed to correlate the rates at different pressures. Thus, the purpose of this investigation was to determine the pressure dependence of hydrogenolysis of propane to gain an insight into the nature of the mechanism by examining both the rates of reaction and the product distributions at various pressures.

The catalyst used for these studies was 0.5 weight percent ruthenium impregnated on  $\gamma$ -alumina, since ruthenium was one of the most active elements in the hydrogenolysis of ethane (2). A continuous stirred-tank catalytic reactor similar to that proposed by Carberry (3) was used because it provided a simple and direct analysis of data. The reactor had the essential features that approach an ideal reactor, and the data acquired are differential so that complicated mathematical procedures could be avoided. This reactor operated over

a wide range of conversions so that the effects of the analytical errors are minimized.

## 1.2 Hydrogenolysis of Hydrocarbons

The earliest reported investigations of the kinetics and mechanism of hydrogenolysis of simple hydrocarbons appear to be those of Taylor and associates (4,5). The reaction of ethane on nickel and cobalt and propane on nickel disclosed the main features of the kinetics of hydrogenolysis; the rate has a surprisingly large inverse dependence on hydrogen pressure. A further study on deuterium exchange reactions revealed that the adsorption-desorption reaction is at equilibrium, and the sole rate determining step is the splitting of carbon-carbon bonds.

A mechanism for the reaction was proposed by Cimino, Boudart and Taylor (6). According to their analysis, the mechanism involved a dissociative adsorption of the hydrocarbon to form an unsaturated surface species which was in equilibrium as



where  $a = (n + 1 - x / 2)$  and  $\text{C}_n\text{H}_x^*$  represents the adsorbed radicals which react with hydrogen to rupture the carbon-carbon bond.



The last step is slow and the adsorbed lower hydrocarbon species may desorb or react with hydrogen to become lower hydrocarbons. Because the slowest step is postulated to be the surface reaction, the Langmuir kinetic treatment can be applied. The fraction of the surface

covered by  $C_n H_x^*$  will be

$$\theta = \frac{k_c (P_c / P_H^a)}{1 + k_c (P_c / P_H^a)} \quad (1.1)$$

where:  $\theta$  - fractional surface coverage

$k_c$  - equilibrium constant for dissociative chemisorption

$P_c, P_H$  - partial pressures of hydrocarbon and hydrogen

For intermediate strengths of adsorption, the relationships over a limited range of pressure may be approximated by

$$\theta = k_c^n (P_c / P_H^a)^n \quad (1.2)$$

Since the rate determining step is the splitting of carbon-carbon bonds, the overall rate is given by the expression

$$r = k' P_H \theta \quad (1.3)$$

Substituting equation (1.2) into equation (1.3) gives

$$r = k P_c^n P_H^{1-na} \quad (1.4)$$

which is a power rate equation, or if equation (1.1) is substituted into equation (1.3) instead of equation (1.2), then

$$r = \frac{k P_c P_H^{1-a}}{(1 + k_c P_c / P_H^a)} \quad (1.5)$$

which is a Hougen - Watson type of rate expression.

The rate expression indicates the hydrogen order depends on "na". Since the adsorbed hydrocarbon is usually highly unsaturated ( $a > 1$ ) but relatively weakly adsorbed ( $n \approx 1$ ), the hydrogen power is usually negative.

There are many polemics upon the proposed mechanism. As reported by Anderson and Baker (7), for the hydrogenolysis of saturated hydrocarbons over evaporated nickel films, the desorption of methane rather than the rupture of carbon-carbon bonds on the surface is the slowest step. The same conclusion is reached by the experiment (8) of the adsorption and desorption and subsequent hydrogenolysis of several hydrocarbons over supported nickel. However, from the deuterium exchange reactions, the exchange of deuterium with hydrocarbons occurs at a much lower temperature than those required for hydrogenolysis (9,10). Therefore, the rate determining step should be the rupture of carbon-carbon bonds, and this statement is further justified by Cuczi et al. (11,12) who found that the hydrogenolysis rates for hydrocarbons of different structures are different, although in all cases the final product is methane. Thus, methane desorption is not the rate controlling step or else the rates should be the same.

Though the mechanism proposed by Cimino et. al. has been criticized because it does not allow for the competitive adsorption of hydrogen (13) or the reaction products, it has been widely used for its ability to explain the strong inhibitory-effect of hydrogen on the reaction rates. It has been used successfully for most kinetics of hydrogenolysis of hydrocarbon except for ethane hydrogenolysis over cobalt (14) and iron (15). The application of power rate law to data for the reaction over cobalt yields hydrogen exponents varying from -1 to 0 with increasing temperature and over iron catalyst the hydrogen exponent is positive. The reversible dissociative adsorption mechanism cannot explain the positive power. Desorption of methane may be the rate controlling step.

Kemball (16) studied the deuterium exchange reaction of hydrocarbons on iron catalyst and found that  $CD_4$  is the main product. This again justifies the postulate that the desorption of methane is rate determining.

The hydrogenolysis of ethane over various metal catalysts has been studied by Sinfelt and co-workers (17,18,19) and has been reviewed by Sinfelt (20). The hydrogenolysis of hydrocarbon in a Carberry reactor over impregnated ruthenium on  $\gamma$ -alumina was first studied by Tajbl (21,22) for the hydrogenolysis of ethane and propane. Further studies of hydrogenolysis over a similar catalyst in a Carberry reactor were made by Kempling (23,24). Table (1.1) is a summary of kinetic parameters obtained by Tajbl and Kempling. The table includes the activation energy, the orders with respect to hydrogen and hydrocarbons and the calculated degree of unsaturation of the adsorbed hydrocarbons.

Since the hydrogenolysis of paraffins results in a mixture of smaller saturated hydrocarbons, the initial fragments except the  $C_1$  species can crack further into smaller products. Kempling reported that for hydrogenolysis of n-butane over impregnated ruthenium, the selectivity which defines as the tendency of a catalyst to produce a particular product is relatively independent of temperature and is not a function of total pressure. The yield of propane decreases with increasing conversion, while methane and ethane increase with increasing conversion. For the hydrogenolysis of propane (25) and n-pentane (26) on nickel catalyst, higher temperature and lower partial pressure of hydrogen favour the formation of smaller hydrocarbon products. For the hydrogenolysis of isobutane on ruthenium (23), propane and methane selectivities approach unity and that of ethane becomes small at lower temperature.

TABLE ( 1.1 )

Hydrogenolysis Data ( 0.5 Weight % Ruthenium On  $\gamma$ -Alumina )

Hydrocarbon	Temperature (°C)	Log A	$E_{act}$	Reaction Orders (a)	(b)	Hydrogen Atoms Lost (n)	Reference
Ethane	160-220	39.08	42	1	-2	6	19
Propane	140-170	36.85	35.8	1.	-1.5	5	19
n-Butane	85-125	22.17	48.1	0.91	-1.34	5.2	20
Isobutane	105-130	13.63	36.2	0.74	-0.66	4.4	21
Isopentane	90-120	19.59	43.2	0.68	-1.07	6.0	22
Neo-pentane	125-153	16.94	43.5	0.89	-0.87	4.2	23

A : Pre-exponential Factor

 $E_{act}$  : Activation Energy ( Kcal/mole )

a : Order of hydrocarbon

b : Order of Hydrogen

The amounts of methane and ethane increase as temperature increases.

A reaction network was proposed by Kempling et. al. and is shown in fig. (1.1) for the hydrogenolysis of n-butane. The network included reversible adsorption and desorption of each hydrocarbon and irreversible rupture of carbon-carbon bonds in the adsorbed species. All of the steps of the process were coupled, i.e., no single rate determining step was assumed. If each of the reactions was assumed to be first order in the hydrocarbon species involved, then when the network is applied to the continuous stirred tank catalytic reactor, the selectivities could be expressed as

$$S_3 = \frac{(1 - F)(k_3' / (k_3^* + k_3'))}{1 + k_3'' / k_4'' (X_4 / (1 - X_4))} \quad (1.6)$$

$$S_2 = \frac{(1 - F - S_3)(k_2' / (k_2^* + k_2'))}{1 + k_2'' / k_4'' (X_4 / (1 - X_4))} \quad (1.7)$$

$$\text{and } S_1 + 2S_2 + 3S_3 = 4 \quad (1.8)$$

where :  $S_i$  - the moles of hydrocarbon containing  $i$  carbon atoms produced per mole of butane reacted.

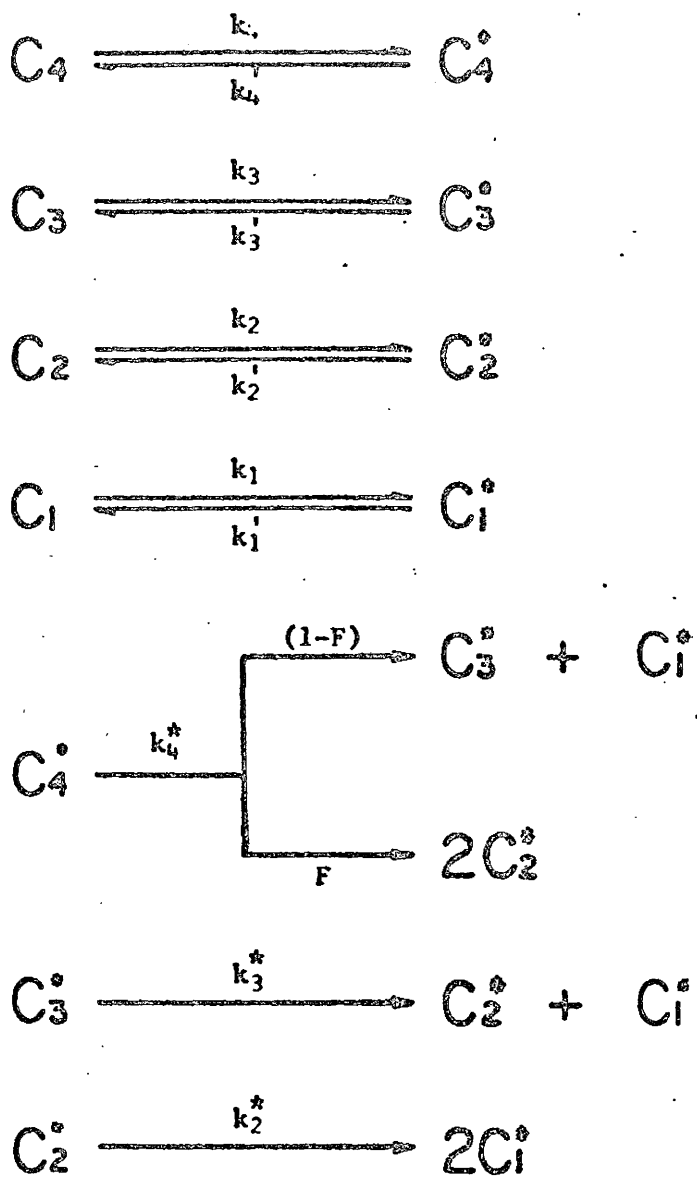
$X_4$  - fractional conversion of n-butane.

$k_i$  - rate constants defined in fig (1.1).

Similar reaction networks have also been successfully applied to hydrogenolysis of propane, neo-pentane and iso-pentane (1).

### 1.3 The Reactor

For laboratory studies of heterogeneous catalysis to obtain kinetic equations, it is imperative that the information derived accurately reflects steady state activity and selectivity. To obtain the most



$C_4, C_3, C_2, C_1$  - gaseous butane, propane, ethane, and methane

$C_4^*, C_3^*, C_2^*, C_1^*$  - adsorbed hydrocarbon species

$k_1$  - adsorption rate constant

$k_1'$  - desorption rate constant

$k_1^*$  - cracking rate constant

$F$  - fractional split factor

$$k_i'' = k_i k_i^* / (k_i^* + k_i')$$

Figure 1.1 N-BUTANE HYDROGENOLYSIS MECHANISM

accurate rate equation, the observed data should involve a minimum of transport effects. The situation is approached for heterogeneous catalytic reactions by laboratory differential reactors operated at high fluid velocities with a fixed bed of small particles. Small particles ensure that intra-particle temperature and concentration gradients are negligible while high fluid velocities eliminate fluid-to-particle temperature and concentration differences (27). The catalyst bed should be isothermal because reaction rates are usually strongly dependent on temperature in a non-linear manner. A simple and well characterized flow pattern should prevail, and the flow pattern should be either of the piston type or thoroughly stirred type (28).

There are various types of small experimental reactors including static and flow, integral and differential. As stated by Carberry, "an ideal reactor is one that operates isothermally over a wide range of conversion in the steady state with respect to the catalyst and reactants under clearly defined residence time conditions while facilitating direct rate law determination." (3). The well stirred continuous flow reactor in principle possesses the ideal characteristic (3,29,30). The essentials of such a reactor are shown in fig. (1.2). Catalyst pellets are placed in wire cages attached to a rotating shaft. The rotating catalyst cages produce perfect mixing. It is shown by Carberry that interphase temperature and concentration gradients are negligible for all except very rapid reactions, and nearly complete conversion can be tolerated in this reactor. Since finite conversions are involved, effluent analysis errors are minimized. However, pressure operation possesses problems in devising effective stirrer seals and bearings that will run at high speeds over a long period of time without contaminating the catalyst and leaking. The ra-

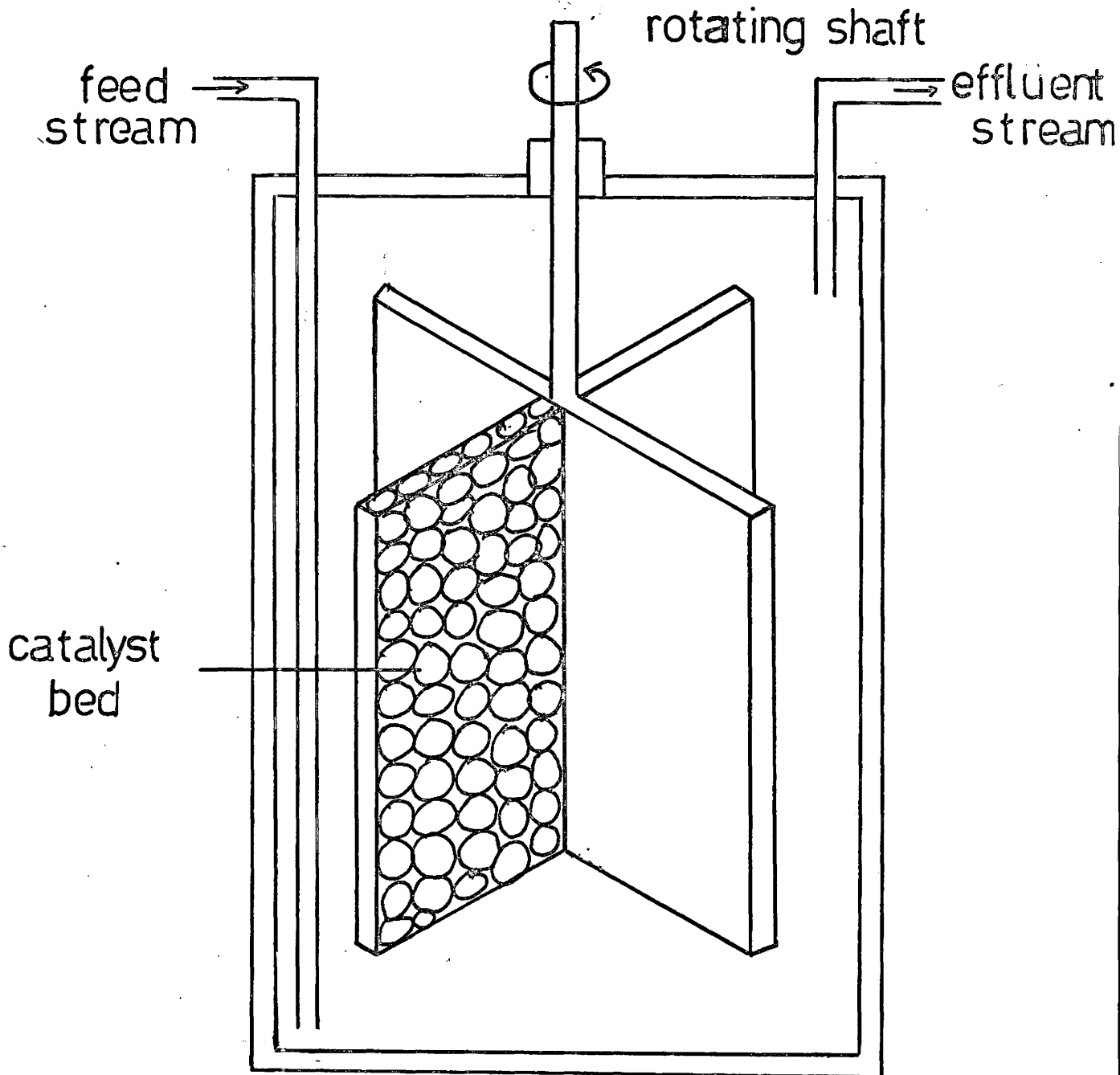


Fig.(1.2) Carberry fixed bed stirred reactor

ther large void volume of the unit renders it unattractive when the possibility of simultaneous homogeneous reaction exists, and also the void volume at higher pressure contains a large amount of the reaction mixture. While no laboratory reactor is truly ideal, this reactor concept appears to be unique in providing a valuable solution of many difficult problems.

Differential data are obtained from this reactor, i.e., they result from one level of concentration and temperature. For each experiment, the differential reaction rate will be :

$$r = \frac{X_i Q_i}{W} \quad (1.9)$$

Where:  $X_i$  - fractional conversion of feed component  $i$

$Q_i$  - the feed rate of  $i$

$W$  - the weight of catalyst

Many kinetic studies employed continuous stirred-tank catalytic reactors, and the data are found to be consistent with those obtained from other reactors. It has been used successfully by Tajbl (21,22) for the hydrogenolysis of ethane on nickel catalyst and ethane and propane on supported ruthenium. Kempling (1) has also studied kinetics of hydrogenolysis of hydrocarbons in the same kind of reactor.

#### 1.4 Analysis of reaction networks.

The equations or mathematical models generally used to correlate kinetics data fall into two broad classifications (31,32). On one hand, there are the power function models which generally are variations of :

$$r = k \prod_i C_i^{a_i} \quad (1.10)$$

where :  $k$  - the rate constant which is a function of temperature

$C_i$  - the concentration of  $i$ th-component

$a_i$  - the order of reaction of the  $i$ -th component.

The rate law utilizes the concept of reaction order and is traditionally called a power-rate law (33). Alternatively, the Hougen-Watson models (34) usually have the general form of :

$$r = \frac{k \prod_i C_i^{a_i}}{(1 + \sum_i k_i^m C_i^m)^n} \quad (1.11)$$

where the denominator is the competition for the catalytic empty sites and  $k_i$  are the corresponding Langmuir adsorption equilibrium constants. Exponents  $m$  and  $n$  are often equal to unity though they may be equal to 1/2 or 2, respectively, in the case of dissociative adsorption and binary reaction.

Normally the rate constants can be expressed by an Arrhenius expression as:

$$k = A \exp(-E/RT) \quad (1.12)$$

where :  $A$  - the pre-exponential factor

and  $E$  - the activation energy.

The power function equations are empirical, but sometimes result from the simplification of a more complex equation with mechanistic significance. The Hougen-Watson model is usually derived from a specific reaction mechanism, assuming the existence of a single rate determining step and the rest of the reactions in equilibrium.

It has been pointed out that the Hougen-Watson models are not useful when adsorbing surfaces are not uniform or when there are interactions between adsorbed molecules. It is also asserted that much of the improved fitting of experimental data results from the great flexibility of the Hougen-Watson model arising from the abundance of parameters in the equa-

tion. Furthermore, kinetic data often contain substantial experimental errors and mathematical forms more complicated than power rate law cannot be justified. However, the Hougen-Watson model offers some insight into the reaction mechanism, and its extrapolation to a region of conditions not experimentally tested usually yields reasonable results.

A useful technique in the study of reaction kinetics is the evaluating of alternative kinetic models by fitting rate data to postulated models and statistically evaluation the results for goodness of fit. These techniques consist of essentially two principal parts : (a) the identification of adequate models and (b) the estimation of the parameters in the best model obtained in the first step (35). There are various methods to determine the acceptance of a model. Analysis of the variance or the analysis of residuals, the difference of the experimental and the fitted values of the dependent variables, could help in examining the degree of fit of a model to experimental data (36). Unacceptable characteristics of the estimated parameters, such as negative rate constants or adsorption coefficients, will result in the rejection of the model (38). Frequently, more than one model is plausible, but the one that fits the experimental data best is chosen.

There are various methods for estimating the parameters. The least squares method is usually selected for convenience and also it usually results in useful quantitative estimation. In this approach, the sum of squares of the errors is minimized. Sometimes the kinetics equations occur in non-linear form; then non-linear least squares methods have to be applied. But some equations are intrinsically linear (37) by taking the reciprocal or

logarithms, and thus can be solved by the linear least squares method. Linearizing equations may distort the goodness of fit criteria. These statistical methods have been described at great length in the literature (38,39,40).

## CHAPTER TWO

### EXPERIMENTAL EQUIPMENT

#### 2.1 Materials

##### A) Catalyst

A commercial catalyst ( courtesy of Engelhard Industries, Inc. ) consisting of a nominal 0.5 weight percent ruthenium impregnated on  $\gamma$ -alumina was used. This catalyst was in the form of 3.2 by 3.2 mm. cylindrical pellets with the ruthenium impregnated on the outer shell of the pellets. The outer shell appeared dark black while the center was white. The concentration profile of ruthenium in the catalyst pellets were determined by an electron probe microanalyzer (1) and the ruthenium concentration gradient is shown in fig. (2.1). The ruthenium layer is about 0.2 mm. thick.

The catalyst has been studied thoroughly by Kempling (1). Table (2.1) summarizes the information obtained from a nitrogen isotherm obtained by the standard volumetric techniques at 77°K over a range of relative pressures from 0.1 to 1.0. In addition, the catalyst was studied by a mercury porosimeter (appendix A). The surface area was found to be 109.9 m<sup>2</sup>/gm. The average pore radius was 62 Å. The pore distribution obtained from the mercury porosimeter is shown in fig. (2.2). The surface area of the supported metal was determined from two hydrogen adsorption experiments which were performed at 20° C and pressures up to 200 Torr. The observed monolayer volume was 0.20 cc(STP) per gram of

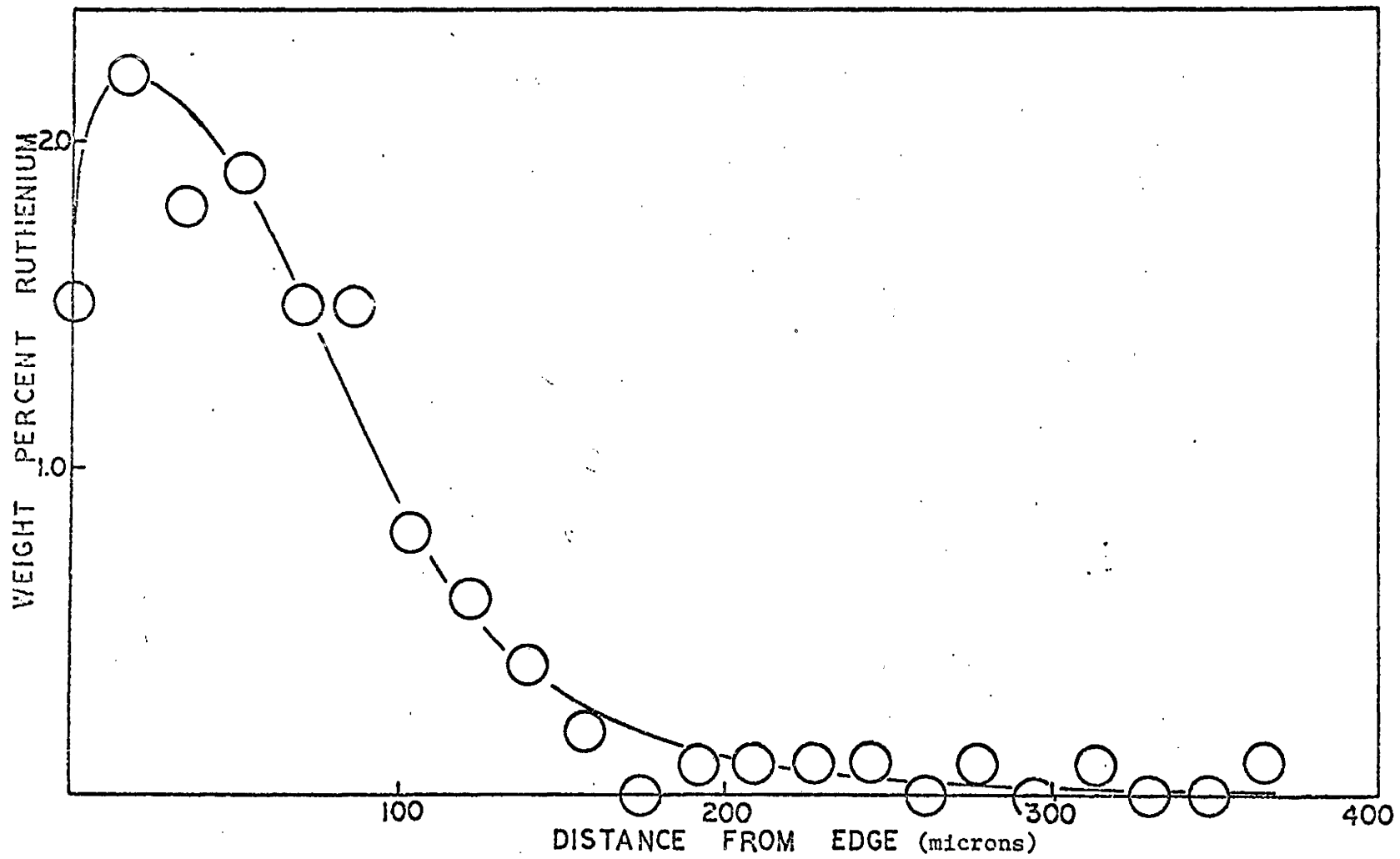


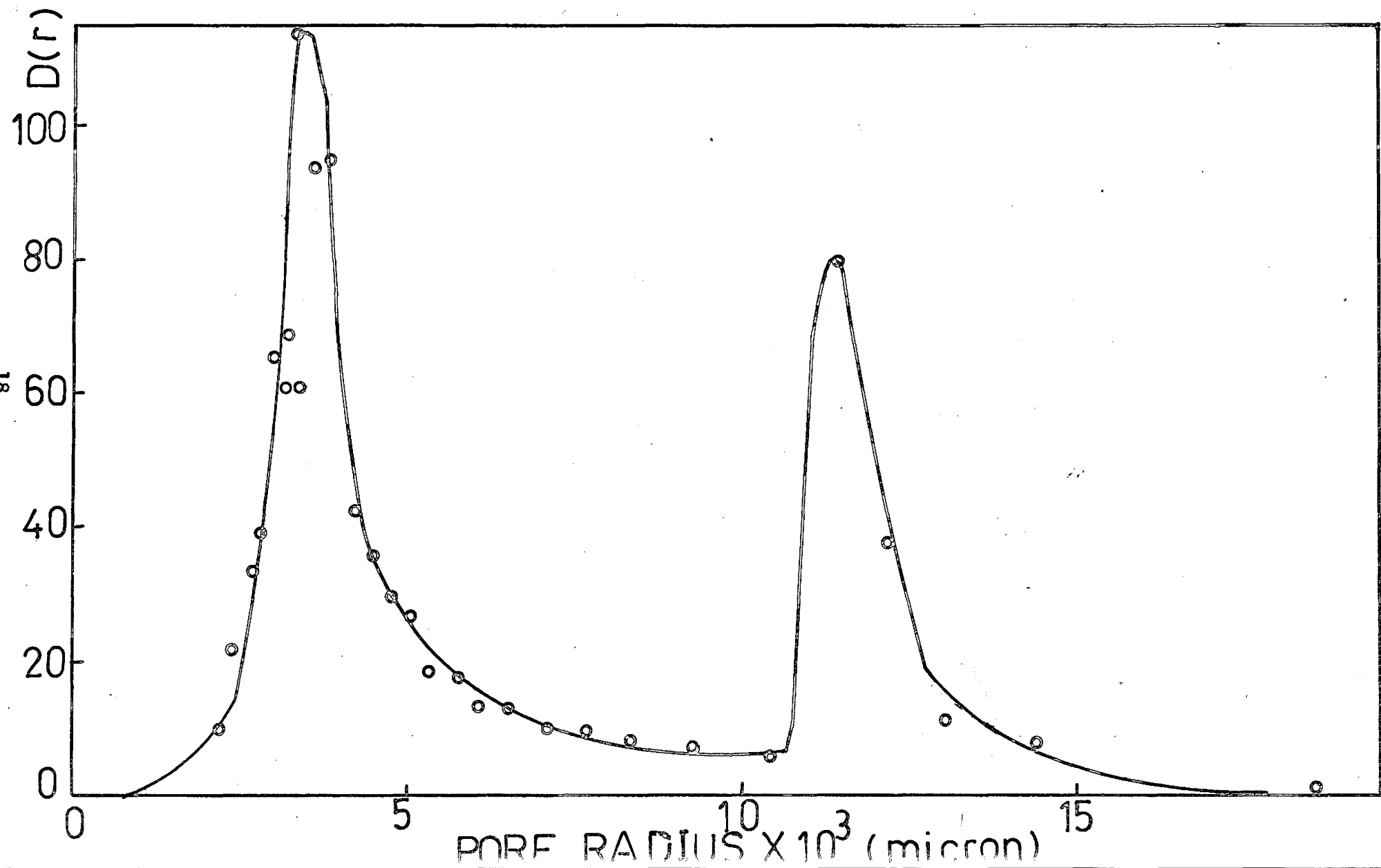
Figure 2.1 : Ruthenium Concentration Gradient

TABLE ( 2.1 )

Summary Of Catalyst Properties Determined From  
Nitrogen Adsorption Isotherm And Porosimeter.

Calculation Method	Surface Area (m <sup>2</sup> /g.)	Pore Volume (cc. (STP)/g.)	"Average" Pore Radius (Å)
Saturation (x=1)	-	180	-
BET Method	87.8	-	60
Universal Thickness Isotherm	84.2	-	-
Pore Distribution			
(i) Adsorption	92.5	175	50
(ii) Desorption	97.7	175	50
Mercury Porosimeter	109.9	-	61

Fig.(22) Pore size distribution



catalyst, and the corresponding ruthenium area was found to be  $0.82 \text{ m}^2/\text{gm.}$  of catalyst or about  $160 \text{ m}^2/\text{gm.}$  of ruthenium. The average crystallite size was  $25 \text{ \AA}$ .

## B) Reactants

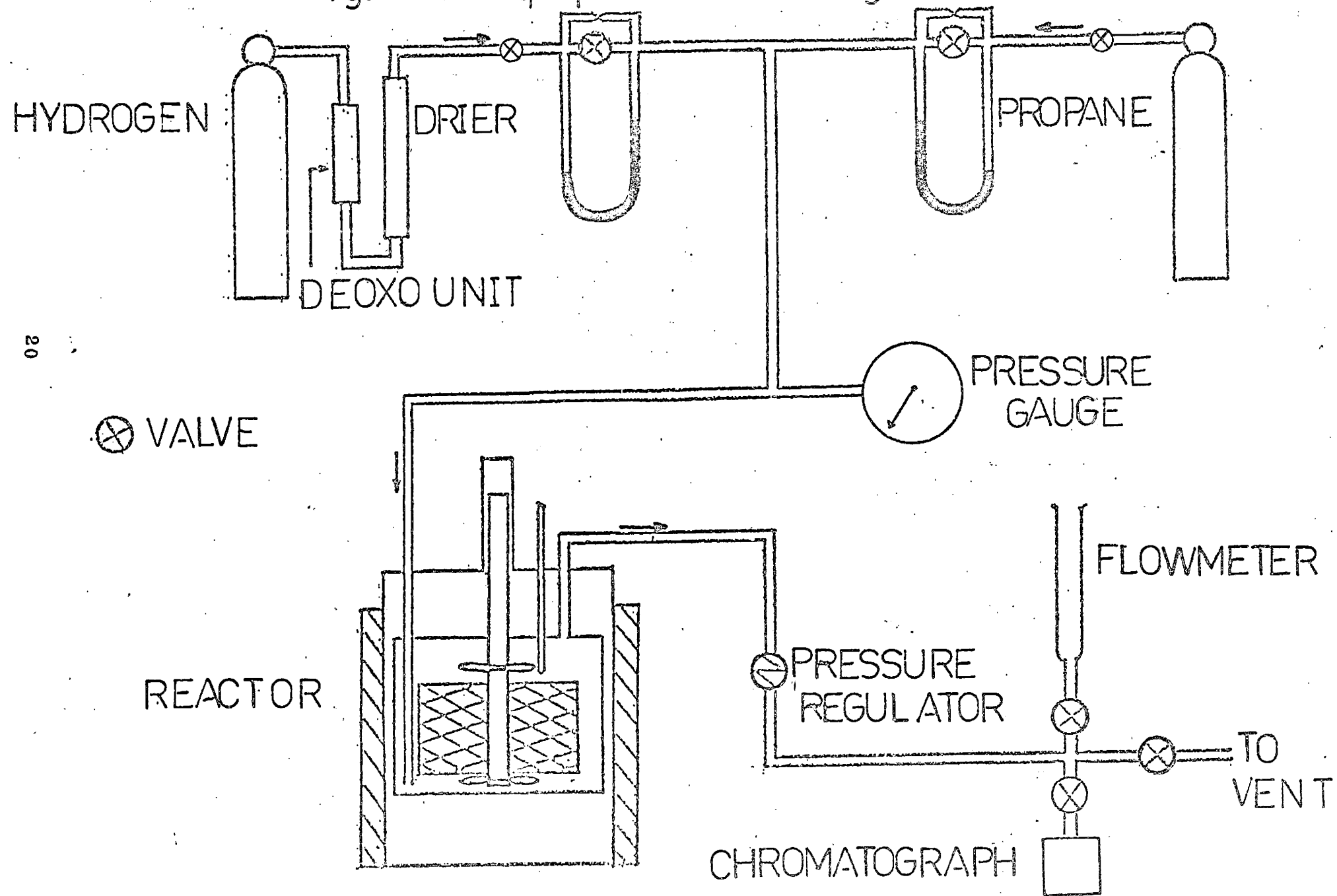
Both hydrogen and propane were obtained from the Matheson Co.. The hydrogen was extra pure grade with a nominal purity of 99.9 percent. The hydrogen was further purified with a de-oxo unit to remove trace quantities of oxygen and then dried over 5A molecular sieve. The hydrocarbon was instrument grade which had a purity of 99.5 percent. From gas-chromatographic analysis, only traces of impurities were found ( 0.35 percent of iso-butane and 0.05 percent of n-butane ). The propane was used directly.

## 2.2 Equipment

A systematic diagram of the apparatus is shown in fig. (2.3). The system could be divided into three sections : the feed system, the reactor and the effluent analysis system.

The feed system consisted of two streams ; hydrogen and propane. The system allowed these two streams to be mixed in definite proportions and introduced into the reactor at a given flow rate. Except where otherwise stated, all the lines were constructed with  $1/4''$  O.D. copper tubing. The hydrogen passed through a deoxo purifying unit for the removal of traces of oxygen and then through a  $9''$  long and  $1\frac{1}{2}''$  O.D. copper tubing which was packed with 5A molecular sieve for drying purposes. The propane was directly introduced into the system without any further purification.

Fig.(2.3) Equipment flow diagram



Both the hydrogen and propane flow rates were controlled by fine metering valves and monitored with capillary type flow meters. The pressure differences were read on glass U-tube manometers which were three feet in length and were filled with Meriam fluid No. D-3166 ( S.G.=1.04 ). The capillary constriction consisted of 1/8" copper tubing which had been crimped. Each manometer had a by-pass valve to allow high flow rates during flushing or changing pressures. The two streams were combined at a 1/4" tee and then passed into the reactor. A precision Bourdon-tube pressure gauge, range 0 - 100 psig. and 12" diameter, was fitted to the feed line just before the reactor to measure the total pressure of the reactor.

The effluent system was used to regulate the pressure of the reactor, to measure the total effluent flow rates, to analyze the effluent stream and to vent the gases. The reactor pressure was regulated by a variable-back pressure regulator ( Brooks instrument Canada, Kendal model 10BP ). The regulator was capable of controlling the reactor pressure in the range of 0 to 125 psig. for variable flow rates and was placed directly downstream of the reactor. Subsequently, the stream was passed through a Swagelok cross in which each outlet line was fitted with a toggle valve. One line was directed to a gas chromatograph sampling valve, the second to a flow meter and the third to a vent line. The flow rates were measured by soap flow meters having different diameters and lengths. The flow meters were capable of measuring flow rates up to 10 ml/sec. The chromatograph consisted of a model 90P-3 Varian Aerograph chromatograph in conjunction with a 125 micro-litre gas sampling valve. A Servo/riter one m.v. recorder was used to record the chromatograms, and an Hewlett-Packard integrator ( model 3373B ) was used to give the corresponding peak areas in number of counts. The best compromise carrier gas for the gas chromato-

graph was helium because it provided a positive hydrogen peak and thus avoided the trouble of changing polarity of the signal during the analysis. The column used was poropak Q,  $1/4$ " in diameter and  $7\frac{1}{2}$  ft. in length. The overall conditions for the chromatographic system and the integrator are listed in Table ( 2.2 ). The retention times of the components are listed in Table ( 2.3 ). The chromatograph was calibrated to determine the calibration factors for each of the components. The factors based on propane as unity are shown in Table ( 2.3 ). The values were the same as literature values within the experimental errors. These factors were used to calculate the mole fractions of the components in the experiments.

The reactor was a modified one-litre magne-drive packless autoclave ( Autoclave Engineering Inc. ) with a magnetic drive to rotate the catalyst assembly. The external driver magnet and a stainless steel housing surrounded an internal magnet encapsulated on a rotor shaft. The strong magnetic field caused the inner shaft to rotate, when the outer magnetic assembly, which was driven by an electric motor, was turned. Two kinds of bearings were used. Initially, graphite bearings were employed. These bearings usually failed to function after three or four weeks of intermittent operations because of the deposition of carbon around the bearings. Finally, rulon bearings were introduced. The rulon contains TFE fluorocarbon and inert substances. These bearings provided a smooth operation for more than two months.

The continuous stirred-tank catalytic reactor was constructed of stainless steel and was a cylindrical vessel of three inches in diameter and nine inches in depth. The volume was reduced to 580 ml with an aluminum block at the bottom of the cavity. A thermocouple was situated within the

TABLE ( 2.2 )

Gas Chromatographic & Integrator Operating Conditions

Column Temperature	---	48° C
Detector Temperature	---	85° C
Injector Temperature	---	50° C
Carrier Gas	---	Helium
Carrier Gas Flow Rate	---	73 ml./min.
Filament Current	---	190 ma.
Attenuation ( Gas Chromatograph )	---	2
Recorder Chart Speed	---	1/2 inch per min.
Attenuation ( Integrator )	---	1
Sensitivity	---	3 or Maximum
Mode of Operation (Integrator)	---	Automatic

TABLE ( 2.3 )

Component Retention Times & Calibration Factors

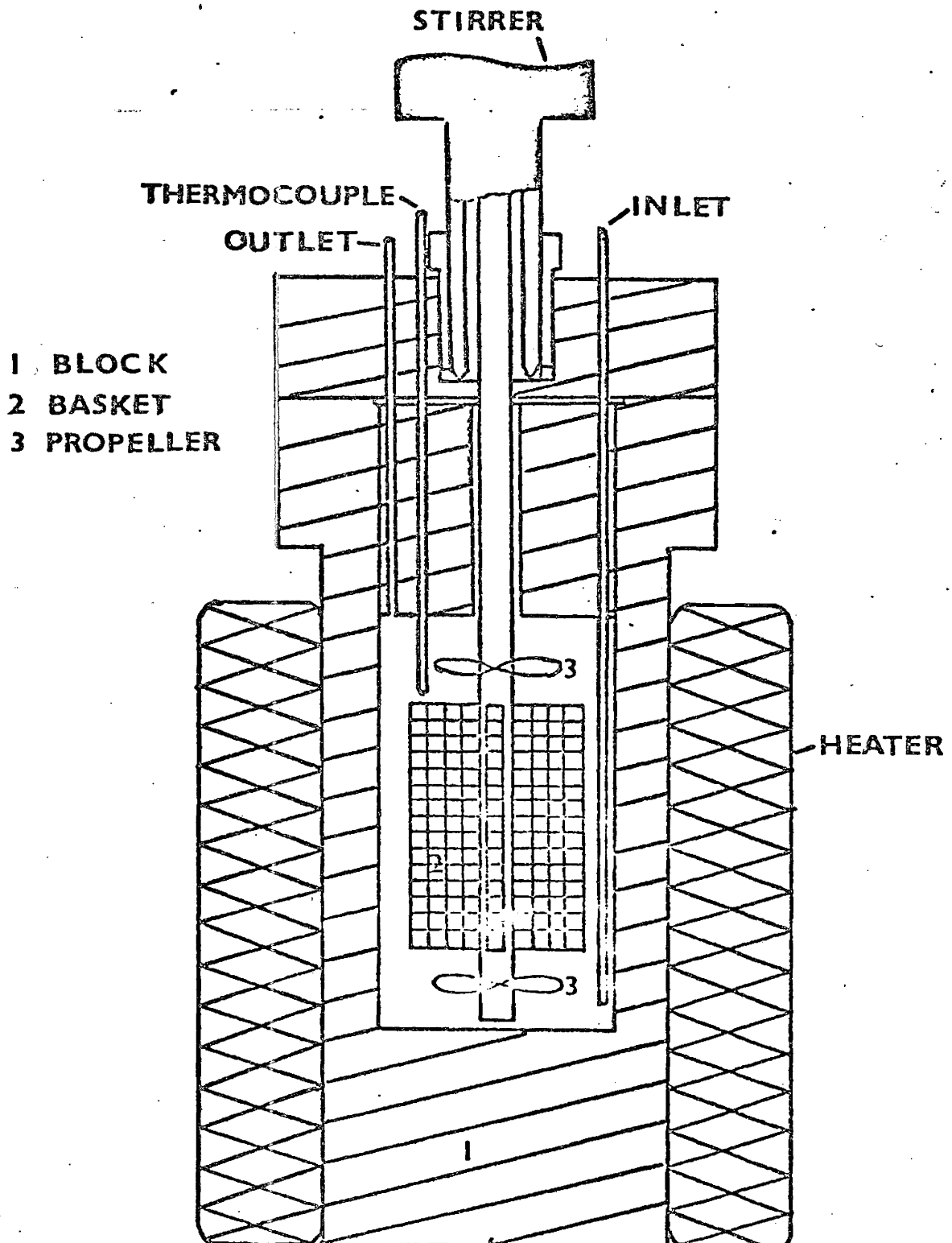
Gases	Retention Time ( min )	Calibration Factor
Hydrogen	0.88	65.85
Methane	1.11	1.902
Ethane	3.37	1.292
Propane	16.63	1.000

reactor and the emf. was measured on a potentiometer ( Croydon Precision Instrument, England. Type P3 ). A chromel-alumel thermocouple with an ice reference junction was used. There are two ports situated near the thermocouple. One is the inlet port which was made of  $1/8''$  stainless steel tubing and was passed to the bottom of the reactor. The effluent port was also made of  $1/8''$  stainless steel tubing, and was located near the top of the reactor. The essential features of the reactor are shown in Fig. (2.4).

The catalyst was contained in a four-vane basket arrangement which was constructed of an aluminum bracket with stainless steel screens placed on both back and front of the spacer. The edges of the screens were then covered with aluminum cover plates. Fig.(2.5) is an exploded view of the basket assembly that contained the catalyst. The whole assembly was bolted to the main body. The two assemblies used were mounted at a  $90^\circ$  angle to give four catalyst chambers. The whole system was attached to the rotating shaft by a screw situated at the top of the shaft. Two propellers, one above and the other below the catalyst basket assembly were attached to the shaft to improve mixing. A nut was screwed onto the end of the shaft which had been threaded so that the whole system would be held firmly in position. Each basket was  $1/4$  inch thick,  $3\frac{1}{2}$  inches long and  $15/16$  inch wide.

The heater of the reactor was a tubular electric furnace supplied by two sources . One of the sources was a Powerstat variable transformer ( model 126-226 ) and was set at a constant voltage. The other source was a proportional controller ( Electronic Control System, model 16C1 ) in which the sensing thermocouple ( chromel-alumel ) was placed in bet-

Fig.(2.4) REACTOR



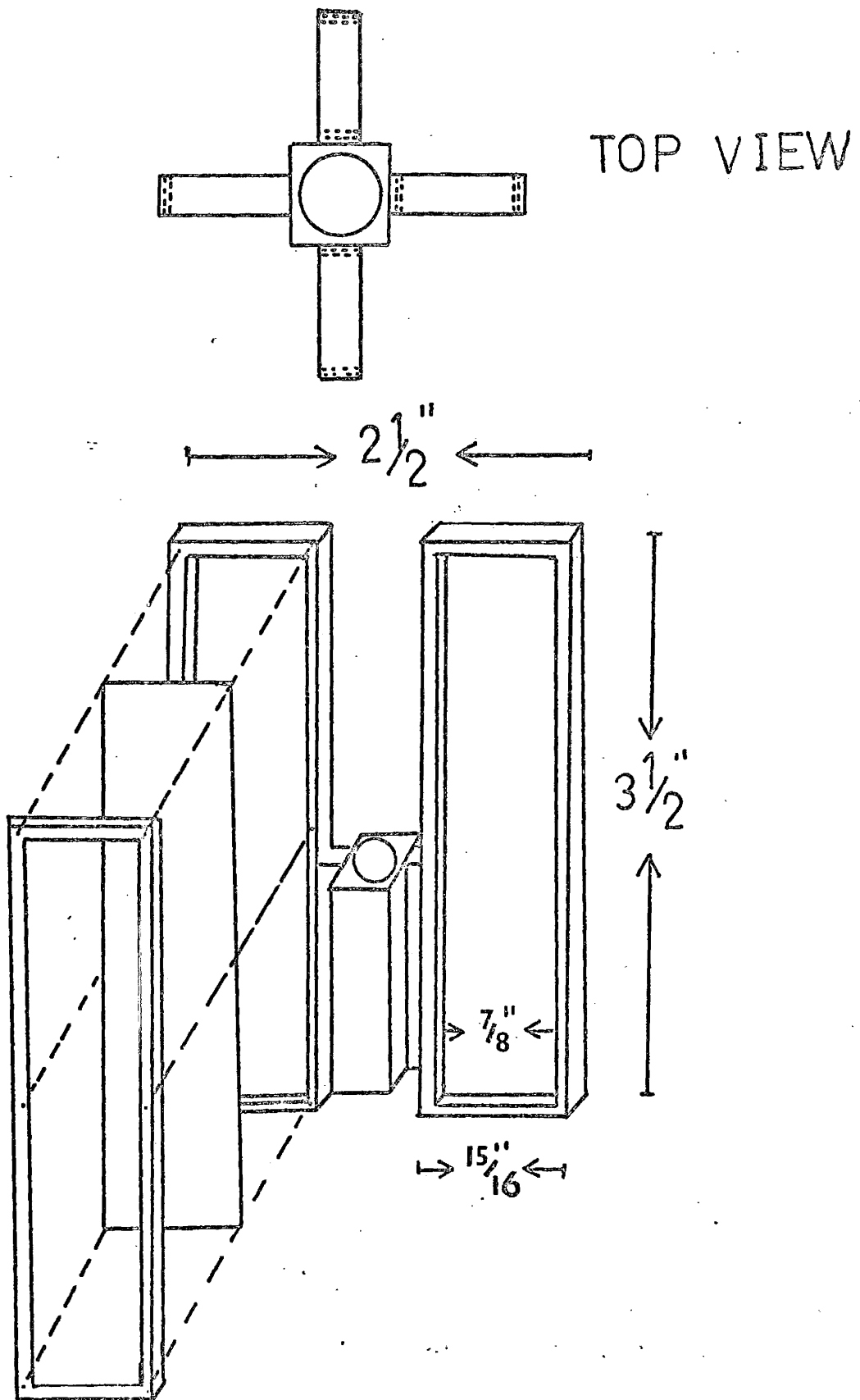


Fig. (25) Paddle basket assembly

ween the heater and the reactor wall.

The performance of the reactor had been checked thoroughly by Kempling (1). The mixing of the reactor was studied by introducing pulses of nitrogen into a steady flow of hydrogen at various flow rates ( 0.08 to 8.77 ml./sec. ) and two stirring speeds ( 1500 and 2000 r.p.m. ). The results showed an exponential decrease in concentration after a sharp increase as would be expected from the equation :

$$C = C^* \exp(-t/\tau) \quad (2.1)$$

where : C - effluent concentration

$C^*$  - maximum concentration of tracer at  $t = 0$

$\tau$  - time constant of reactor =  $V/Q$

t - time

V - volume of reactor

Q - flow rate of hydrogen

This test proved that the reactor provided a perfectly mixing of reactants. For a 5:1 mixture of hydrogen and n-butane, the mass and heat transfer coefficients were estimated to be  $3.8 \times 10^{-4}$  moles/cm<sup>2</sup>-sec-atm. and  $2.1 \times 10^2$  cal/cm<sup>2</sup>-sec-°C respectively. Varying the stirring speeds between 1500 and 1900 r.p.m. had no effect on the observed reaction rates for n-butane hydrogenolysis. This shows that interparticle concentration gradients were negligible over the range of the stirring speeds. Thus, the stirring speed was fixed at 1500 r.p.m. in the experiments.

### 2.3 Operating Procedure

Initially, the catalyst was weighed and then placed on the catalyst basket. The whole basket assembly was carefully balanced on a knife-edge static balance before attaching to the rotating shaft. This procedure eliminated vibration of the basket during rotation in which the heavier vane would cause excessive bearing wear and make the system inoperative. The reactor was closed tightly with a torque wrench and checked for leaks with soap solution using hydrogen.

The catalyst was then reduced in the reactor for about 12 hours at 250°C with a hydrogen flow of 10 ml./min. and a stirring speed of 1500 r.p.m.. Once the catalyst had been reduced, the reactor was not opened again to avoid catalyst contamination with air. The same batch of catalyst was used until it became deactivated. The catalyst was kept in a flow of hydrogen when not used for hydrogenolysis studies.

A continuous flow system was employed in which the feed gas mixture entered the reactor from the bottom and the effluent left at the top. An experiment consisted of setting the reactor conditions and the feed flow rates and ratios. When steady state conditions had been established, the effluent flow rate was measured and its composition was analyzed by gas chromatograph.

To begin an experiment, the reactor was filled with hydrogen to the desired pressure. The reactor temperature was set by the proportional temperature controller. The stirring mechanism was activated. When the required experimental conditions had been obtained, the hydrogen flow rate was set and propane was then added to the hydrogen flow. When

the temperature became constant, the effluent composition was analyzed by a gas chromatograph. As soon as the integrator showed that the peak area of each component was constant for about fifteen minutes, steady state was assumed to have been reached. The effluent flow rate was determined with the soap flow meter. The final reactor temperature was taken and a final analysis of the effluent was made. The propane flow was then discontinued, and the hydrogen flow was increased to flush the reactor for the next experiment. A set of six or seven runs was made on a working day with one of the runs at standard conditions to check for the activity of the catalyst. The activity usually remained essentially constant,  $\pm 5\%$  for nearly a month. A new batch was introduced every five or six weeks, and corrections were made for activity changes, if required, in the last part of this period.

## CHAPTER THREE

### HYDROGENOLYSIS OF PROPANE

#### 3.1 General

The hydrogenolysis of propane was investigated at various temperatures and pressures using a Carberry reactor. The rates obtained were differential and can be calculated as (1) :

$$r = \frac{F}{W} \frac{Y_1 + 2Y_2}{3} \quad (3.1)$$

where :  $r$  - differential rate

$F$  - effluent flow rate

$W$  - weight of catalyst

and  $Y_i$  - mole fraction of hydrocarbon containing  
i carbon atoms

The strategy for developing rate expressions was divided into two parts. Firstly, a simple power rate equation was assumed as

$$r = k P_{C_3}^a P_{H_2}^b \quad (3.2)$$

where :  $k$  - rate constant

$P_{C_3}$  - partial pressure of hydrogen

$P_{H_2}$  - partial pressure of propane

$a$  - exponent for propane

$b$  - exponent for hydrogen.

The rate expression was linearized by taking the logarithms and then linear least squares was applied to estimate the parameters  $k$ ,  $a$  and  $b$ . The values of  $a$  and  $b$  were tested for other temperatures by plotting  $r$  against  $P_{C_3H_2}^a P_{H_2}^b$ . The dependence of the rate constant was represented by an Arrhenius expression as :

$$k = A \exp(-E/RT) \quad ( 3.3 )$$

where :  $A$  - pre-exponential factor

$E$  - activation energy

$R$  - gas constant

and  $T$  - temperature in  $^{\circ}K$

Equation (3.2) and (3.3) were tried at various pressures and temperatures to evaluate the values of  $a$ ,  $b$  and  $E$ .

The equation derived from the mechanism proposed by Cimino et. al. (6) was found by Kempling (1) to be unable to correlate the rate data at various pressures. The mechanism has been described in detail in Chapter One. It includes a reversible adsorption-desorption of hydrocarbon in equilibrium and a surface cracking reaction which is the rate determining step. The rate expression derived from this mechanism could be simplified as :

$$r = k P_{C_3H_2}^n P_{H_2}^{(1-n\alpha)} \quad ( 3.4 )$$

where  $\alpha$  is the number of hydrogen atoms lost by propane upon adsorption.

Comparing equations (3.4) and (3.2), value of  $\alpha$  can be estimated as :

$$\alpha = 2(1-a)/b \quad ( 3.5 )$$

The mechanism proposed by Cimino et. al. was criticized by Kemball

(13) because it does not allow the competition of hydrogen on adsorption. Various mechanisms were proposed and equations were derived from the mechanisms. The equations that were proposed and tested are shown in Appendix (B). The criteria for equation rejection are a lack of fit as shown by an excessively large residual root mean square and unacceptable characteristics of the estimated parameters. The mechanism that fits the experimental observations reasonably well is shown in fig. (3.1). It involves an initial dissociative adsorption of hydrogen and propane. The adsorbed  $C_3$  species dissociates further to lose more hydrogen, forming a second hydrocarbon species denoted by  $C_3'$ . The adsorbed  $C_3'$  species reacts with adsorbed hydrogen to form  $C_1$  and  $C_2$  adsorbed species. The surface coverage of adsorbed  $C_3$  and hydrogen can be represented as :

$$\theta_{C_3} = \frac{k_{C_3}^P C_3^P H_2^{-1/2}}{1 + k_H^P H_2^{1/2} + k_{C_3}^P C_3^P H_2^{-1/2}} \quad (3.6)$$

$$\theta_H = \frac{k_H^P H_2^{1/2}}{1 + k_H^P H_2^{1/2} + k_{C_3}^P C_3^P H_2^{-1/2}} \quad (3.7)$$

The coverage of the surface by species  $C_3'$  is assumed to be negligibly small. If the rate determining step is assumed to be the cracking of carbon-carbon bond of the adsorbed  $C_3'$  species, then

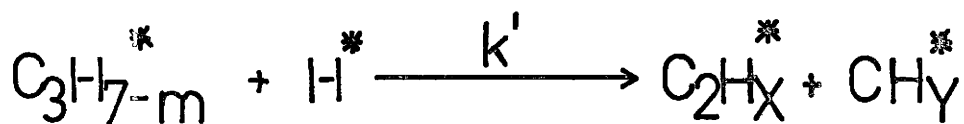
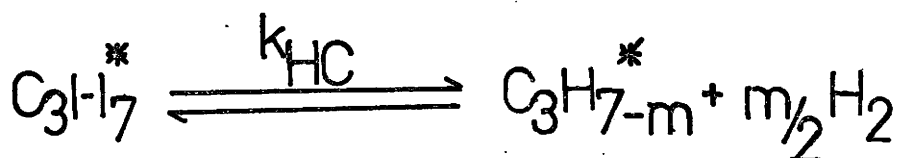
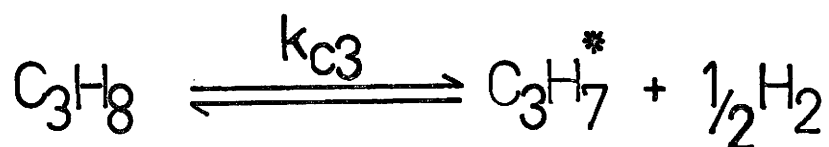
$$r = k' \theta_{C_3'} \theta_H \quad (3.8)$$

$$\text{where } \theta_{C_3'} = k_{HC} \theta_{C_3}^P H_2^{-m/2} \quad (3.9)$$

Substituting equations (3.7) and (3.9) into equation (3.8) yields

$$r = \frac{k^P C_3^P H_2^{-m/2}}{\left( 1 + k_H^P H_2^{1/2} + k_{C_3}^P C_3^P H_2^{-1/2} \right)^2} \quad (3.10)$$

Fig.(31) Mechanism for hydrogenolysis  
of propane



$k_{\text{C3}}$  - Adsorption constant for propane

$k_{\text{H}}$  - Adsorption constant for hydrogen

$k_{\text{HC}}$  - Equilibrium constant

$k'$  - Cracking rate constant

$\text{C}_3\text{H}_8$  and  $\text{H}_2$  - Gaseous propane and hydrogen

$\text{C}_3\text{H}_7^*$ ,  $\text{C}_3\text{H}_{7-m}^*$ ,  $\text{C}_2\text{H}_X^*$  and  $\text{CH}_Y^*$  - Adsorbed hydrocarbon species

$\text{H}^*$  - Adsorbed Hydrogen

The parameters in equation (3.10) were estimated by linear least squares method. Sometimes, nonlinear least squares method was applied to improve the value of the parameters.

### 3.2 Experimental Results

The experimental data are shown in Table A(1) to A(10). The data were obtained at different temperatures and pressures with different feed rates and ratios. The following were the ranges of the experimental conditions.

Temperature	-	115-155 °C
Pressure	-	2 - 80 psig.
Feed ratio ( $H_2/C_3H_8$ )	-	2.5 - 7
Effluent flow rate	-	0.9 - 10 ml/sec.
Propane conversion	-	10 - 90 %

Equation (3.2) was linearized by taking the logarithms as :

$$\log r = \log k + a \log P_{C_3} + b \log P_{H_2} \quad (3.11)$$

Equation (3.11) was fitted to the experimental data shown on Table A(1) to A(6) by linear least squares. The parameters  $k$ ,  $a$  and  $b$  obtained are listed in table (3.1). The propane exponents are positive and hydrogen exponents are negative and large. The overall orders of the reaction are negative. The values for  $a$  and  $b$  are different for different pressures. Fig.(3.2) is a comparison of the observed and calculated reaction rates. The figure demonstrates that the fit was reasonably good ca.  $\pm$  8%. The values of  $a$  and  $b$  were used to explore their fit at other temperatures at the same pressure by plotting  $r$  as a function of  $P_{C_3}^a P_{H_2}^b$  and are shown in fig.(3.3) to fig.(3.7). These figures show that the

TABLE ( 3.1 )

Parameters of Equation (3.2)

$P_T$ (psig)	Temp. ( $^{\circ}\text{C}$ )	Residual Sum of Squares	Residual Root Mean Square	$a \pm$ 95% Confidence Interval	$b \pm$ 95% Confidence Interval	$k$
2	120	$1.29 \times 10^{-14}$	$2.54 \times 10^{-8}$	$.785 \pm .097$	$-1.22 \pm .26$	$2.18 \times 10^{-5}$
15	114.5	$8.15 \times 10^{-15}$	$1.84 \times 10^{-8}$	$.632 \pm .072$	$-1.22 \pm .235$	$5.47 \times 10^{-7}$
20	126	$7.12 \times 10^{-14}$	$4.18 \times 10^{-8}$	$.618 \pm .082$	$-1.87 \pm .184$	$1.67 \times 10^{-6}$
40	144.5	$5.17 \times 10^{-14}$	$4.36 \times 10^{-8}$	$.770 \pm .073$	$-1.52 \pm .176$	$8.33 \times 10^{-6}$
60	147.5	$4.60 \times 10^{-14}$	$4.90 \times 10^{-8}$	$.861 \pm .129$	$-1.57 \pm .450$	$9.02 \times 10^{-6}$
80	150	$2.59 \times 10^{-14}$	$4.03 \times 10^{-8}$	$.453 \pm .129$	$-1.60 \pm .189$	$4.97 \times 10^{-6}$

Units of  $k$  :  $\frac{\text{Mole atm.}^{-(a+b)}}{\text{sec. gm.-cat.}}$

Fig.( 32)

Comparison of Experimental & Calculated Rates

( Eqn. 3.2 )

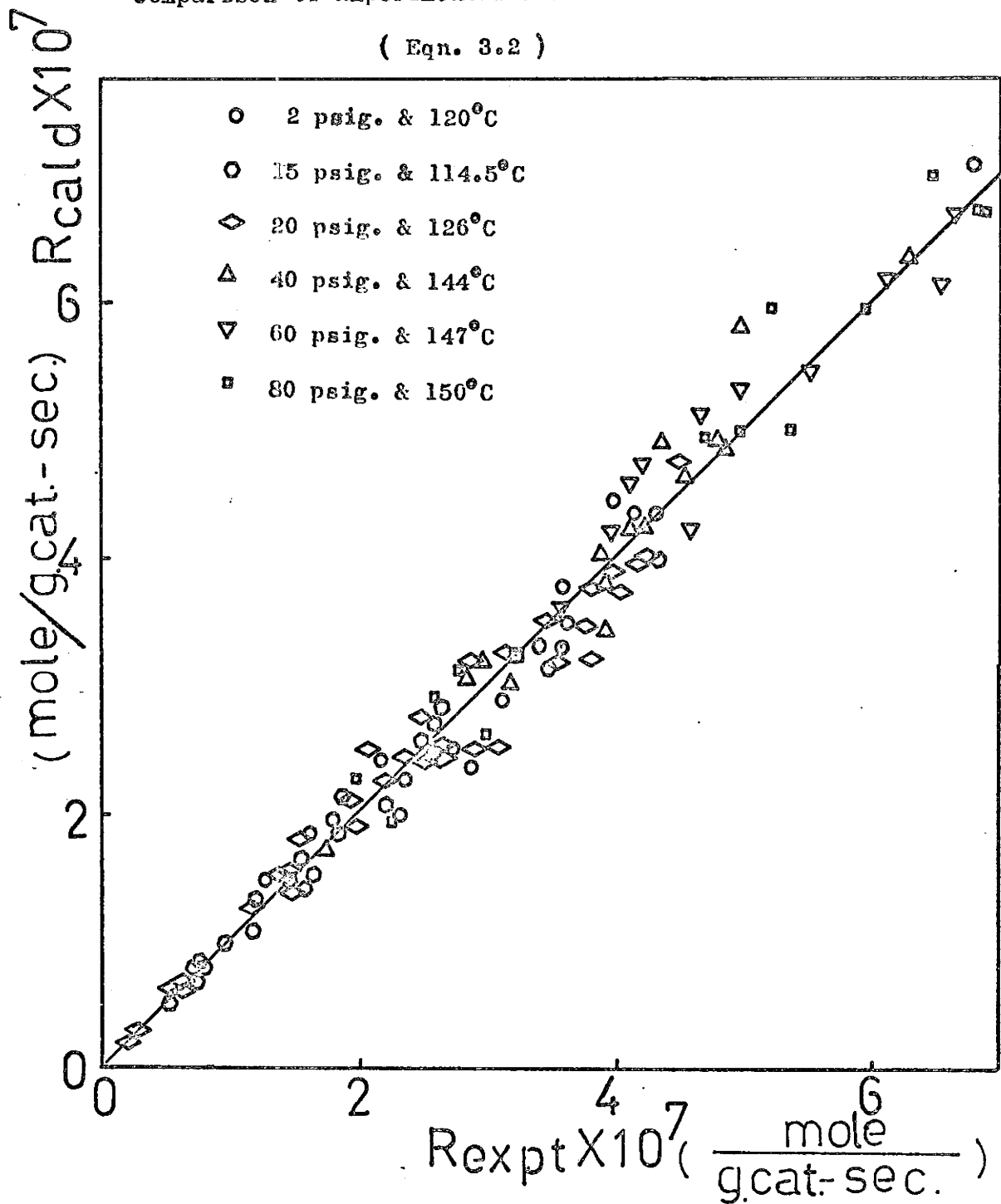


Fig.(3.3)

Propane Hydrogenolysis Kinetics at  $P_T = 15$  psig.

( $a = .632$  &  $b = -1.22$ )

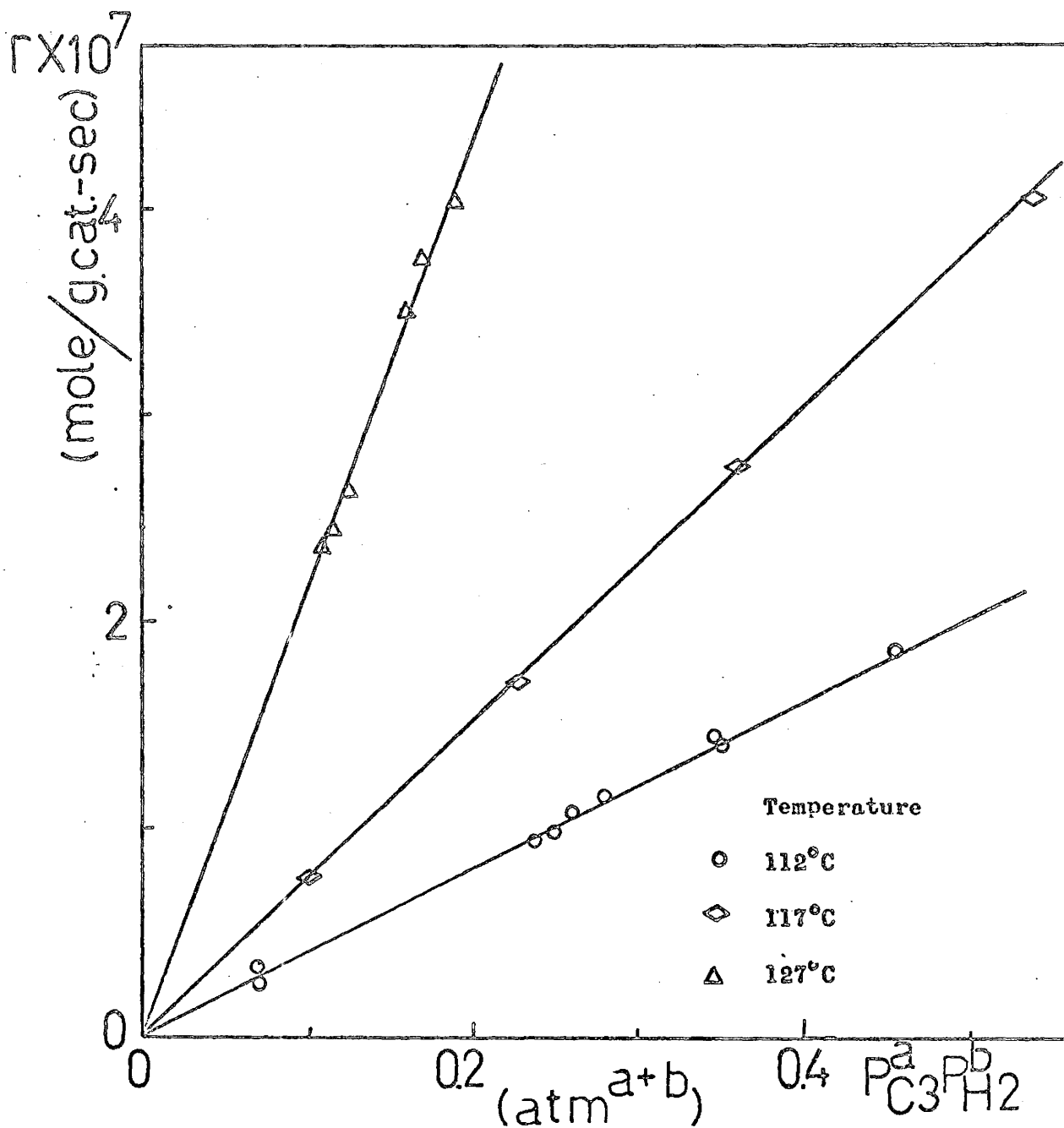
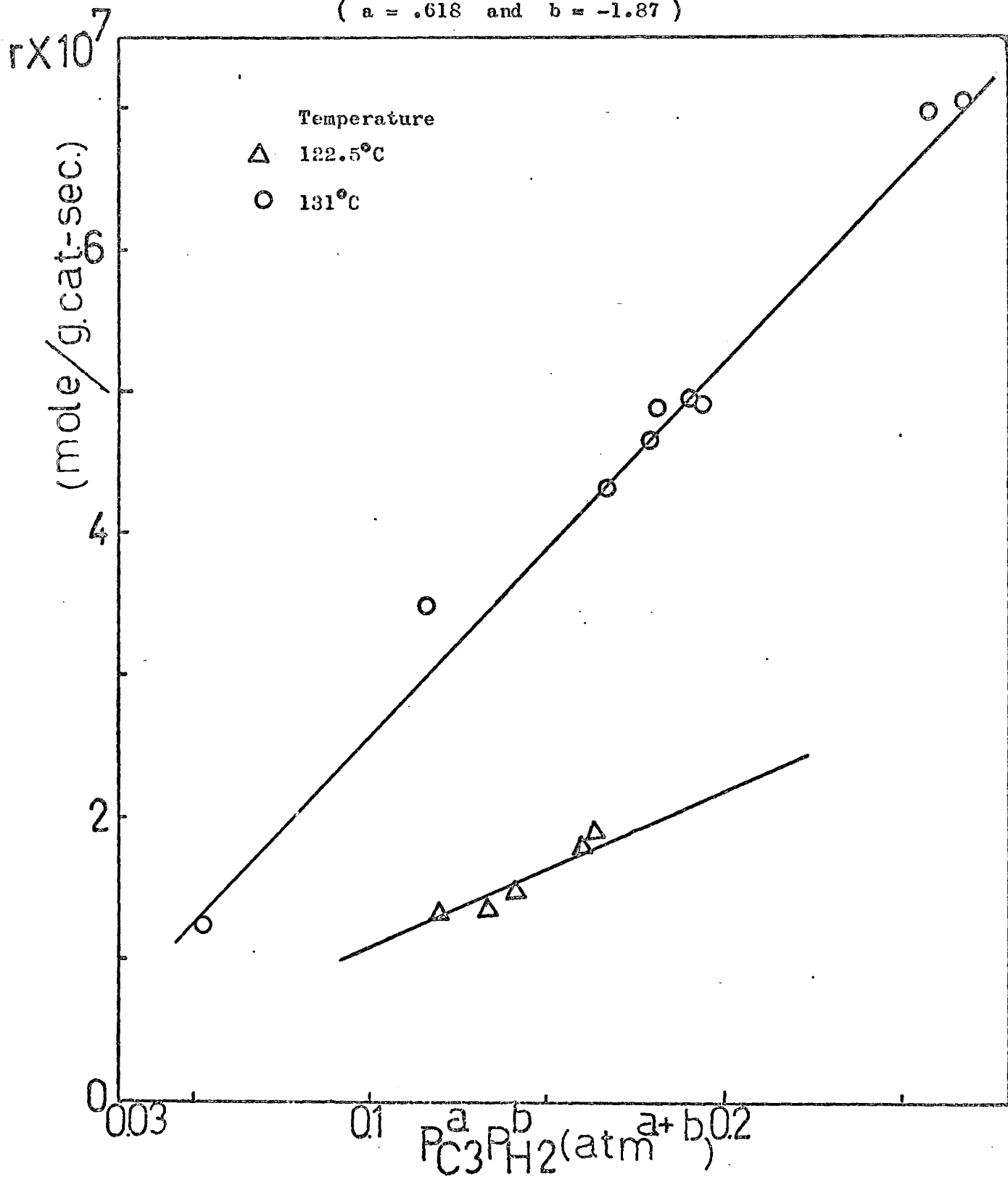


Fig.(34)

Propane Hydrogenolysis Kinetics at  $P_T = 20\text{psig}$ .

(  $a = .618$  and  $b = -1.87$  )



# Fig.(35)

Propane Hydrogenolysis Kinetics at  $P_T = 40\text{psig.}$

(  $a = .770$  and  $b = -1.52$  )

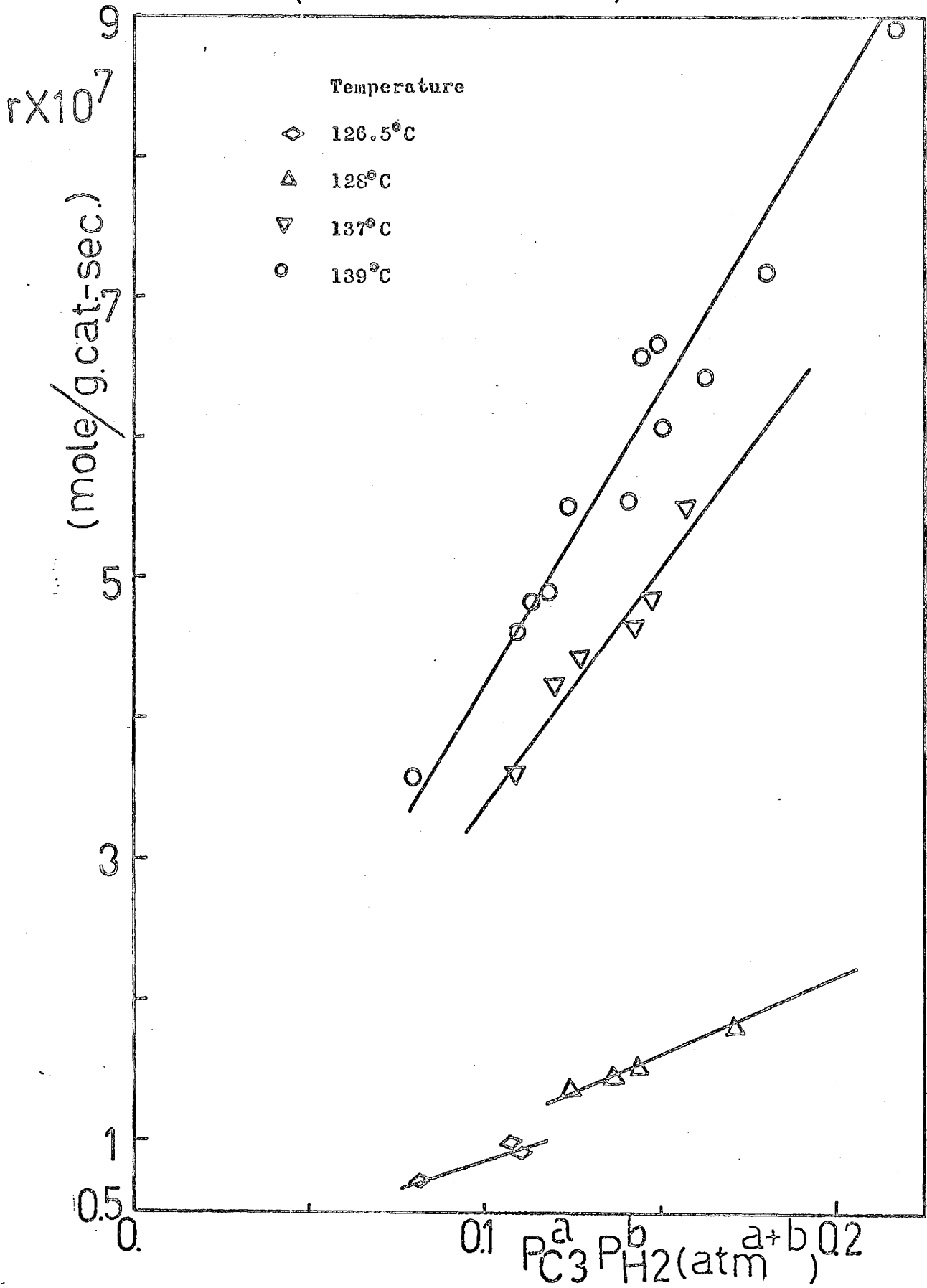
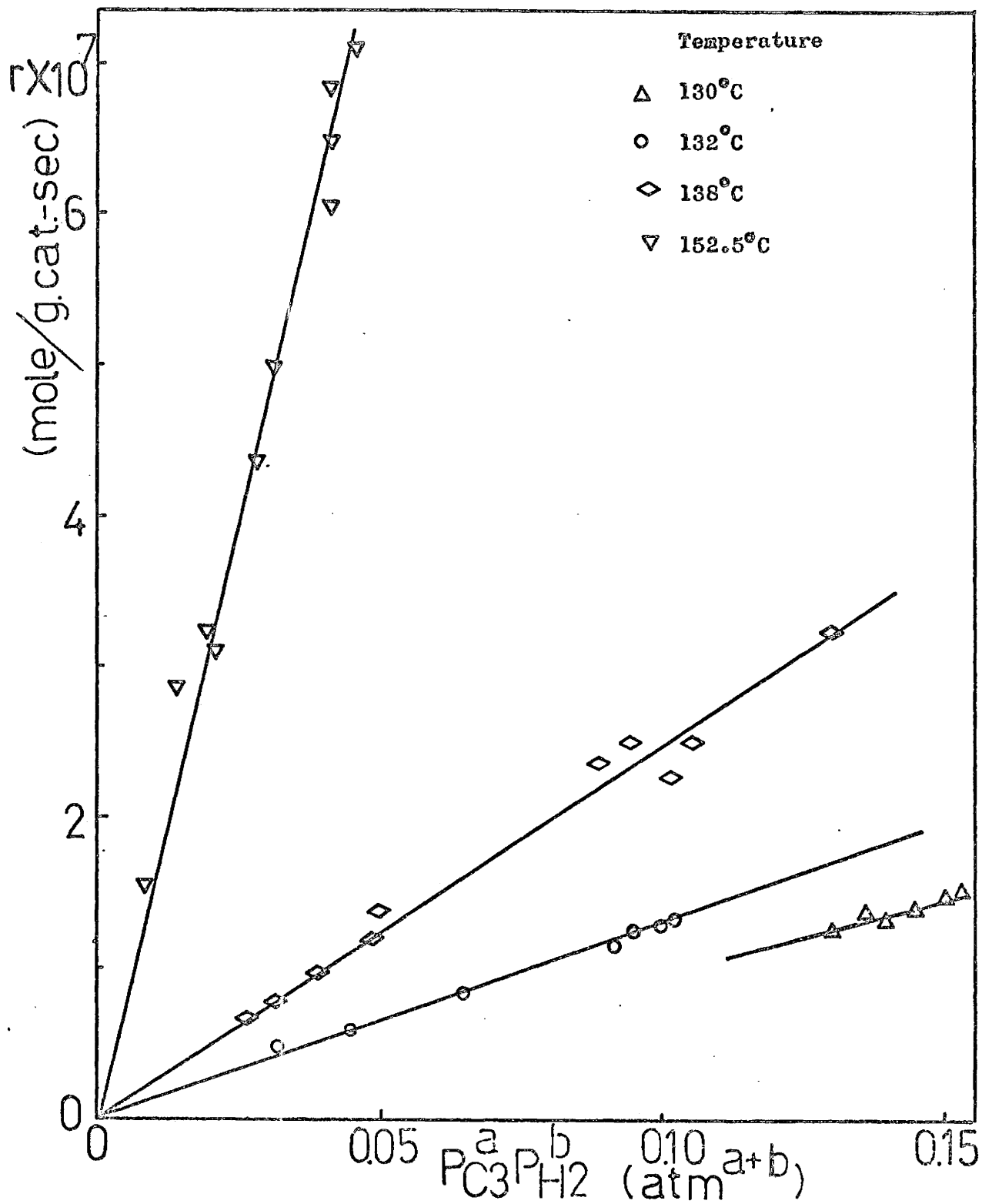


Fig.(3.6)

Propane Hydrogenolysis Kinetics at  $P_T = 60$  psig. $( a = .861 \text{ and } b = -1.57 )$ 



exponents of propane and hydrogen remain the same over the temperatures examined. The slope of the plots of  $r$  as a function of  $P_{C_3}^a P_{H_2}^b$  is the rate constant. Table (3.2) shows the rate constants at different temperatures and pressures. The dependence of the rate constant on temperature was represented by equation (3.3). Fig.(3.8) presents Arrhenius plots for data at constant pressures. The values of the pre-exponential factor and activation energy are given in Table (3.3). The activation energy increases with increasing pressure.

Experiments at constant temperatures with pressures varying were performed. The experimental data are shown in Tables B(1) to B(4). Experiments at four different temperatures (128, 139, 143.5 and 148°C) with pressures ranging from 10 to 90 psig. were made. The data given in Tables B(1) to B(4) were fitted to equation (3.10). The value of  $m$  was first assumed. The equation was then linearized by inversion and examined using linear least squares. The most appropriate value of  $m$  is that which yields the smallest residual sum of squares and positive rate constants. The values of the parameters are shown in Table (3.4).  $k$  is the rate constant for the hydrogenolysis of propane.  $k_H$  and  $k_{C_3}$  are the equilibrium constants for the adsorption of hydrogen and propane respectively.  $n/2$  ( $n = m + 1$ ) is the total number of hydrogen molecules lost by propane in forming adsorbed  $C_3'$  species that undergoes cracking reaction.

The values of  $n$  are between 5 and 5.3. An integral value of 5 was taken. The dependence on temperature of the parameters is expressed as :

$$k = A \exp(-E/RT) \quad (3.12)$$

$$k_H = A_H \exp(Q_H/RT) \quad (3.13)$$

$$\text{and } k_{C_3} = A_{C_3} \exp(Q_{C_3}/RT) \quad (3.14)$$

where  $A$ ,  $A_H$  and  $A_{C_3}$  are the pre-exponential factors,  $E$  is the activation energy and  $Q_H$  and  $Q_{C_3}$  are the heat of adsorption for hydrogen and propane.

The parameters in equations (3.12), (3.13) and (3.14) were obtained by plotting  $\log k$ ,  $\log k_H$  and  $\log k_{C_3}$  as a function of  $1/T$ . The plots are shown in fig. (3.9) and (3.10) and the parameters are listed in Table (3.5). The activation energy for the hydrogenolysis of propane is large. The adsorption of propane is endothermic;  $Q_{C_3}$  is  $-2.19$  kcal/mole. The adsorption of hydrogen is exothermic;  $Q_H$  is  $7.95$  kcal/mole. Fig. (3.11) is the comparison of the calculated and the experimental reaction rates. The figure demonstrates that the fit is good.

Finally, the dependence of reaction rates on total pressure was studied. This was done by performing experiments with constant feed rate, feed ratio and temperature. The experimental data are shown in Table B(5). Fig.(3.12) shows the trend of the reaction rates with pressure while fig.(3.13) shows the trend of the conversions with pressure. If the dependence of the reaction rate on reaction pressure was assumed to be

$$r = k P_T^d \quad (3.15)$$

where  $P_T$  is the total reaction pressure and  $d$  is the order of the pressure dependence. Value of  $d$  would be obtained by plotting  $\log r$  as a function of  $\log P_T$ . The plot is shown in fig.(3.14) and values of  $d$  are  $-0.93$ ,  $-0.88$  and  $-0.87$  for the temperatures of  $128$ ,  $139$  and  $148$  C. An average value of  $-0.90$  was taken. Values of  $k$  obtained were  $3.97 \times 10^{-6}$ ,  $9.71 \times 10^{-6}$  and  $1.99 \times 10^{-5}$

TABLE ( 3.2 )

Rate Constant Obtained from Plots of  $r$  vs  $P_{C3}^a P_{H2}^b$

$P_T$ (psig.)	Temperature ( $^{\circ}C$ )	$k$
15	112	$4.00 \times 10^{-7}$
15	117	$7.40 \times 10^{-7}$
15	127	$2.16 \times 10^{-6}$
20	122.5	$1.04 \times 10^{-6}$
20	130.5	$2.59 \times 10^{-6}$
40	126.5	$8.96 \times 10^{-7}$
40	128	$1.06 \times 10^{-6}$
40	137	$3.34 \times 10^{-6}$
40	139	$4.28 \times 10^{-6}$
60	130	$9.94 \times 10^{-7}$
60	132	$1.30 \times 10^{-6}$
60	138	$2.52 \times 10^{-6}$
60	152.5	$9.02 \times 10^{-6}$
80	131	$5.70 \times 10^{-7}$
80	147	$3.75 \times 10^{-6}$

Units of  $k$  :  $\frac{\text{mole atm.}^{-(a+b)}}{\text{sec. gm.-cat.}}$

Fig.(38)

Arrhenius Plots for Rate Constants at Various pressures ( Eqn. 3.2 )

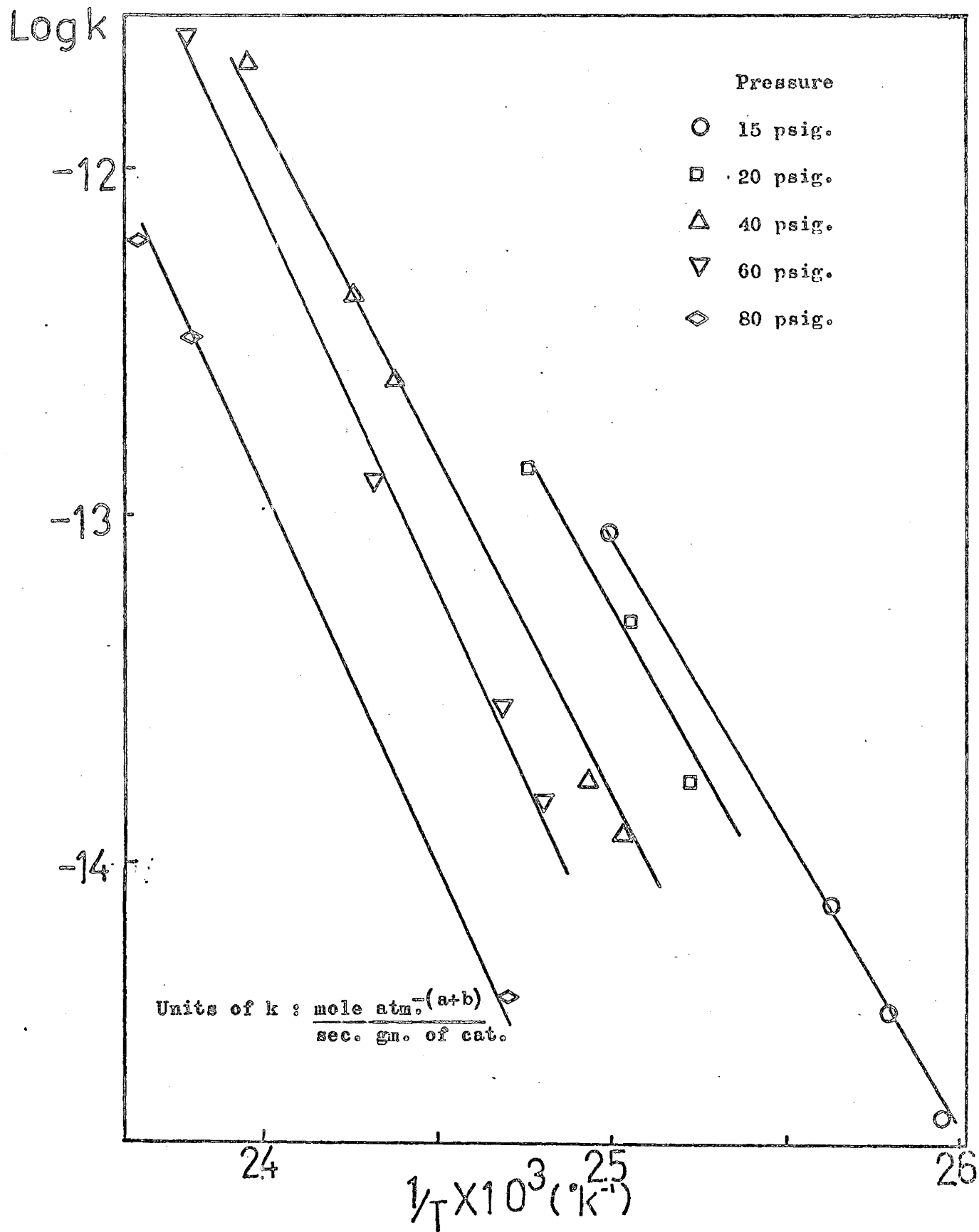


TABLE ( 3.3 )

Summary of Parameters from The Analysis of Equations ( 3.2 ) and ( 3.3 )

$P_T$ (psig)	Temp. Range ( $^{\circ}C$ )	$a \pm$ 95% Confidence Interval	$b \pm$ 95% Confidence Interval	$E_{act}$ $\frac{kcal}{mole}$	Log A
2	120	.785 $\pm$ .097	-1.22 $\pm$ .26	-	-
15	112 - 127	.632 $\pm$ .072	-1.22 $\pm$ .235	33.6	29.21
20	122 - 131	.618 $\pm$ .082	-1.87 $\pm$ .180	36.1	32.18
40	126 - 144	.770 $\pm$ .073	-1.52 $\pm$ .176	38.4	34.51
60	130 - 142	.861 $\pm$ .129	-1.57 $\pm$ .450	40.2	36.30
80	131 - 150	.453 $\pm$ .129	-1.60 $\pm$ .189	42.9	38.90

TABLE ( 3.4 )

Analysis Of Rate Data Using Equation ( 3.10 )

Reaction Pressure Range (psig)	10 - 50	20 - 60	40 - 60	40 - 90
Reaction Temperature (°C)	128	139	143.5	148
Number of Observation	37	43	19	41
Residual Degree of Freedom	34	40	16	38
Residual Sum of Squares ( $\times 10^{13}$ )	1.04	1.26	.379	1.59
Residual Root Mean Squares ( $\times 10^8$ )	5.31	5.4	4.47	6.23
Coefficient of Multiple Correlation	0.98	0.97	0.96	0.96
Values of n ( m + 1 )	5.0	5.3	5.1	5.0
Values of k ( $\times 10^5$ ) ( mole-atm./sec.-gm.-cat. )	1.78	4.66	6.77	9.67
Values of $k_H$ ( atm. <sup>-1/2</sup> )	1.08	0.78	0.72	0.66
Values of $k_{C_3}$ ( atm. <sup>-1/2</sup> )	1.58	1.73	1.77	1.81

Fig.(3.9)

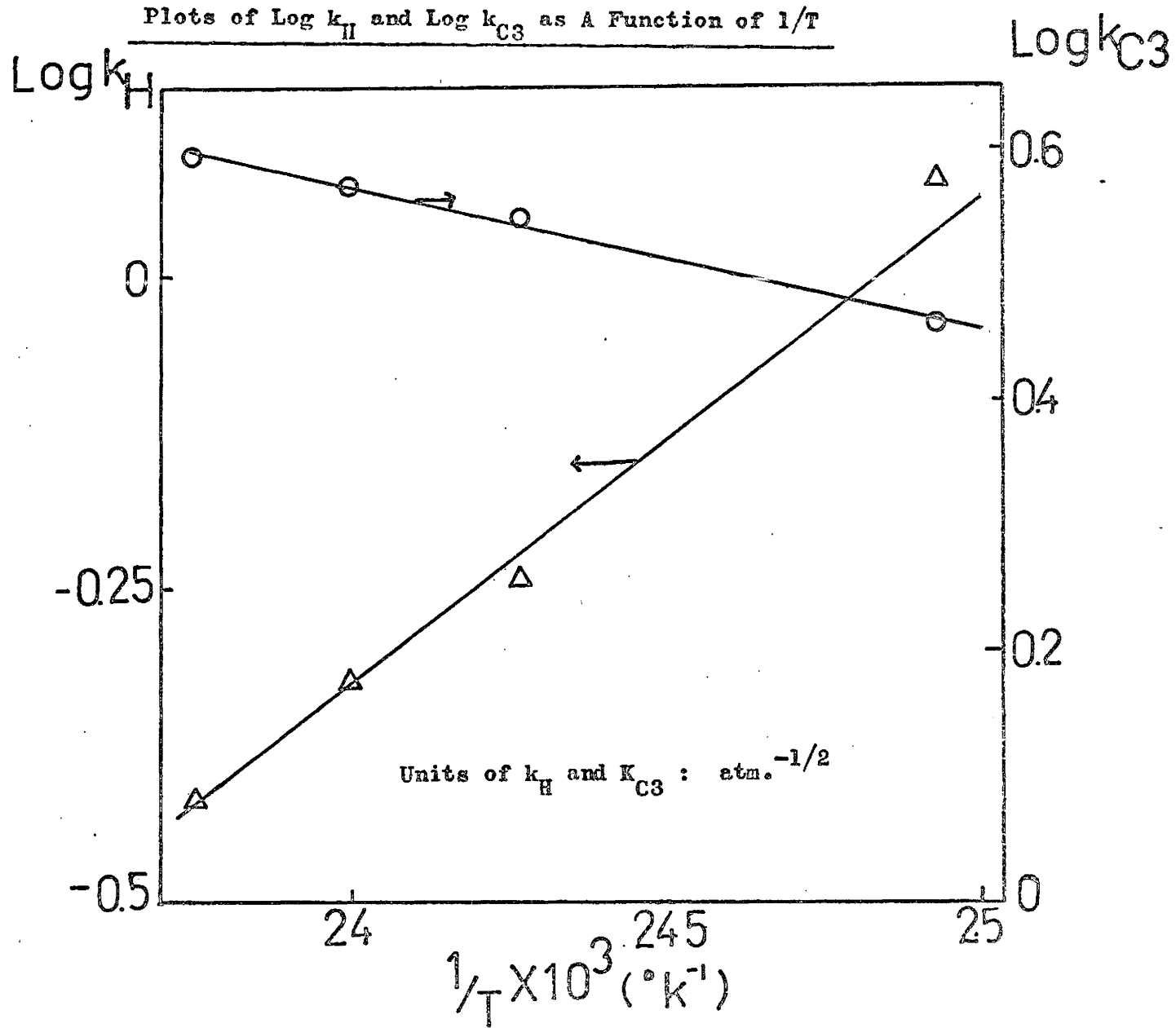


Fig.(3.10)

Arrhenius Plot For Hydrogenolysis Rate Constants ( Eqn. 3.10 )

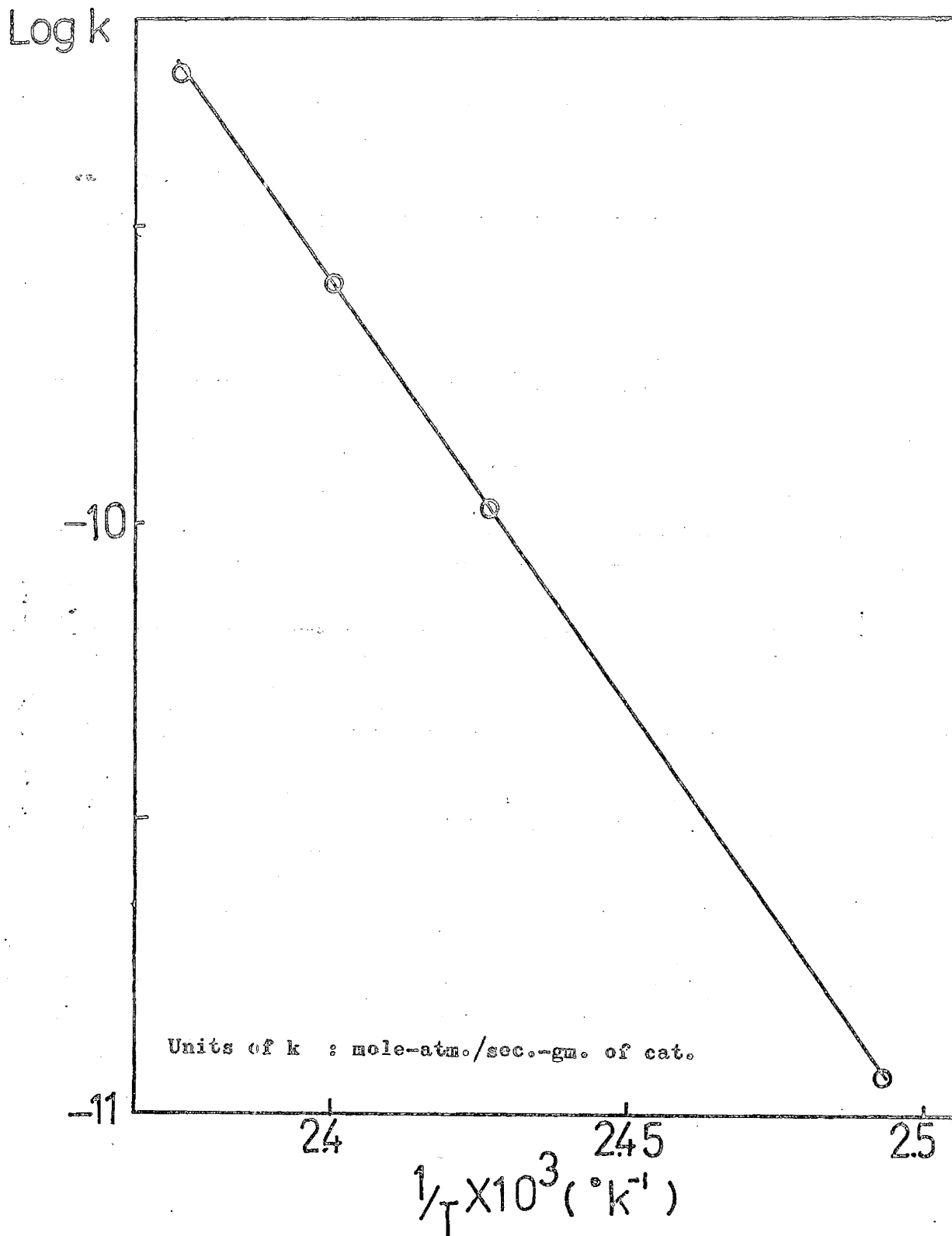


Fig.( 3.11)

Comparison of Experimental &amp; Calculated Rates ( Eqn. 3.10 )

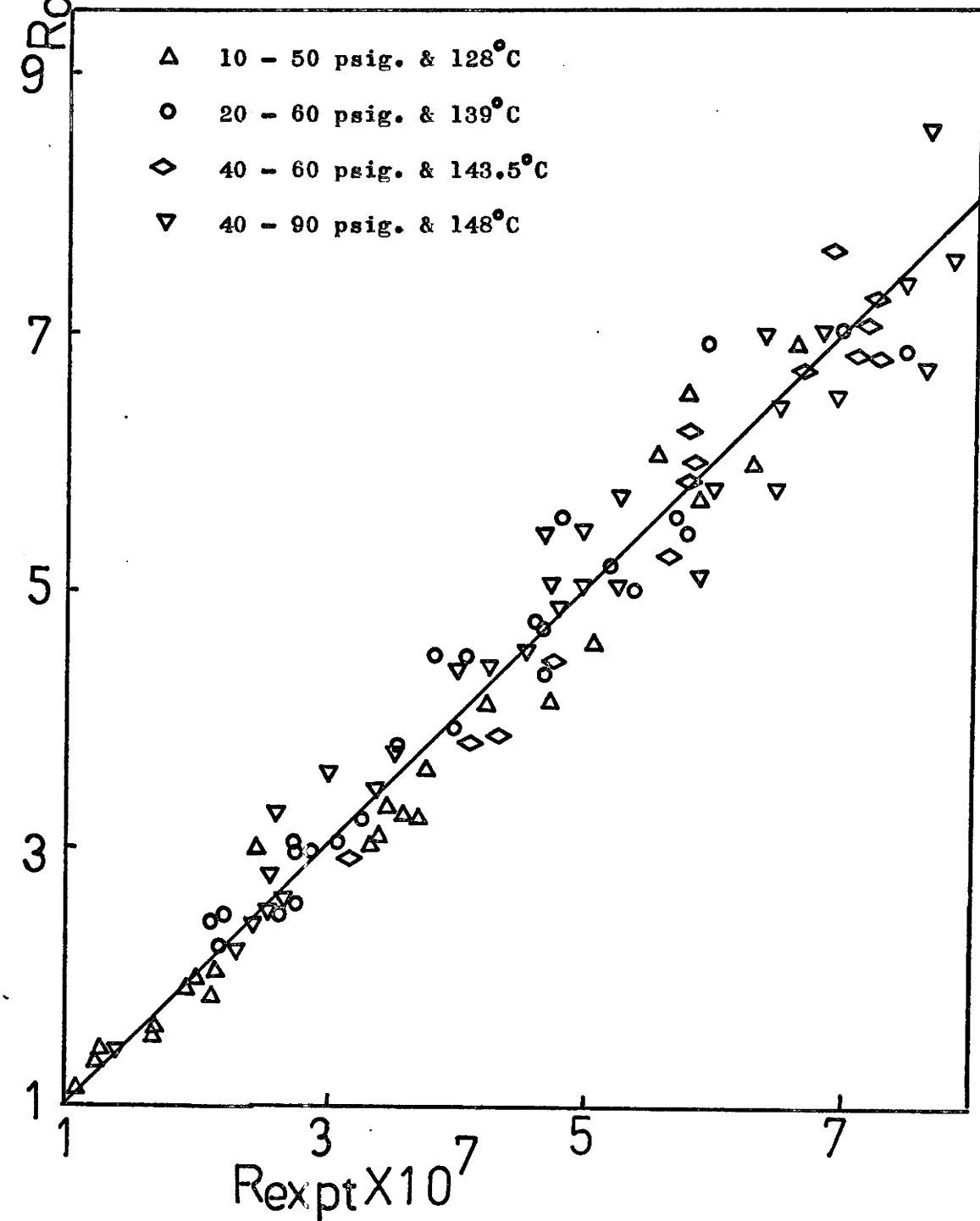


Fig.(3.12)

Dependence of Reaction Rates on Pressure

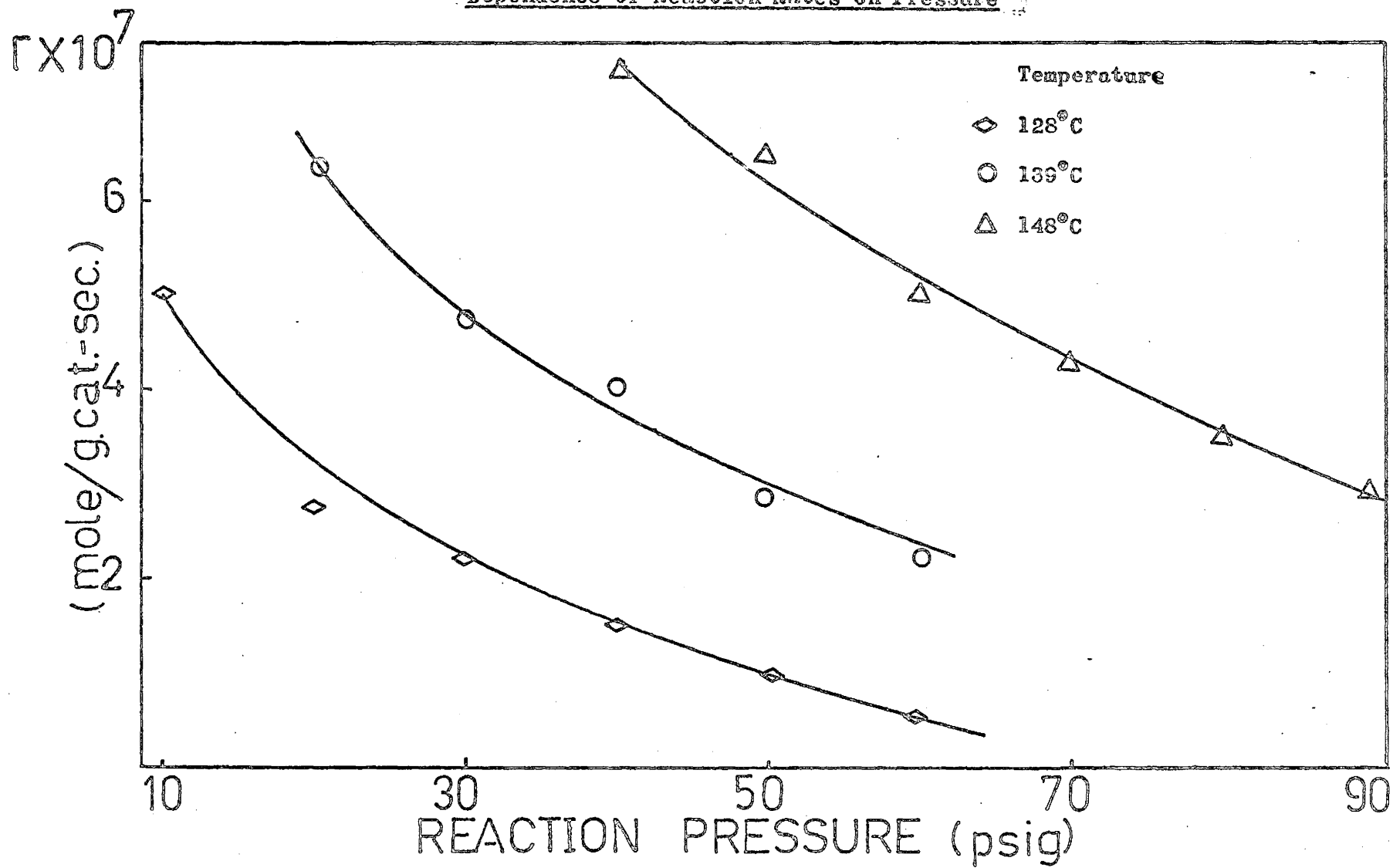


Table ( 3.5 )

Activation Energies and Heat of Adsorption ObtainedFrom Equation ( 3.10 )

	Kcal./mole	Pre-exponential Factor (log A)
Hydrogenolysis *	28.7	24.8
Hydrogen **	7.95	-12.2
Propane **	-2.19	2.58
Cracking *	34.4	34.3

\* Activation energy

\*\* Heat of Adsorption

Fig.(3.13)

Dependence of Propane Conversion on Pressure

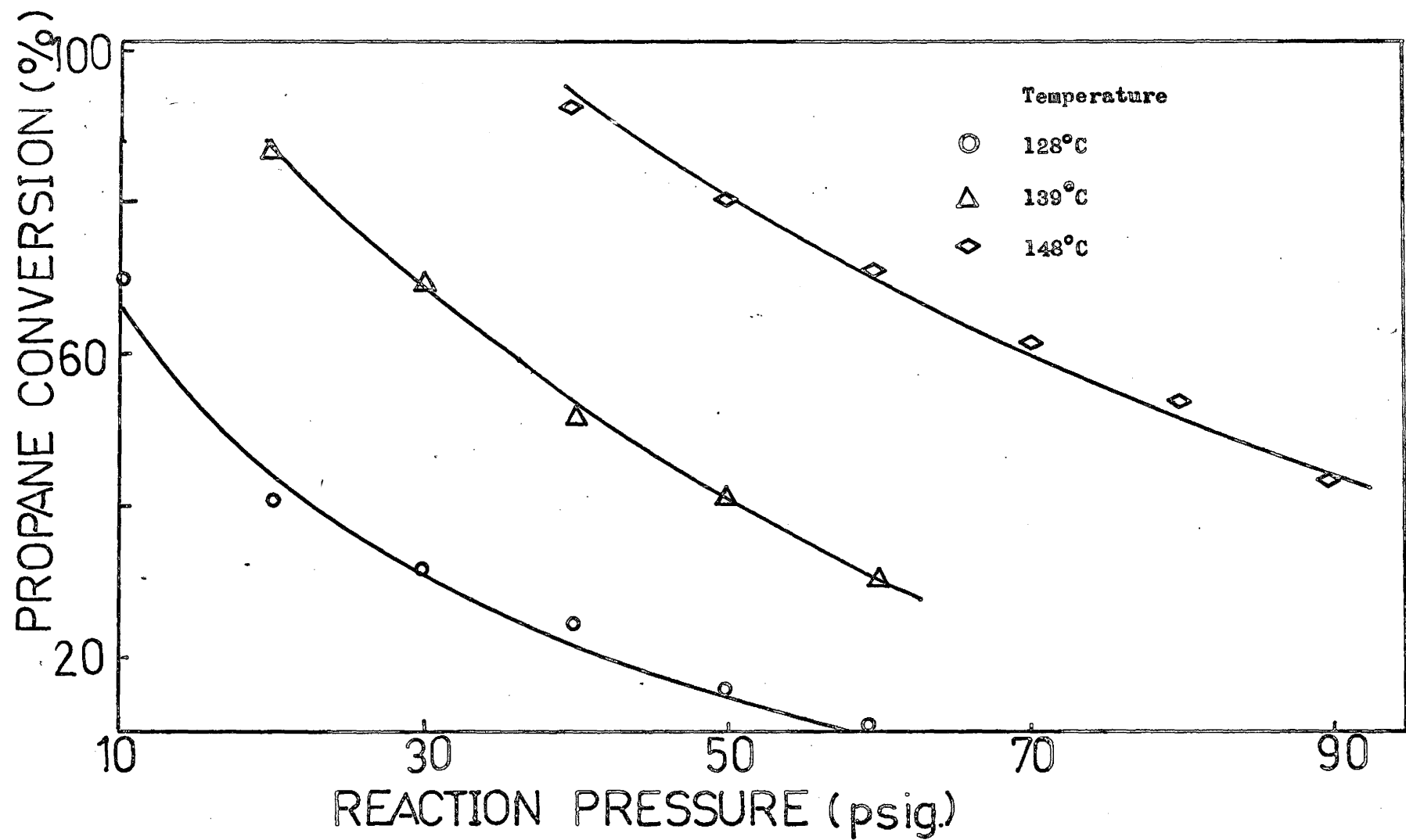
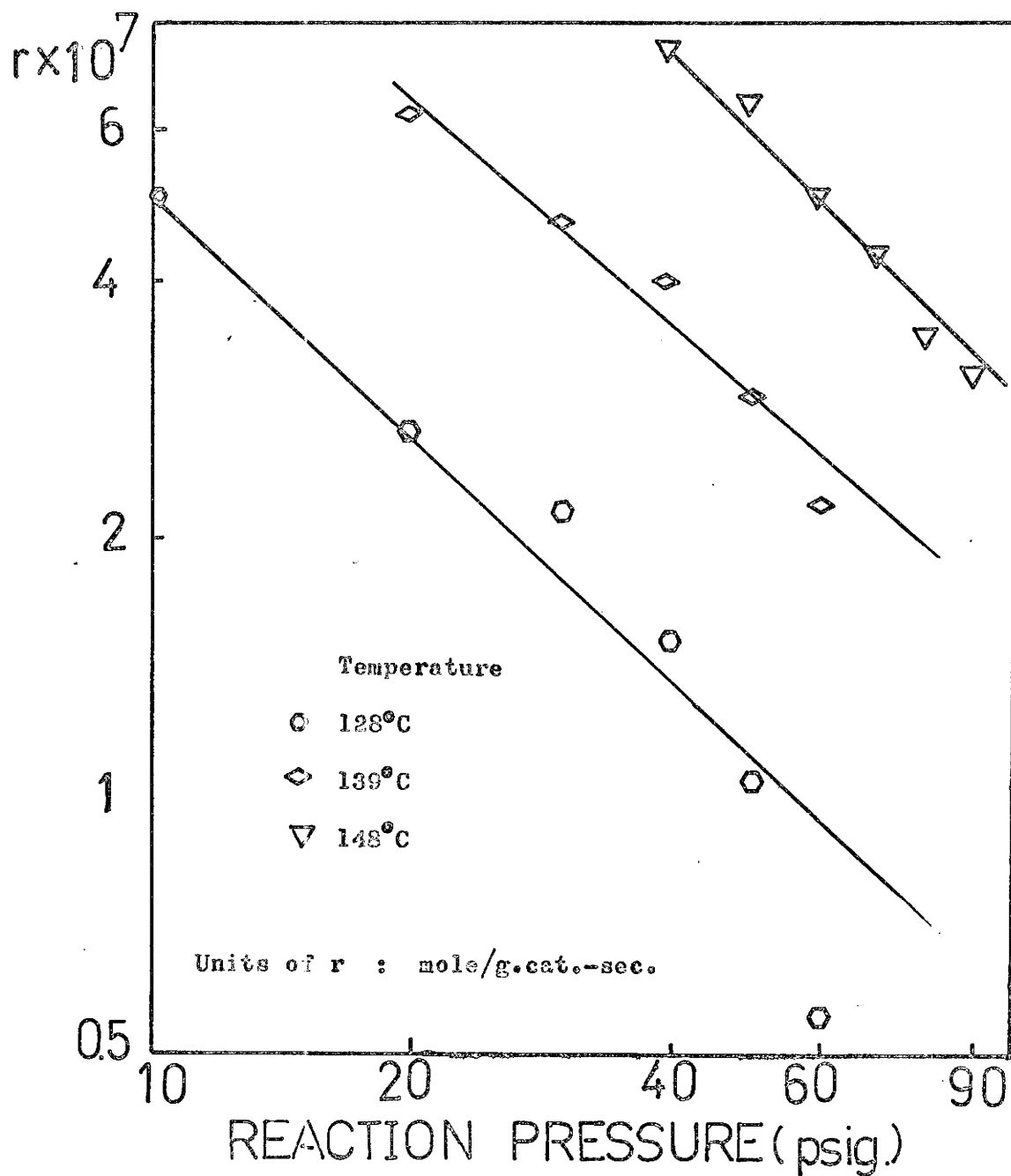


Fig.(3.14)

Dependence of rates on total pressure



for temperatures of 128, 139 and 148 °C. The dependence of  $k$  on temperature is represented as

$$k = A \exp(-E/RT) \quad (3.16)$$

where  $A$  is the pre-exponential factor and  $E$  is the activation energy. The plot of  $\log k$  against  $1/T$  is shown in fig.(3.15) and  $E$  was found to be 27.9 kcal/mole. The value is close to the value of activation energy for hydrogenolysis of propane obtained from equation (3.11).

### 3.3 Discussion and Summary

A power rate equation was assumed for the hydrogenolysis of propane. Experimental data were fitted to the equation at various pressures and temperatures to obtain the rate constants and exponents for hydrogen and propane at their 95% confidence intervals. Exponents for propane are positive and for hydrogen are negative. The overall dependence of reaction rate on pressure is negative. Apparently the power rate law will work only moderately well over a limited range of partial pressures of hydrogen and propane. Each set of data at different operating pressures requires a new set of constants, and no set of constants will fit data at several operating pressures accurately. This has also been observed by Kempling (1). The values for the exponents of hydrogen and propane, the pre-exponential factors and the activation energies for different operating pressures are shown in Table (3.3). Average values of exponents for hydrogen and propane at various pressure were estimated from fig.(3.15). The best values seem to be  $a = 0.65$  and  $b = -1.55$ . The reliability of the values is about  $\pm 35\%$ .

The mechanism proposed by Cimino et al. provided a fundamental significance to the hydrogen and hydrocarbon exponents. The number of hydrogen atoms lost on adsorption of propane is given by equation (3.5). The values of  $\alpha$  were 5.6, 7.0, 9.3, 6.5, 6.0 and 11.5 for total pressures of 2, 15, 20, 40, 60 and 80 psig.. The values of  $\alpha$  are not constant. Since values of  $\alpha$  greater than 8 are not possible for the hydrogenolysis of propane, the power rate equation seems to be unrelated to the mechanism and only an empirical relationship. At 2 psig., the value of  $\alpha$  is 5.6. This value is close to the value of 5 obtained by Tajbl (22).

Various rate equations derived from different mechanisms were proposed and tested. The one that fits the experimental observations reasonably well is equation (3.10). The equation was derived from the mechanism shown in fig.(3.1). The equation not only provides positive rate constants but also the smallest residual sum of squares. The equation was developed from the consideration of the equilibrium adsorption of propane and hydrogen. The proposed mechanism assumes that the majority of the surface is covered by hydrogen and  $C_3$  species which are only slightly dissociated. The fractional coverages of hydrogen and  $C_3$  were obtained by the application of the Langmuir equation to the dissociative adsorption of hydrogen and propane. The initial  $C_3$  species dissociates further to lose more hydrogen molecules, forming a second reactive species denoted by  $C_3'$ . The adsorption of propane and hydrogen were assumed to be in equilibrium and the rate determining step to be the surface cracking reaction of adsorbed hydrogen and  $C_3'$  species. A Hougen-Watson type of rate expression was obtained as shown in equation (3.10). The parameters were evaluated by least squares methods. The reliability of the equation and mechanism proposed was demonstrated by the small residual sum of squares.

The value of  $n$ , corresponding to the total number of hydrogen atoms lost upon adsorption to form reactive adsorbed  $C_3^1$  species is 5. Thus, the activated surface radical in cracking is  $C_3H_3^*$ . It has been proposed by Cuczi et al. (12) for hydrogenolysis of propane on Ni-catalyst, that 1,2-diadsorbed species is more favourable than 1,3-diadsorbed species intermediate. The diadsorbed intermediate perhaps is either in the form of  $C=C-CH_3$  or  $C-C-CH_3$ , i.e., propane adsorbed on two adjacent carbon atoms which are stripped of their hydrogen. The intermediates proposed here are identical with those proposed by Tajbl (22).

The parameters,  $k$ ,  $k_H$  and  $k_{C_3}$  are the rate constant for hydrogenolysis, adsorption constant for hydrogen and adsorption constant of propane. The activation energy for propane hydrogenolysis is 28.7 kcal/mole. The heat of adsorption of propane is -2.19 kcal/mole, i.e., the adsorption reaction is endothermic. It has been proposed by Sinfelt (43) that the adsorption of hydrocarbon is endothermic. Kempling (1) has also found an endothermic adsorption of hydrocarbons. The endothermicity must be due to an equilibrium reaction between adsorbed radical and gas phase propane, because adsorption processes are exothermic (41). The heat of adsorption of hydrocarbon is 7.9 kcal/mole. The adsorption reaction is exothermic.

The activation energy for  $k$  of equation (3.10) was lower than the activation energy obtained by Tajbl (22), 35.8 kcal/mole. However, Tajbl's activation energy was obtained from the constant of a power rate law. The rate constant  $k$  in equation (3.10) is the product of the rate constant for the splitting step and the adsorption constants for  $C_3$  species and hydrogen.

The dependence of the reaction rate on total pressure was also determined. The dependency can be represented as

$$r = kP_T^{-0.9} \quad (3.17)$$

where  $k$  depends on temperature and  $P_T$  is the total reaction pressure in atmosphere. The activation energy of  $k$  was obtained from an Arrhenius plot. The value was 27.9 kcal/mole which is similar to the value obtained from equation (3.10). If the exponents for hydrogen and propane in the power rate equation are taken as the values, 0.65 and -1.55, respectively, then the overall dependence of reaction rate on pressure would be to the power of -0.9, which is similar to the exponent in equation (3.17).

As a conclusion, a single power rate expression fails to correlate the reaction rates of hydrogenolysis of propane at various pressures. The mechanism proposed by Cimino et al. does not fit the kinetics data at higher pressures. This mechanism has been criticized because it does not allow the competition of hydrogen for adsorbed sites. A mechanism allowing both hydrogen and propane to compete for empty sites was proposed. A Hougen-Watson type equation was derived from the proposed mechanism. The equation was found to be consistent with the experimental observations.

Fig.(3.15)

Arrhenius plot for Equation (3.15)

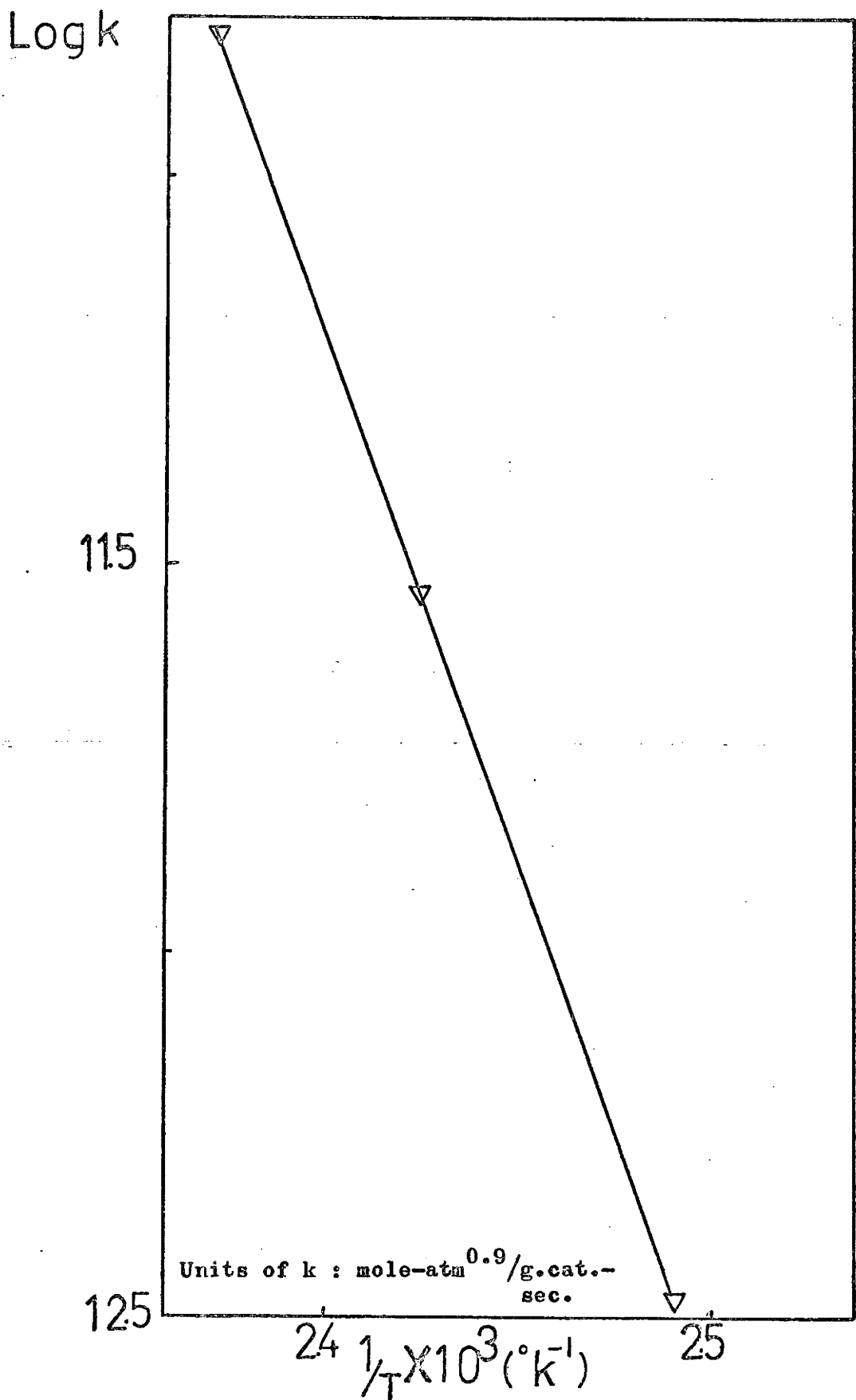
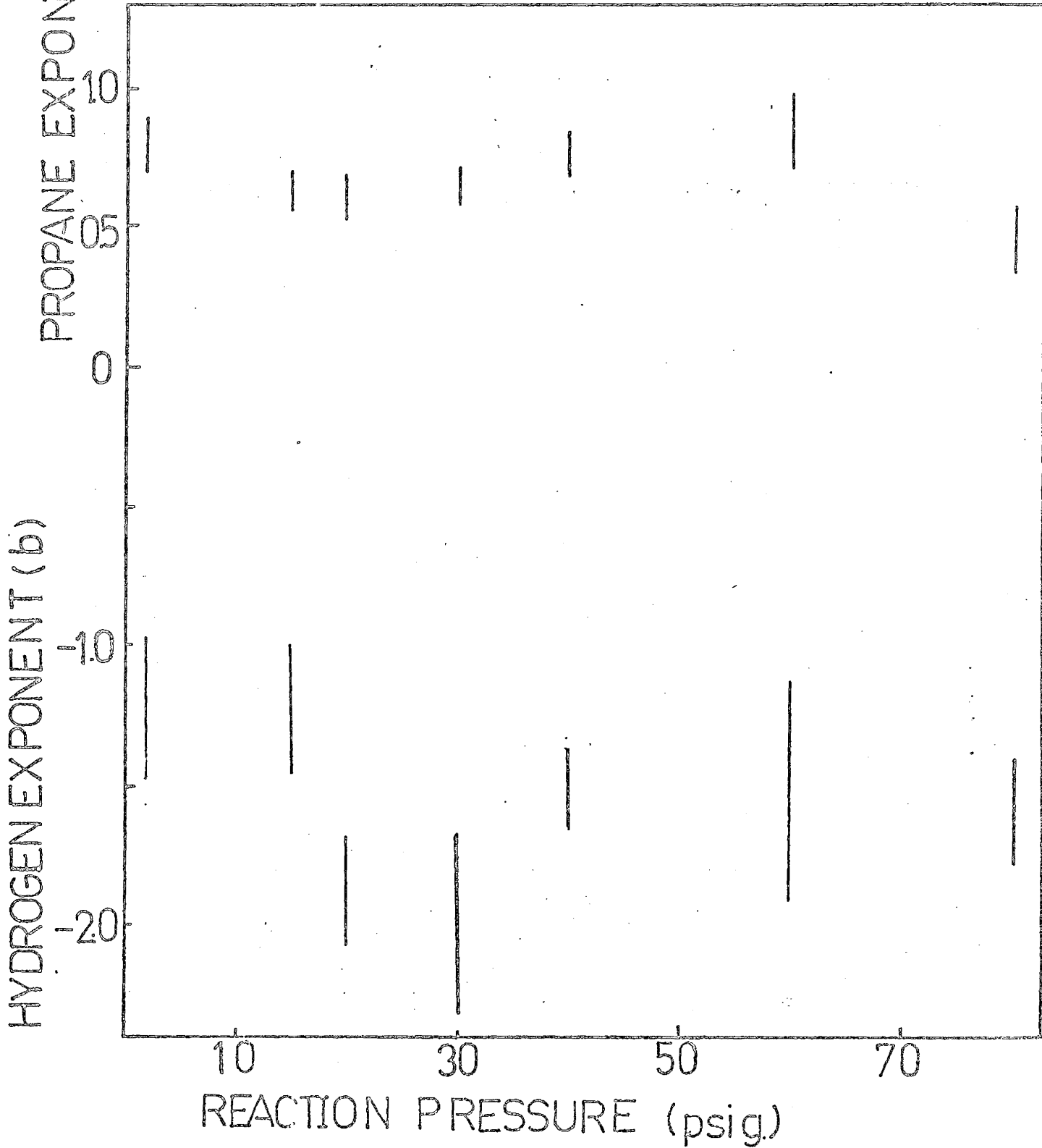


Fig.(3.15)

The Ranges of a and b



CHAPTER FOUR  
PRODUCT DISTRIBUTION

4.1 Introduction

The hydrogenolysis of propane over ruthenium yields methane and ethane. Since the adsorbed species  $C_2^*$  formed can crack further into methane, the quantity of methane and ethane in the product should not be identical. The product distribution is usually reported in terms of selectivity which is defined as the tendency of a catalyst to produce a particular product or quantitatively as the ratio of moles of a particular product formed to the moles of feed hydrocarbon consumed. If  $S_1$  and  $S_2$  represent selectivities of methane and ethane, then in terms of the effluent compositions, they are

$$S_1 = \frac{3Y_1}{Y_1 + 2Y_2} \quad (4.1)$$

$$S_2 = \frac{3Y_2}{Y_1 + 2Y_2} \quad (4.2)$$

where  $Y_i$  is the mole fraction of hydrocarbon with  $i$ -number of carbon atoms.

The selectivity changes with experimental conditions and relates to the reaction mechanism. It is a function of the extent of reaction. The

selectivity at zero conversion represents the cracking of only the feed hydrocarbon, i.e. products of the primary reaction.

A reaction network proposed by Kempling was used throughout this study. The network is shown in fig.(4.1) and the analysis of the network is given in detail in the appendix. Each of the hydrocarbons was assumed to adsorb and desorb reversibly to produce reactive species on the metal surface. The adsorbed species was then reacted irreversibly leading to the rupture of carbon-carbon bonds to produce smaller adsorbed fragments. All the reactions were assumed to be first order with respect to the gaseous hydrocarbon involved and the concentration of adsorbed hydrocarbon species. The effect of the hydrogen partial pressure was assumed to be nearly constant and incorporated in the rate constants. According to the analysis of the network, selectivity for methane and ethane can be predicted by the equations

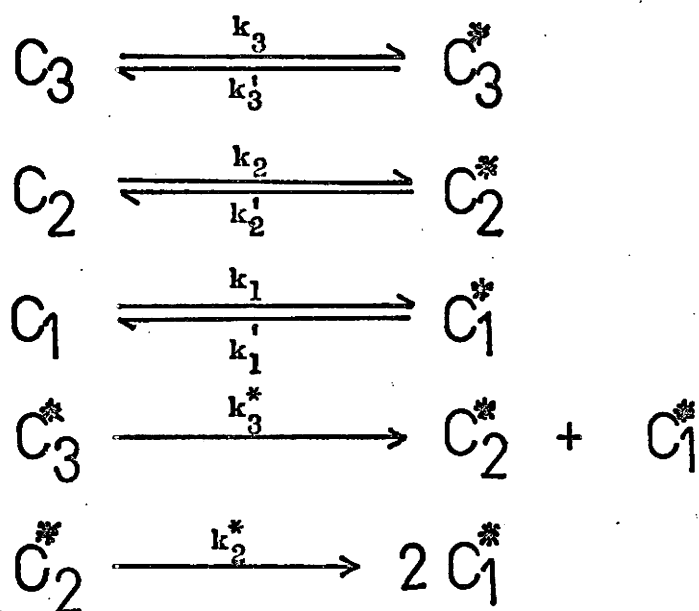
$$S_2 = \frac{k_2' / (k_2' + k_2^*)}{1 + k_2'' / k_3'' (X / (1 - X))} \quad (4.3)$$

and 
$$S_1 + 2S_2 = 3 \quad (4.4)$$

where  $x$  is the fractional conversion of propane and  $k$ 's are defined in fig. (4.1).

The parameter  $k_2' / (k_2' + k_2^*)$  corresponds to the relative rates of desorption and cracking of adsorbed  $C_2$  species. If the rate of carbon-carbon bonds splitting is the rate determining step, the parameter  $k_2' / (k_2' + k_2^*)$  should approach unity. The term  $k_2'' / k_3''$  is the ratio of the overall rate constants of ethane hydrogenolysis to propane. It is the ratio of overall rates of hydrogenolysis of ethane to propane since all the reactions were assumed to be first order in hydrocarbon.

By taking the reciprocal of equation (4.3), the following equation



$C_3, C_2, C_1$  - gaseous propane, ethane and methane

$C_3^*, C_2^*, C_1^*$  - adsorbed hydrocarbon species

$k_i$  - adsorption rate constant

$k_i'$  - desorption rate constant

$k_i^*$  - cracking rate constant

$$k_i'' = k_i k_i^* / (k_i^* + k_i')$$

Fig. (4.1)

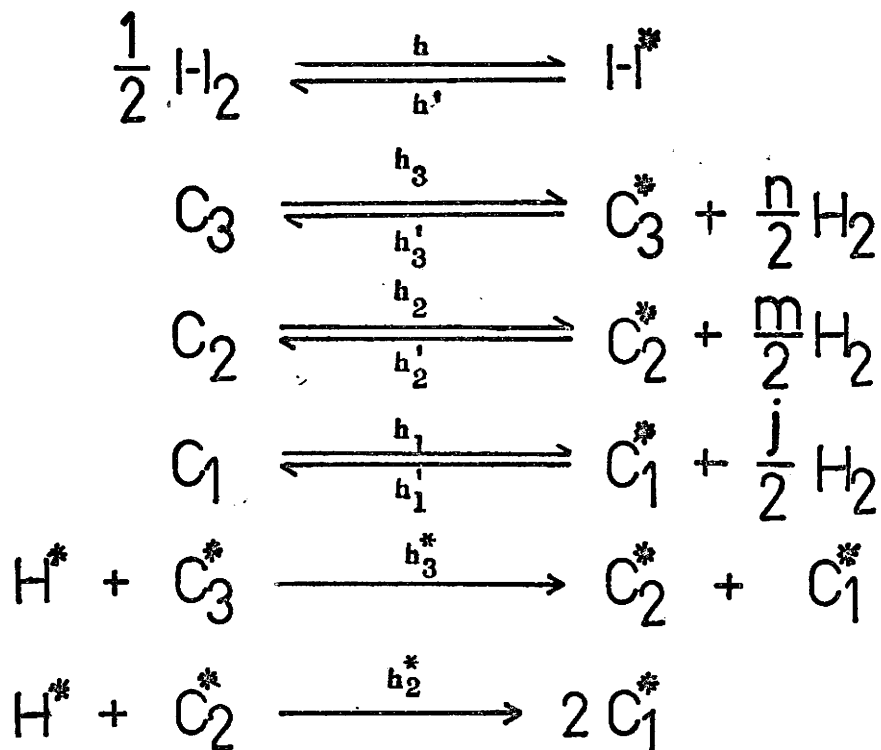
## Propane Hydrogenolysis Mechanism

is obtained

$$\frac{1}{S_2} = \frac{1}{k_2'/(k_2' + k_2^*)} + \frac{k_2''/k_3''}{k_2'/(k_2' + k_2^*)} \frac{X}{1 - X} \quad (4.5)$$

The values of the parameters were obtained from the slope and intercept of the plot of the reciprocal of ethane selectivity as a function of  $X/(1 + X)$ . The ratio of ethane cracking rate to its desorption ( $k_2^*/k_2'$ ) is the ( intercept - 1 ). The experimental data were plotted according to equation (4.5).

Equation (4.3) has a shortcoming in that it includes the hydrogen partial pressure in the rate constants. This simplification is often reasonable because the variation of hydrogen pressures at a given total pressure is small. The parameters in equation (4.3) are only good for the specific pressure being studied. This assumption is good when the reaction pressure ranges are small. In the present studies, the pressures ranged from 2 psig. to 90 psig., therefore it is better to include hydrogen pressures in the selectivity equations. The network in fig. (4.1) was modified so that the reactions would be functions of both hydrogen and hydrocarbon partial pressures. The network is shown in fig. (4.1a). The desorption of propane was found in Chapter Three to be 2.5 order in hydrogen. The surface cracking involves an adsorbed hydrocarbon species and an adsorbed hydrogen species. The surface coverage of adsorbed hydrogen is assumed to be proportional to  $P_{H_2}^{-1/2}$ . The hydrogen order for desorption of ethane was estimated from the selectivity data. The detail of the derivation for the selectivity equation is shown in the Appendix. A general equation for the ethane selectivity at different pressures is



$\text{C}_3, \text{C}_2, \text{C}_1$  - gaseous propane, ethane and methane

$\text{C}_3^*, \text{C}_2^*, \text{C}_1^*$  - adsorbed hydrocarbon species

$h_i$  - adsorption rate constant

$h_i'$  - desorption rate constant

$h_i^*$  - cracking rate constant

$\text{H}_2$  and  $\text{H}^*$  - gaseous and adsorbed hydrogen

Fig.(4.1a)

## Propane Hydrogenolysis Mechanism

$$S_2 = \frac{1}{1 + \frac{h_2^*}{h_2} P_{H_2}^{\frac{1}{2} - \frac{m}{2}} + \frac{h_2 h_2^*}{h_3 h_3^*} \left\{ \frac{h_3}{h_2} P_{H_2}^{\frac{5}{2} - \frac{m}{2}} + \frac{h_3^*}{h_2} P_{H_2}^{\frac{1}{2} - \frac{m}{2}} \right\} \frac{X}{1-X}} \quad (4.6)$$

Equation (4.6) permits the evaluation of more rate constants than equation (4.3). For estimating parameters of equation (4.6), values of  $m$ , the hydrogen power for the desorption of ethane, were assumed and residual sum of squares of the reciprocal of  $S_2$  was calculated by linear least squares. The most appropriate value of  $m$  yields the smallest residual sum of squares.

Equation (4.3) evaluates the ratio of the rates of hydrogenolysis of ethane to propane and the ratio of the rates of cracking of ethane to its desorption. Equation (4.6) yields the ratio of the rate constant of cracking to the desorption for ethane and propane and also the ratio of adsorption rates of ethane to propane.

#### 4.2 Experimental Results

Three individual sets of experiments were made. Initially, selectivity experiments at constant temperatures and pressures were performed, followed by experiments at constant pressures but at different temperatures in order to study the temperature dependence of the selectivity. Lastly, experiments at different pressures but at constant temperatures were performed to obtain an insight into the pressure dependence of the selectivity. The range of the experimental conditions were :

Temperature	-	115 - 155°C
Pressure	-	2 - 90 psig.
Propane Conversion	-	10 - 90%
Feed flow rate	-	0.9 - 10 ml./sec.
Feed ratio ( $H_2/C_3H_8$ )	-	2.5 - 7

Fig.(4.2), (4.3) and (4.4) show the product distribution at the temperatures and pressures shown on the figures. The experimental data are also given in Table (C1), (C2) and (C3). Low conversions could not be obtained under these conditions because the catalyst was very active. The methane selectivity for the three cases increases with conversion. while that of ethane decreases with conversion. Each experiment yielded one conversion with one set of selectivities. The selectivity for methane is higher at lower pressure and decreases as the pressure increases for the same conversion.

Plots of  $1/S_2$  as a function of  $X/(1 - X)$  were made for the three cases and are shown in fig.(4.5), (4.6) and (4.7). The straight lines are drawn to fit most of the points. The values for the intercept and slope are shown in Table ( 4.1 ), as well as the parameters  $k_2''/k_3''$  and  $k_2^*/k_2'$ . The solid curves in fig. (4.2), (4.3) and (4.4) were obtained from the parameters in Table (4.1) by using equation (4.3) and (4.4). The experimental selectivities and the calculated curves agreed very well. Values of  $k_2''/k_3''$  are far smaller than unity, i.e. the rate of hydrogenolysis of ethane is much slower than propane. The parameter,  $k_2^*/k_2'$  which is very much less than unity indicating that the desorption rate of ethane is much faster than its cracking rate.

Fig.(4.2)

Product Distribution at 120°C and 2 psig.

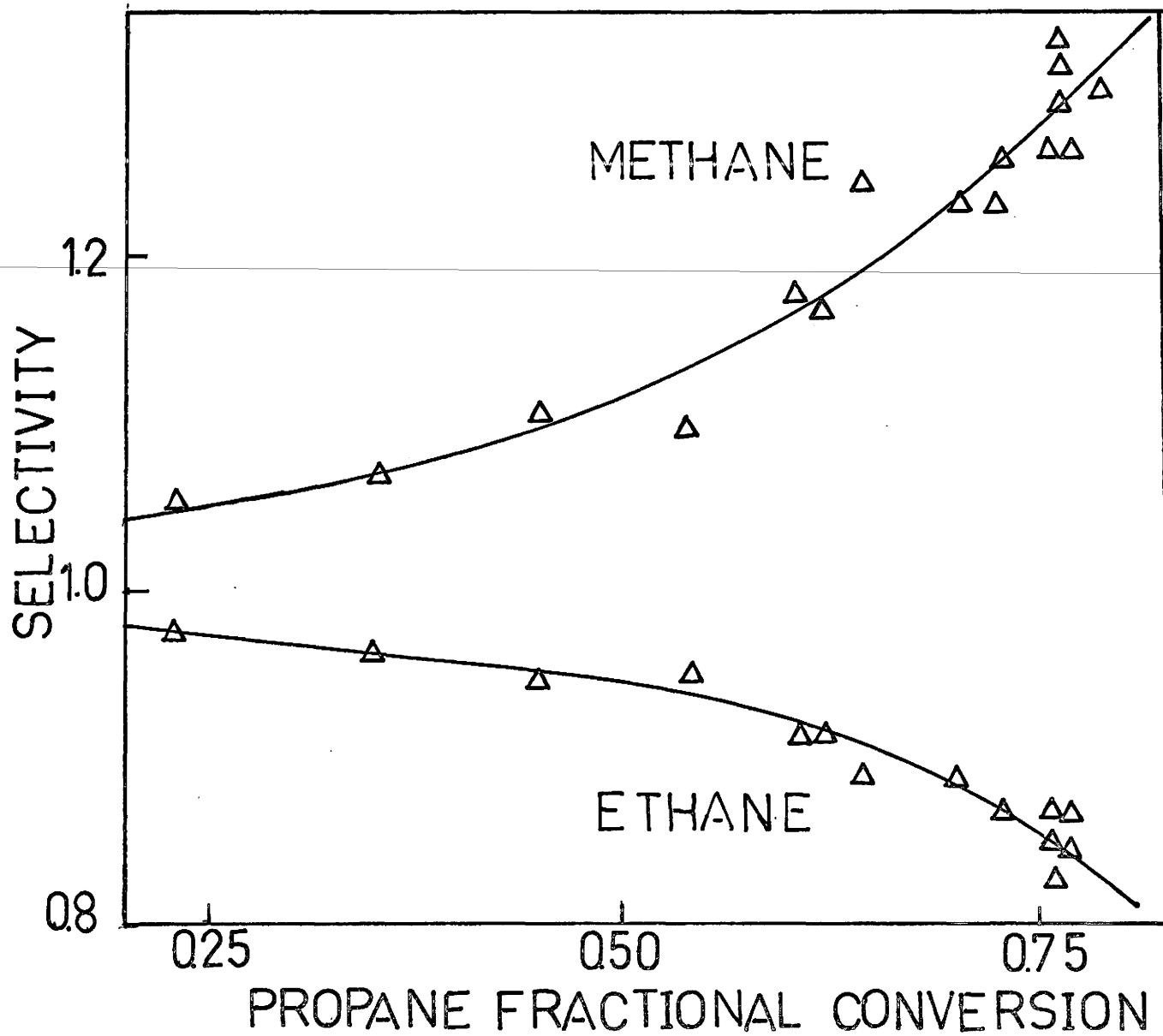


Fig.(4.3)

Product Distribution at 130°C and 30 psig.

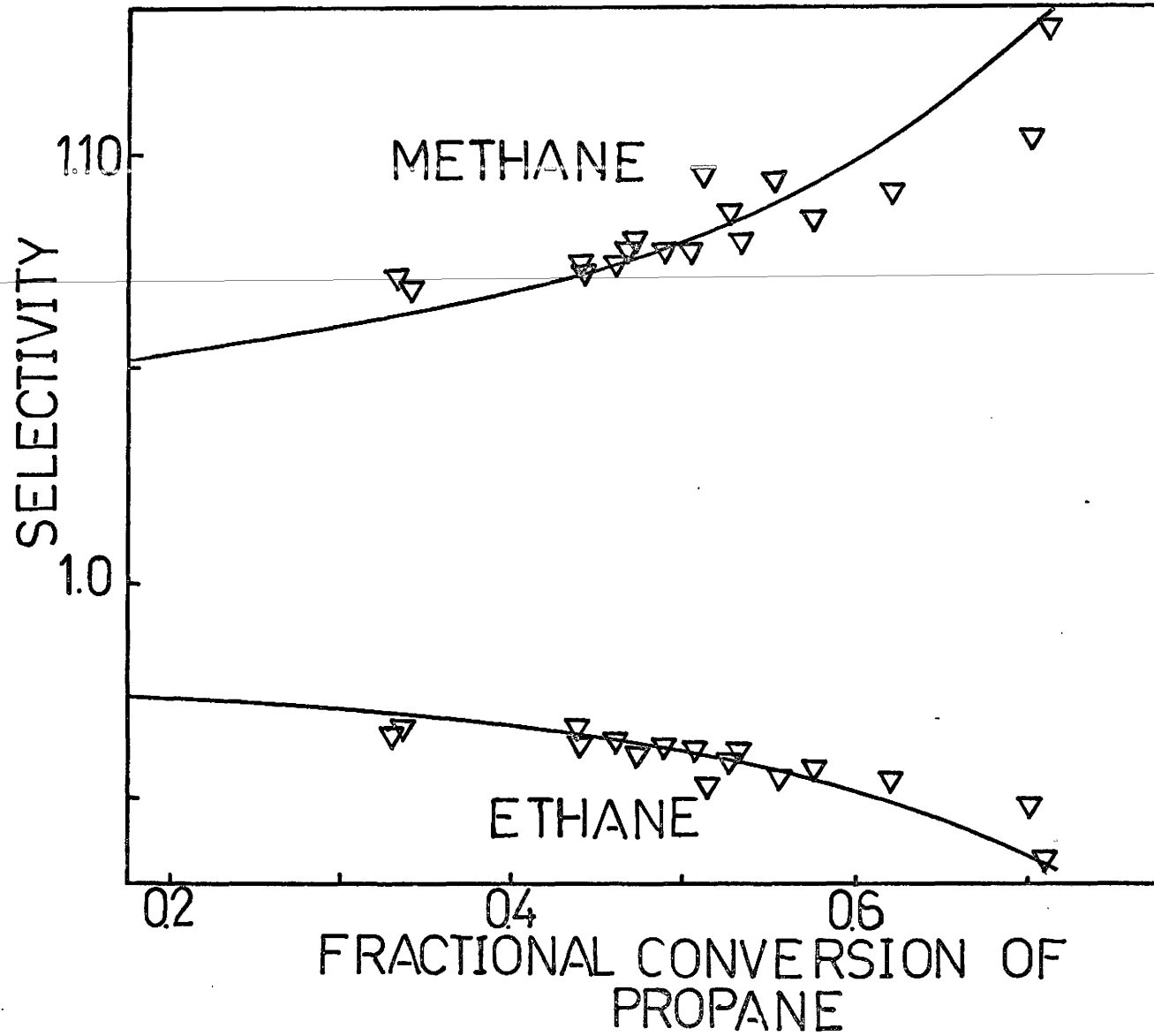


Fig.(4.4)

Product Distribution at 150°C and 80 psig.

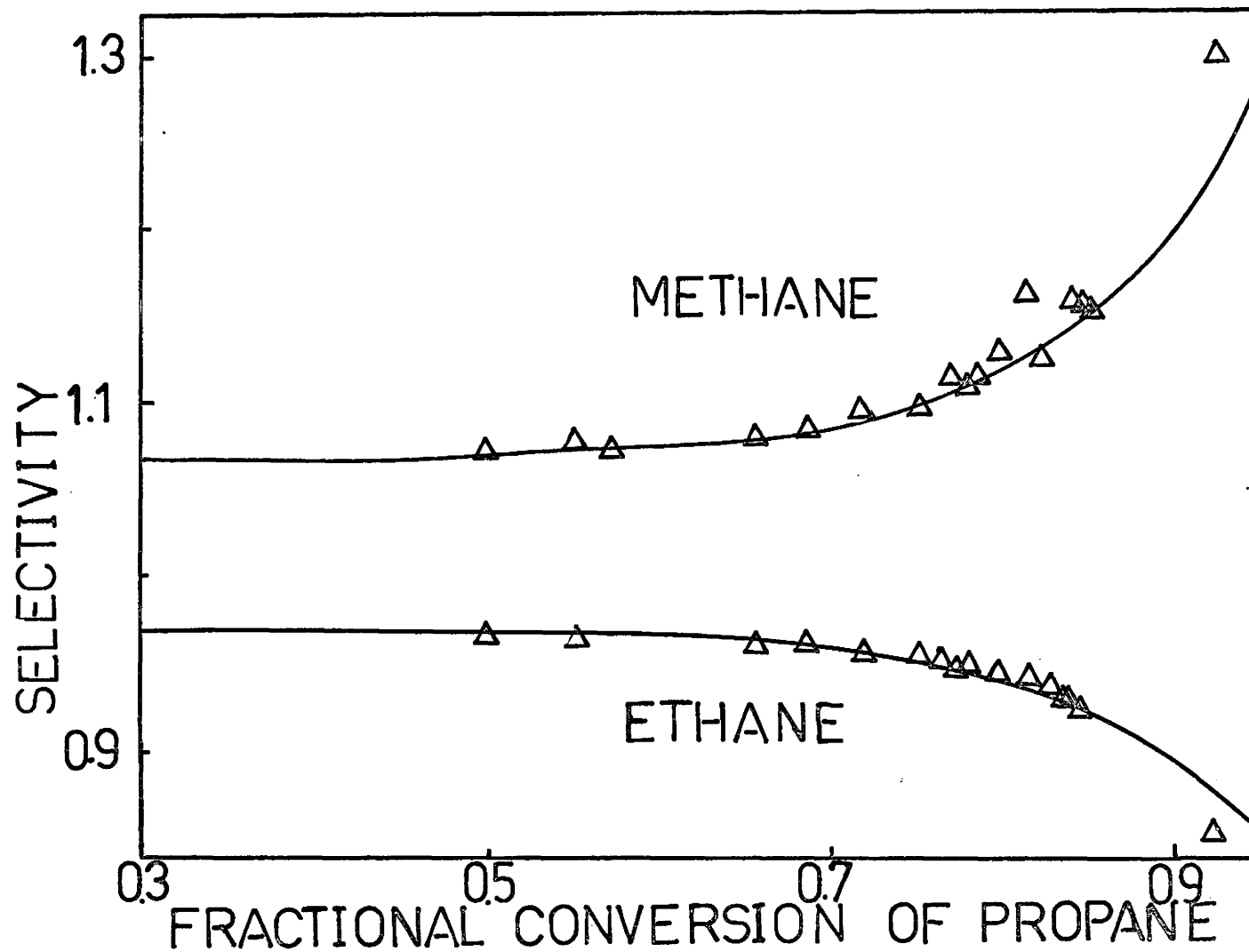


Fig.(4.5)

Product Distribution Analysis at 120°C and 2 psig.

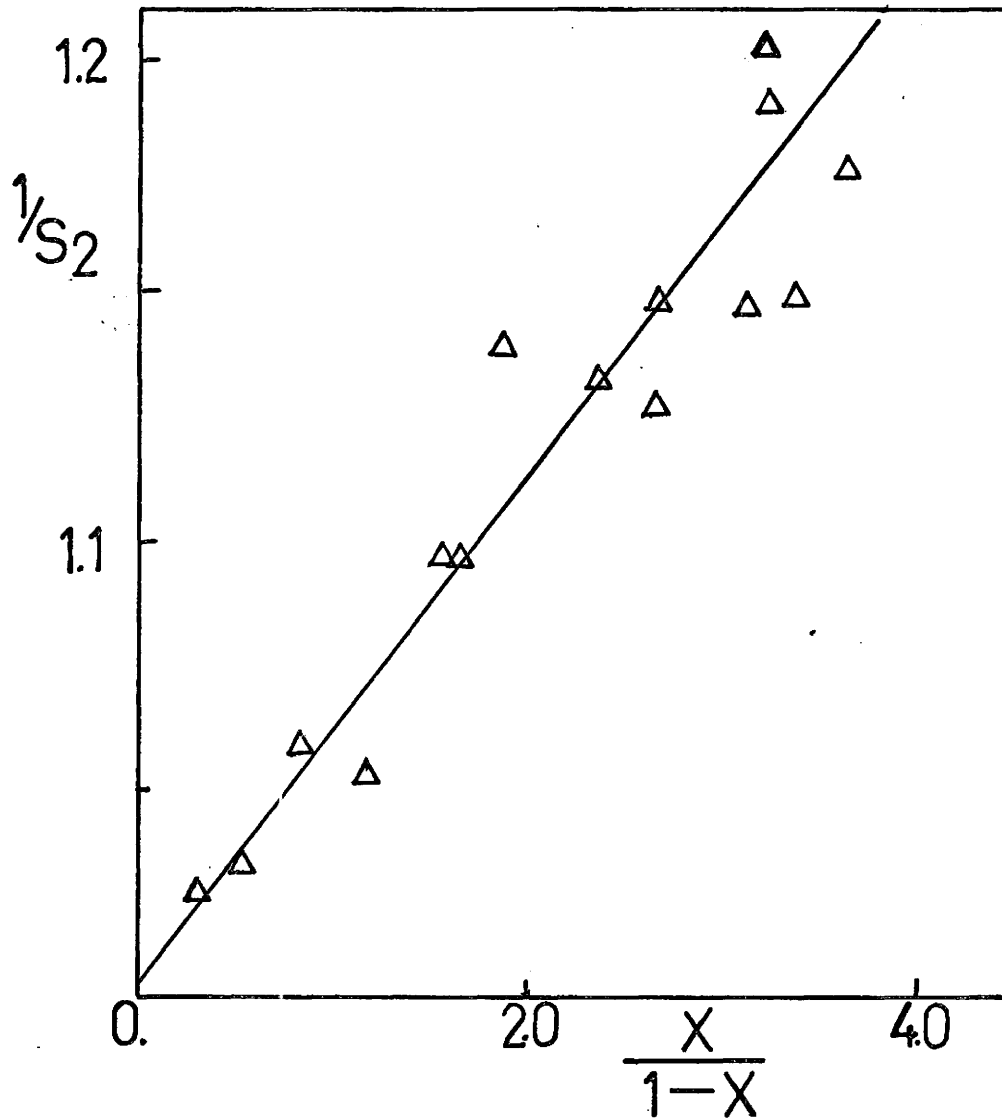


Fig.(4.6)

Product Distribution Analysis at 130°C and 30 psig.

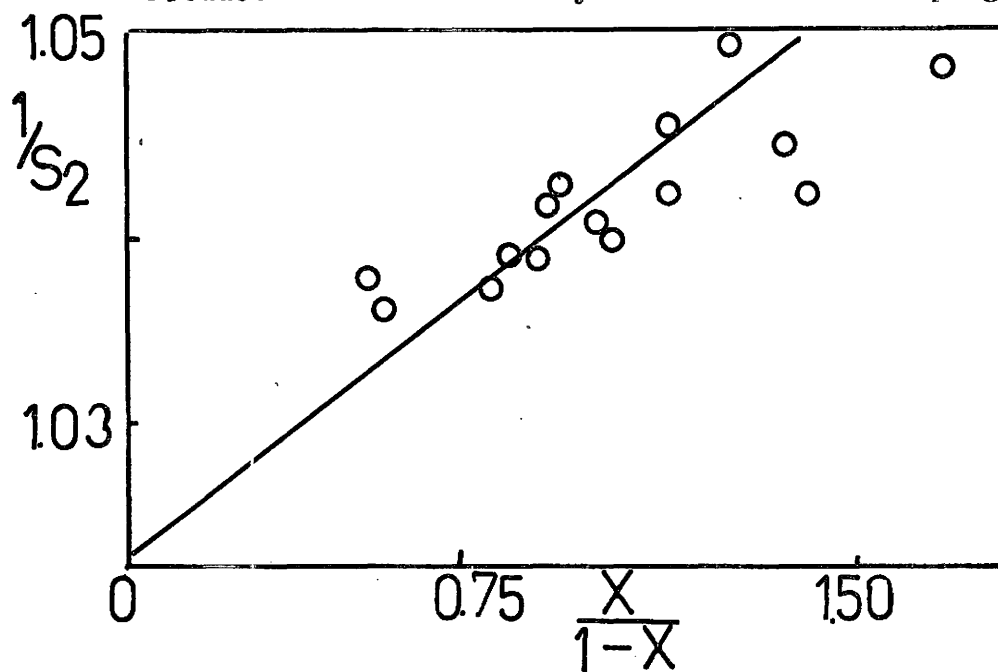


Fig.(4.7)

Product Distribution Analysis at 150°C and 80 psig

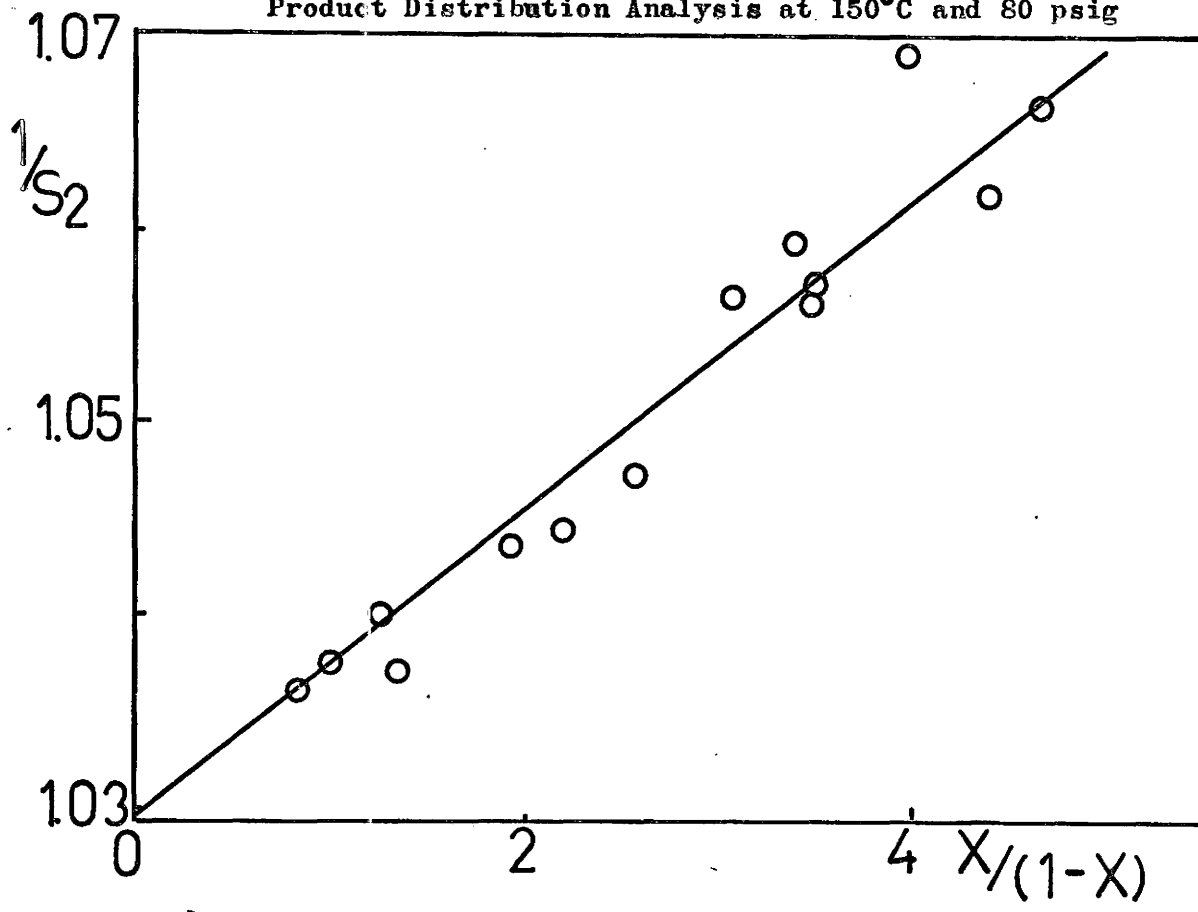


TABLE ( 4.1 )

Product Distribution Analysis ( Eqn. 4.3 )

$P_T$ (psig)	Temp. ( $^{\circ}$ C)	Slope	Intercept	$k_2^*/k_2'$	$k_2''/k_3''$
2	120	0.0525	1.0095	0.0095	0.052
30	130	0.0191	1.0225	0.0225	0.0187
80	150	0.0079	1.0295	0.0295	0.0077

The product distribution was then studied at different temperatures at constant pressures. Fig.(4.8), (4.9) and (4.10) or Table (C4), (C5) and (C6) are the product distribution data. Higher temperature favours the formation of methane. Plots of  $1/S_2$  as a function of  $X/(1 - X)$  were made and are shown in fig.(4.12), (4.13), (4.14) and (4.15). The straight lines were drawn to fit most of the points. The intercepts and slopes, together with the parameters  $k_2''/k_3''$  and  $k_2^*/k_2'$  are given in Table (4.2). The solid curves in fig.(4.8), to (4.10) were calculated from these parameters. It is noted that  $1/S_2$  vs  $X/(1 - X)$  plots are not always too good, yet the selectivity curves fit quite well. Both the values of  $k_2''/k_3''$  and  $k_2^*/k_2'$  are far less than unity. For a given pressure, values of  $k_2''/k_3''$  and  $k_2^*/k_2'$  increase with increasing temperature.

The catalyst was too active to allow low conversion determinations, but the selectivity was extrapolated by equation (4.5) to zero conversion. Fig.(4.11) is the zero conversion selectivity as a function of temperature. These selectivities correspond to the primary cracking of feed propane alone. Low pressure favours methane formation. The curvature of the plots decreases with increasing pressure, and at 60 psig., the curve is essentially linear.

The dependence of the two parameters on temperature by Arrhenius expressions as :

$$\frac{k_2^*}{k_2'} = A_{22} \exp(-E_{22}/RT) \quad (4.7)$$

and

$$\frac{k_2''}{k_3''} = A_{23} \exp(-E_{23}''/RT) \quad (4.8)$$

here,  $A_{22}$  and  $A_{23}$  are the pre-exponential factors and  $E_{22}$  and  $E_{23}''$  are

the apparent activation energies for the corresponding rate ratio. Fig. (4.16) and (4.17) are the Arrhenius plots for the parameters  $k_2''/k_3''$  and  $k_2^*/k_2'$  respectively. The slope of the plots, the pre-exponential factors and the activation energies are given in Table (4.3) and (4.4). The activation energies for  $k_2''/k_3''$  can be regarded as the difference between the activation energies of hydrogenolysis of ethane and propane. The values for these activation energies seem to be constant with an average value of 11.2 kcal/mole. Thus, hydrogenolysis of ethane has an activation energy of 11.2 kcal/mole greater than propane. The activation energy for  $k_2^*/k_2'$  is the difference between the activation energy of cracking and desorption of ethane. The values seem to be decreasing with increasing pressure. The accuracy of these values are low. The values of  $k_2^*/k_2'$  were obtained from ( intercept - 1 ) of the plots of  $1/S_2$  vs  $X/(1 - X)$ . The intercept is about 50 times larger than  $k_2^*/k_2'$ , therefore a small error in the intercept would result in a great error in the value of  $k_2^*/k_2'$ . Never-the-less, the activation energy for cracking of ethane is greater than that of desorption.

The product distribution study was then shifted to constant temperatures with pressures varying. Table (C7), (C8), (C9) and (C10) are the selectivity data at four different temperatures. Fig.(4.18), (4.19) and (4.20) are the product distribution plots. Lower pressure favours the formation of methane.  $1/S_2$  was plotted as a function of  $X/(1 - X)$  as shown in fig.(4.21), (4.22) and (4.23). The parameters at different temperatures and pressures are shown in Table (4.5). The solid curves in fig.(4.18), (4.19) and (4.20) were drawn from these parameters obtained

Fig.(4.8)

Product Distribution at 40 psig.

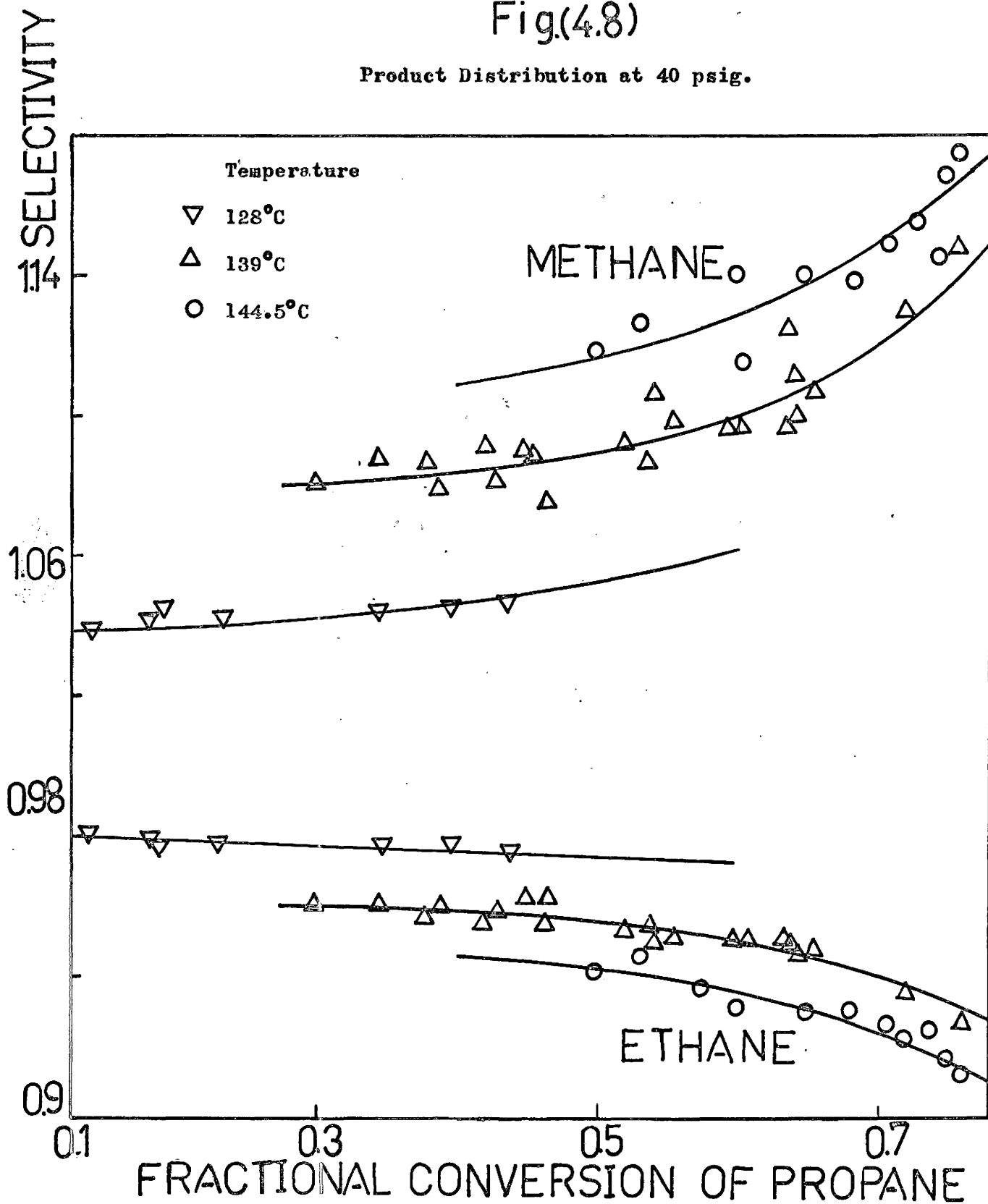


Fig.(4.9)

Product Distribution at 50 psig.

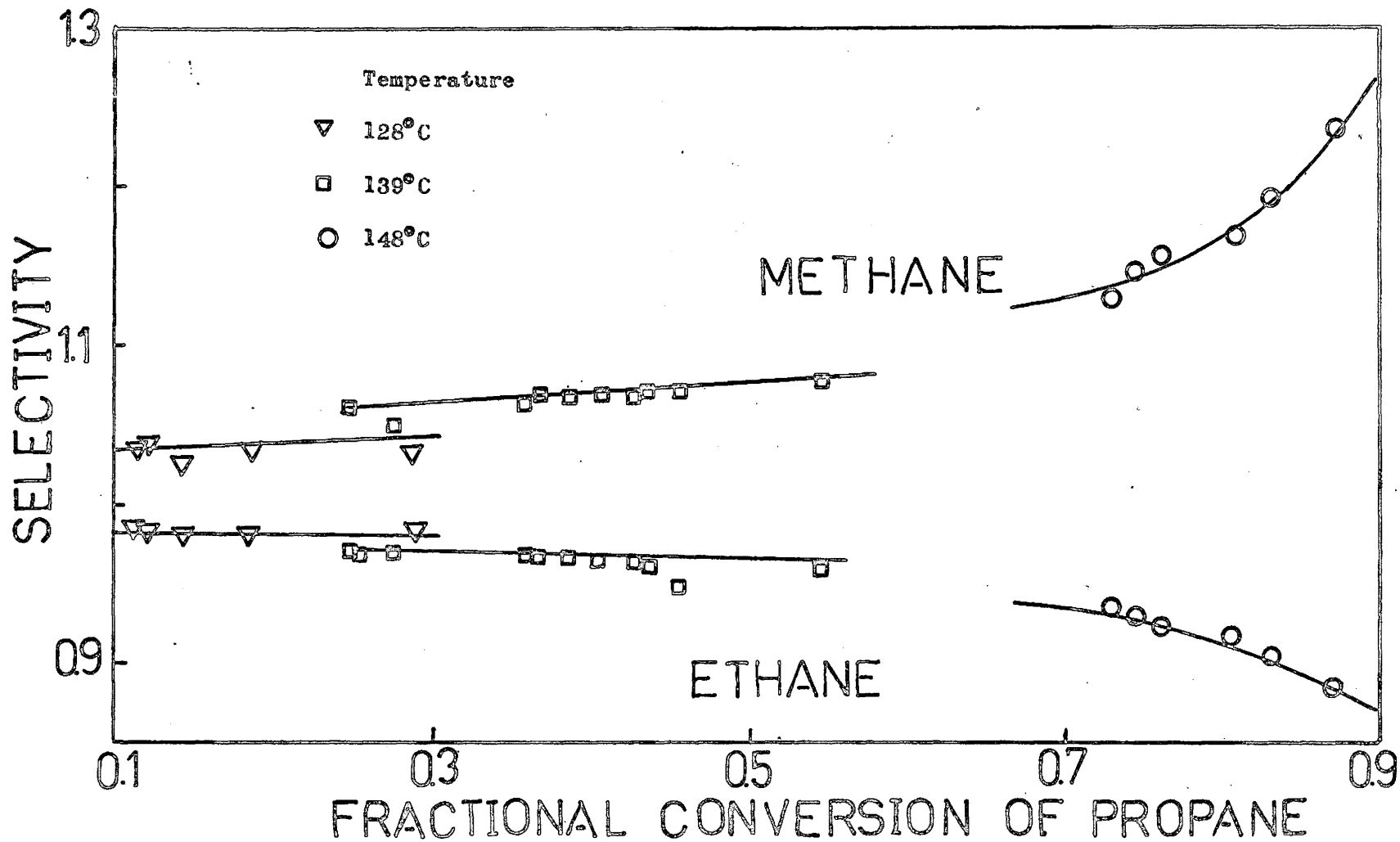


Fig.(4.10)

Product Distribution at 60 psig.

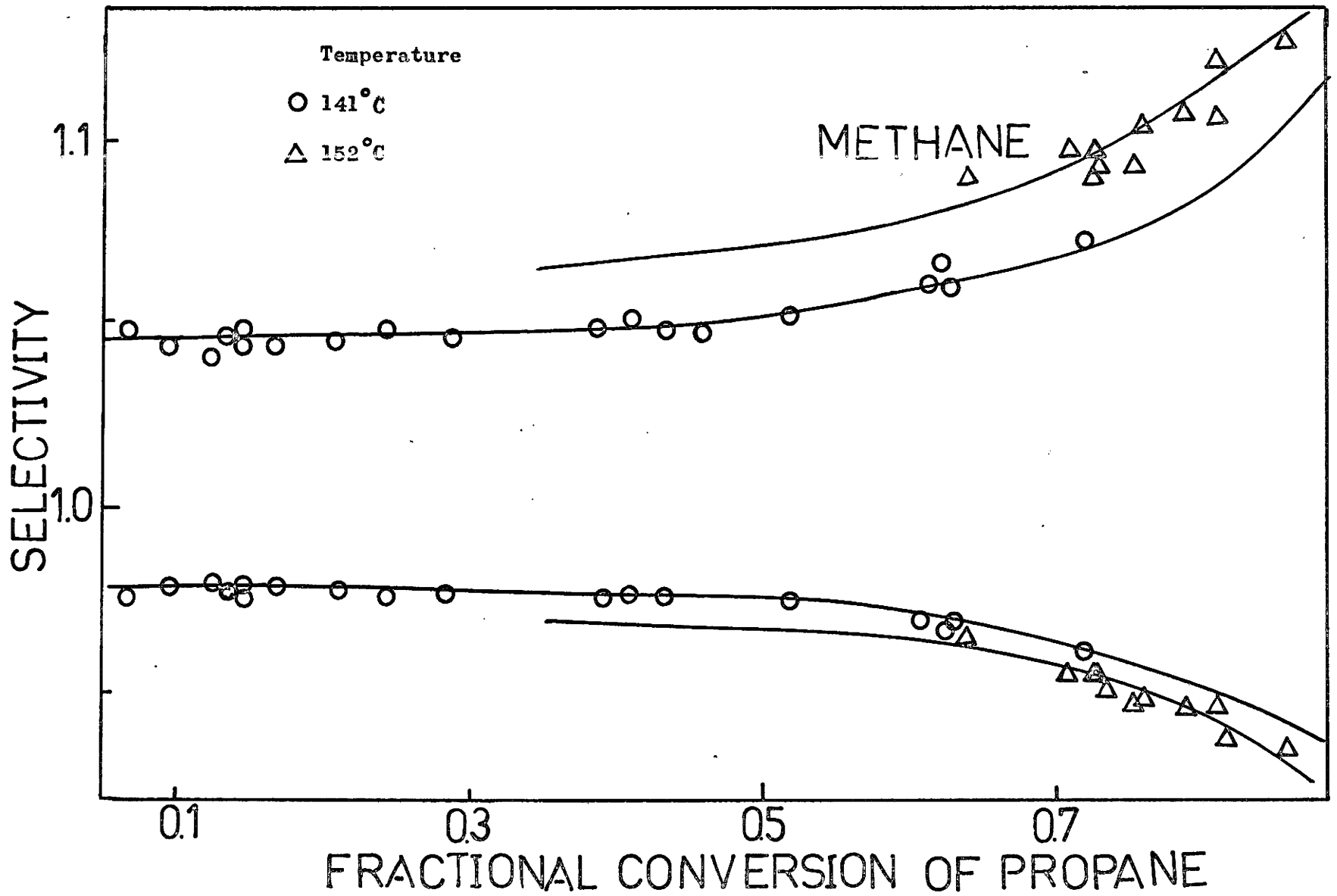


Fig.(4.11)

Product Distribution at Zero Conversion at Several Pressures

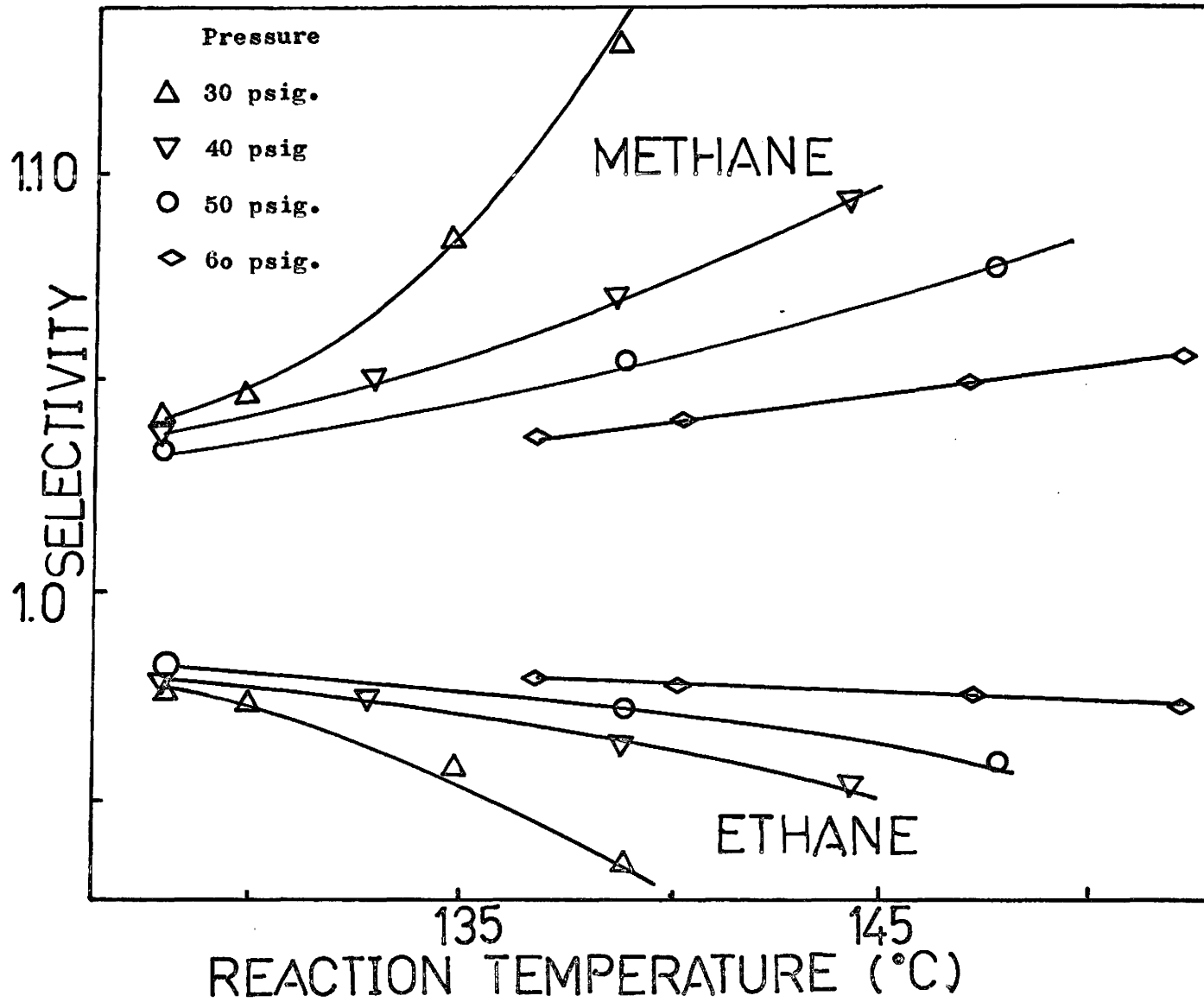


Fig.(4.12)

Product Distribution Analysis at 30 psig.

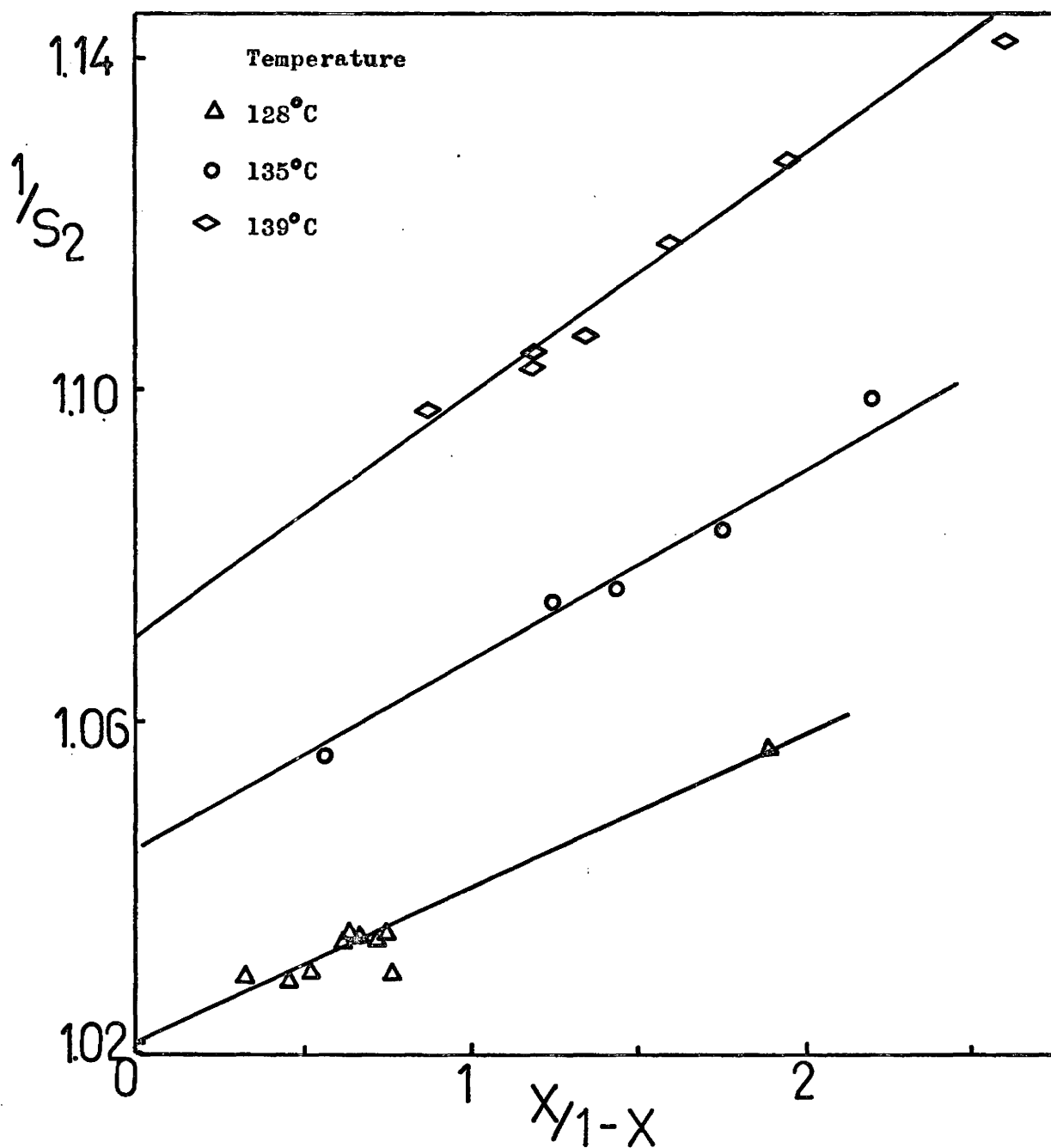


Fig.(4.13)

Product Distribution Analysis at 40 psig.

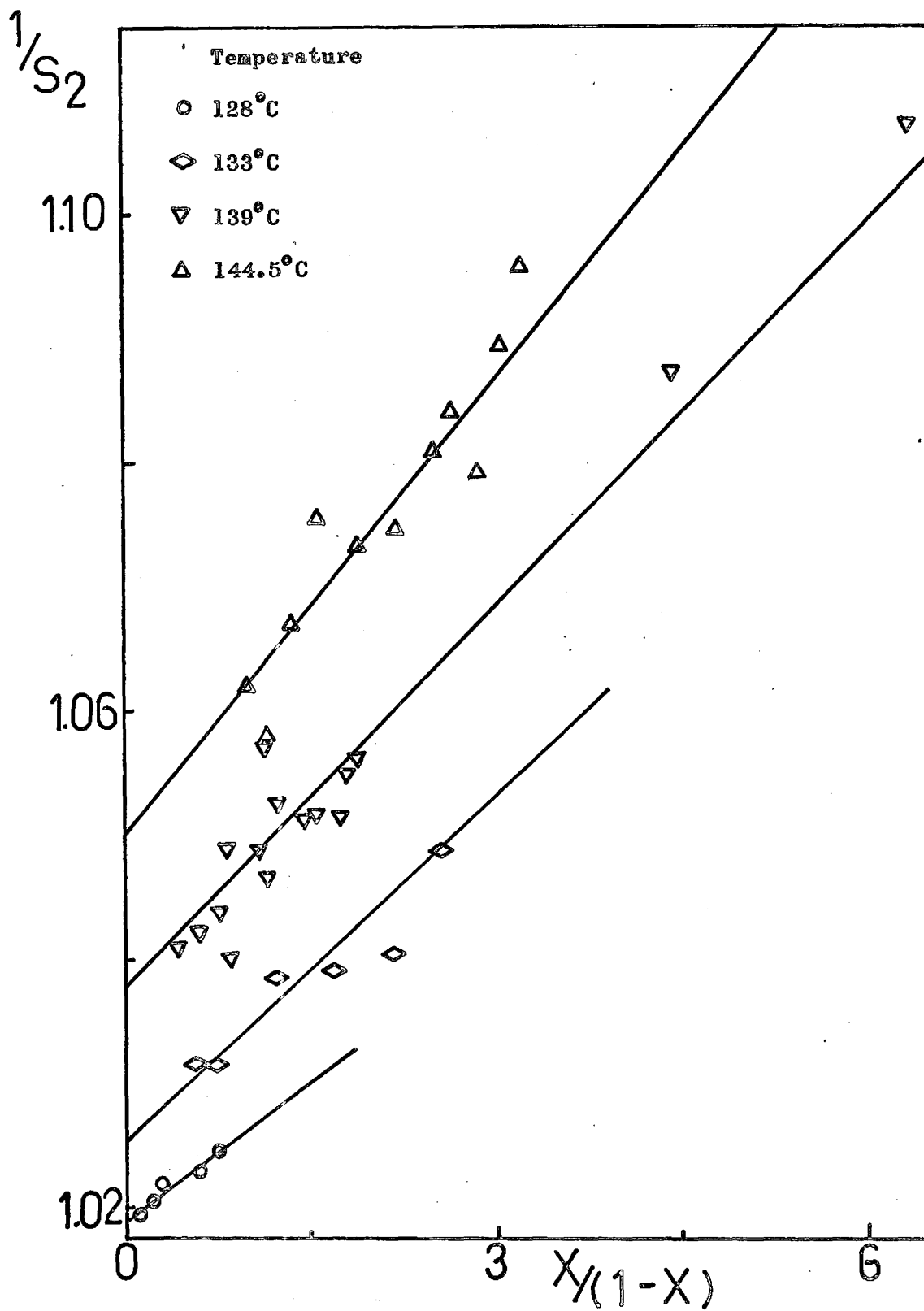


Fig.(4.14)

Product Distribution Analysis at 50 psig.

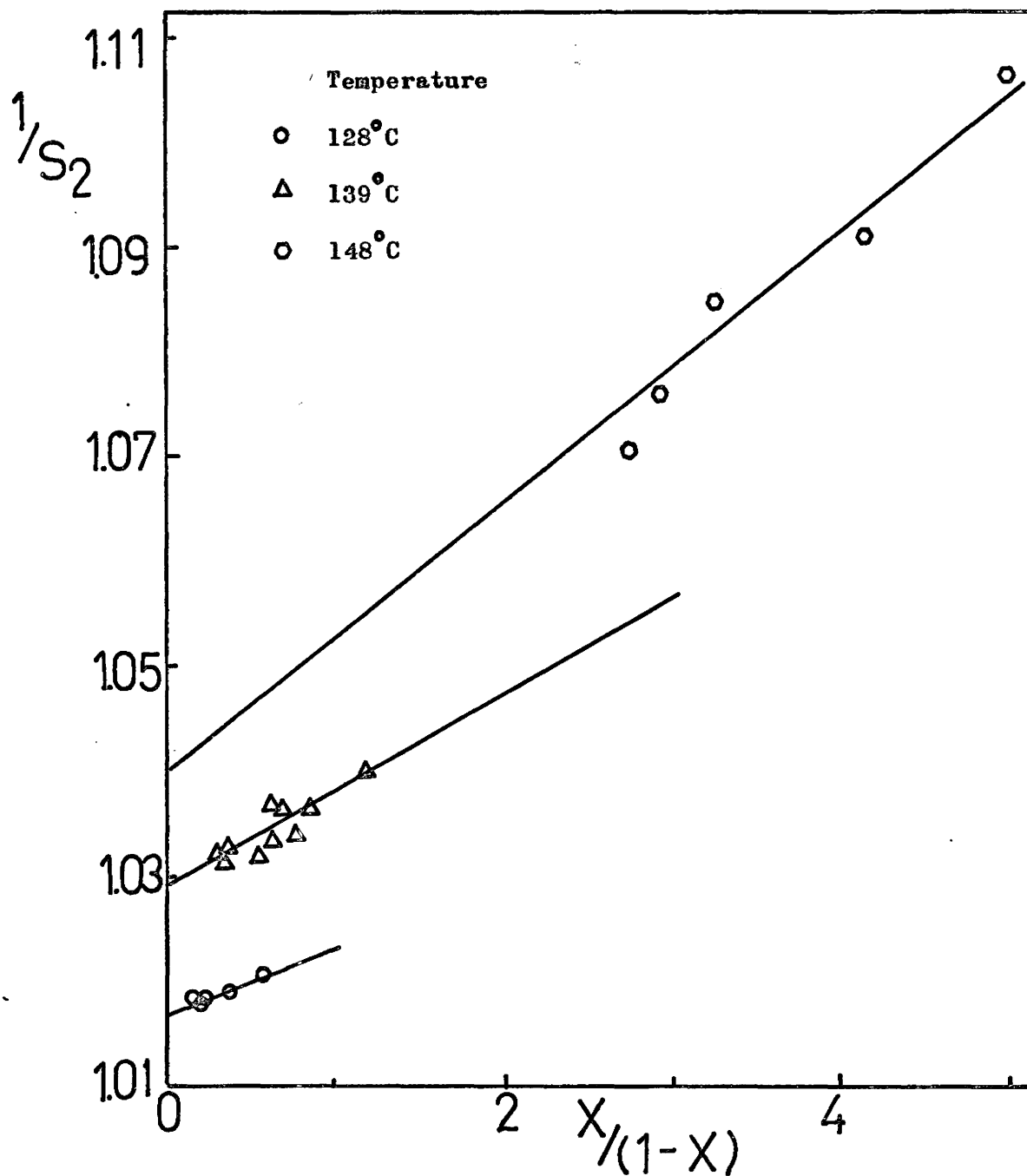


Fig.(4.15)

Product Distribution Analysis at 60 psig.

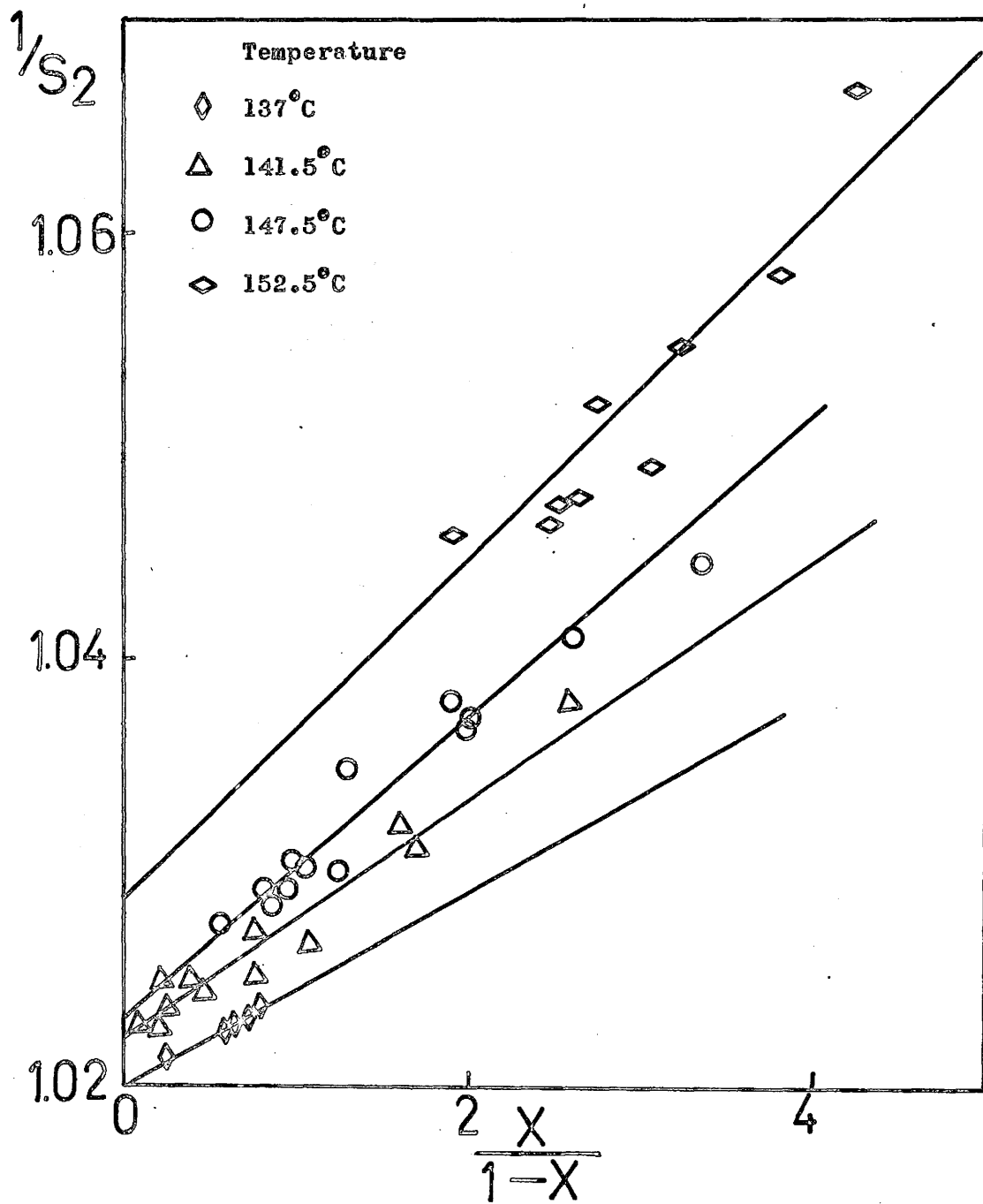


TABLE ( 4.2 )

Product Distribution Analysis ( Eqn. 4.3 )

$P_T$ (psig)	Temp. ( $^{\circ}C$ )	Slope	Intercept	$k_2^*/k_2'$	$k_2''/k_3''$
30	128	0.0186	1.0214	0.0214	0.0182
30	130	0.0191	1.0225	0.0225	0.0187
30	135	0.0243	1.0442	0.0442	0.0233
30	139	0.0285	1.0705	0.0705	0.0266
40	128	0.0078	1.0190	0.0190	0.0076
40	133	0.0093	1.0255	0.0255	0.0091
40	139	0.0108	1.0375	0.0375	0.0104
40	144.5	0.0132	1.0495	0.0495	0.0126
50	128	0.0062	1.0170	0.0170	0.0061
50	139	0.0090	1.0290	0.0290	0.0088
50	148	0.0132	1.0405	0.0405	0.0127
60	137	0.0049	1.0199	0.0199	0.0048
60	141.5	0.0055	1.0220	0.0220	0.0054
60	147.5	0.0066	1.0230	0.0230	0.0065
60	152.5	0.0079	1.0288	0.0288	0.0077

Fig.(4.16)

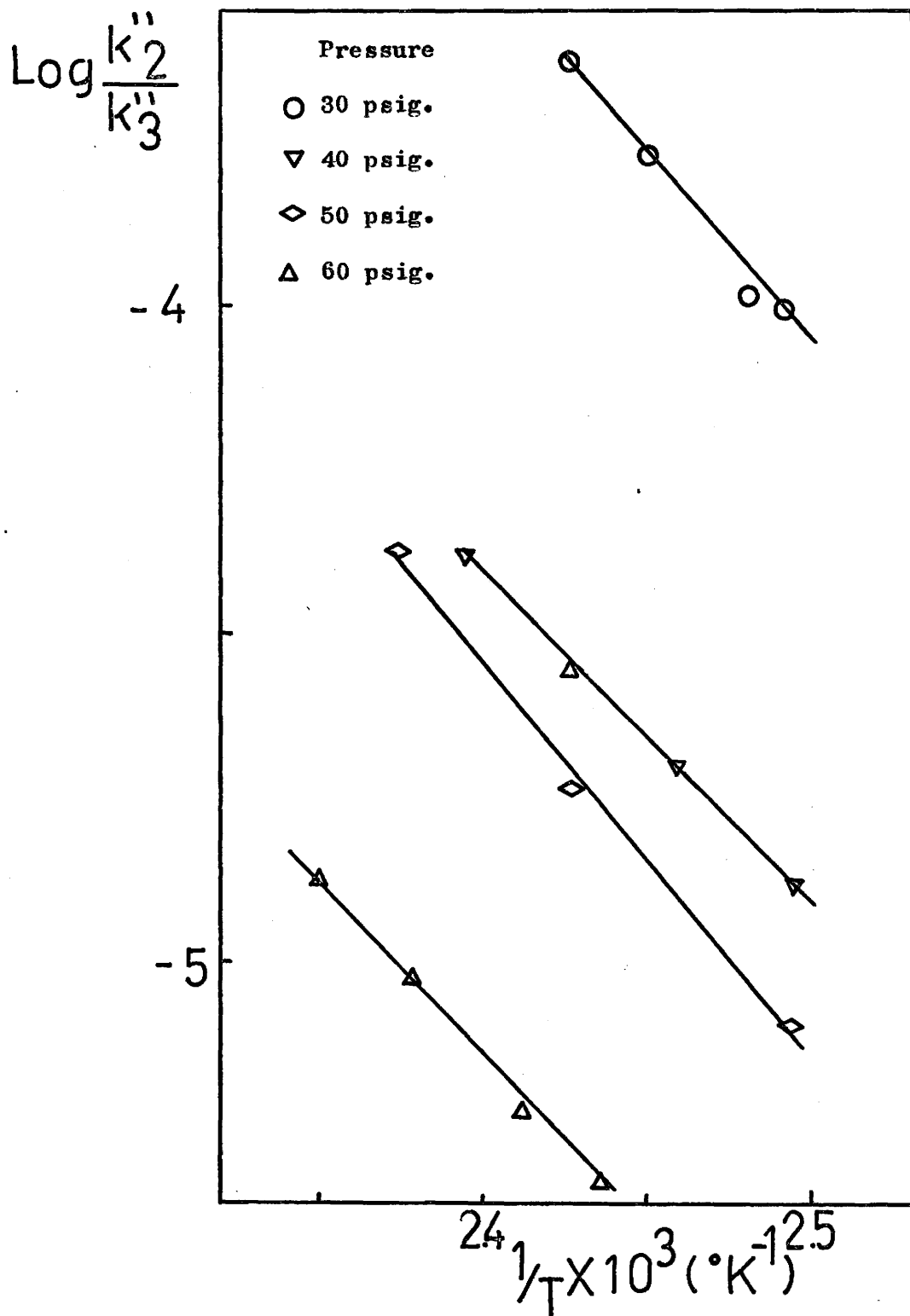
Arrhenius Plot for  $k_2''/k_3''$ 

Fig.(4.17)

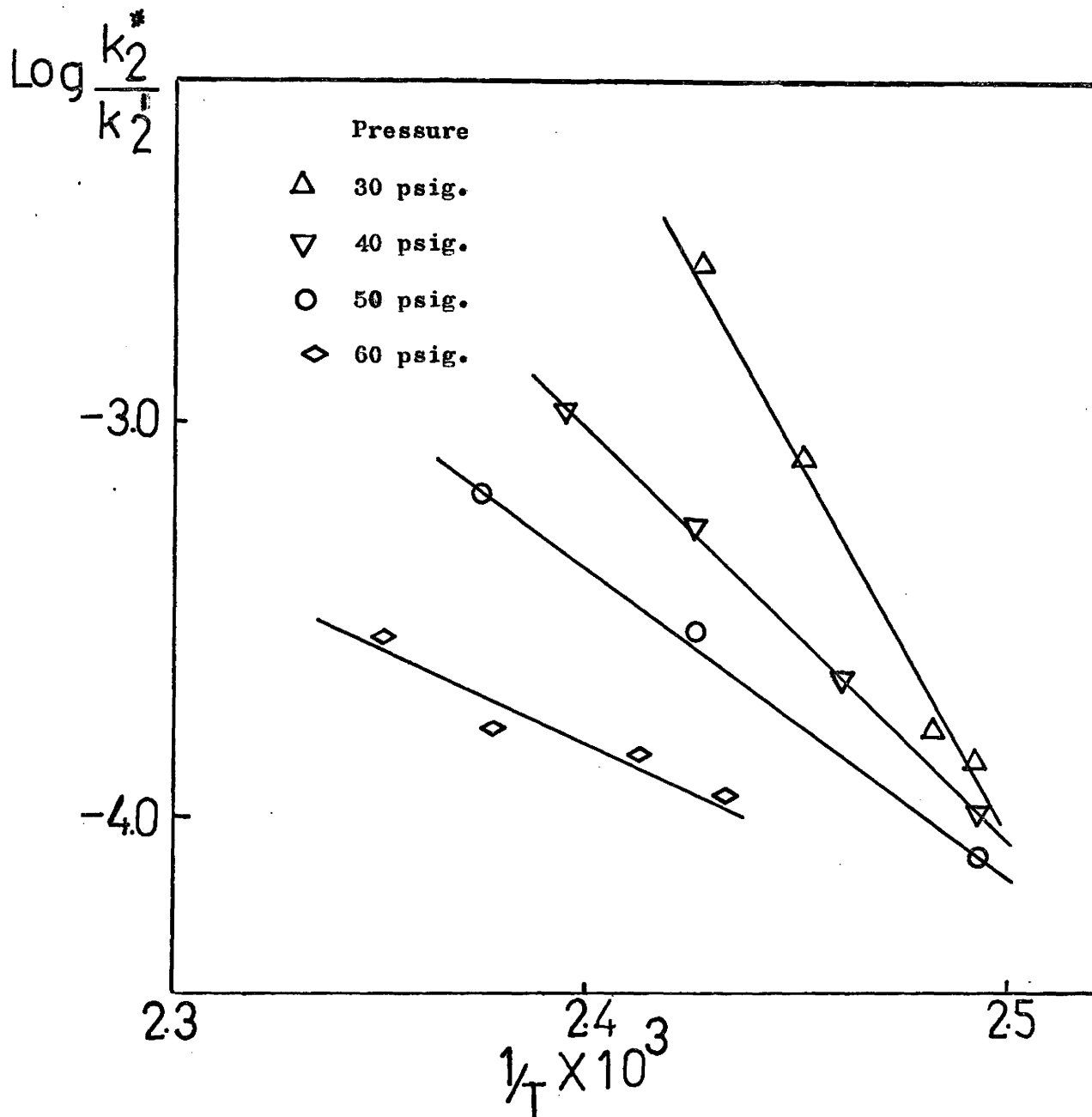
Arrhenius Plot for  $k_2^*/k_2'$ 

TABLE ( 4.3 )

Pre-exponential Factors and Activation Energies for  $k_2''/k_3''$

$P_T$ (psig)	Slope $\times 10^{-3}$	Log $A_{23}''$	$E_2'' - E_3''$ ( kcal/mole ) *
30	5.81	10.47	11.6
40	5.20	8.08	10.4
50	5.92	9.67	11.8
60	5.50	8.06	11.0

TABLE ( 4.4 )

Pre-exponential Factors and Activation Energies for  $k_2^*/k_2^0$

$P_T$ (psig)	Slope $\times 10^{-3}$	Log $A_{22}$	$E_2^* - E_2^0$ ( kcal/mole ) **
30	16.2	14.0	32.2
40	9.9	20.6	19.6
50	7.4	14.4	14.7
60	4.4	5.8	8.8

\*  $E_{23}''$

\*\*  $E_{22}$

Fig (4.18)

Product Distribution at 128 °C

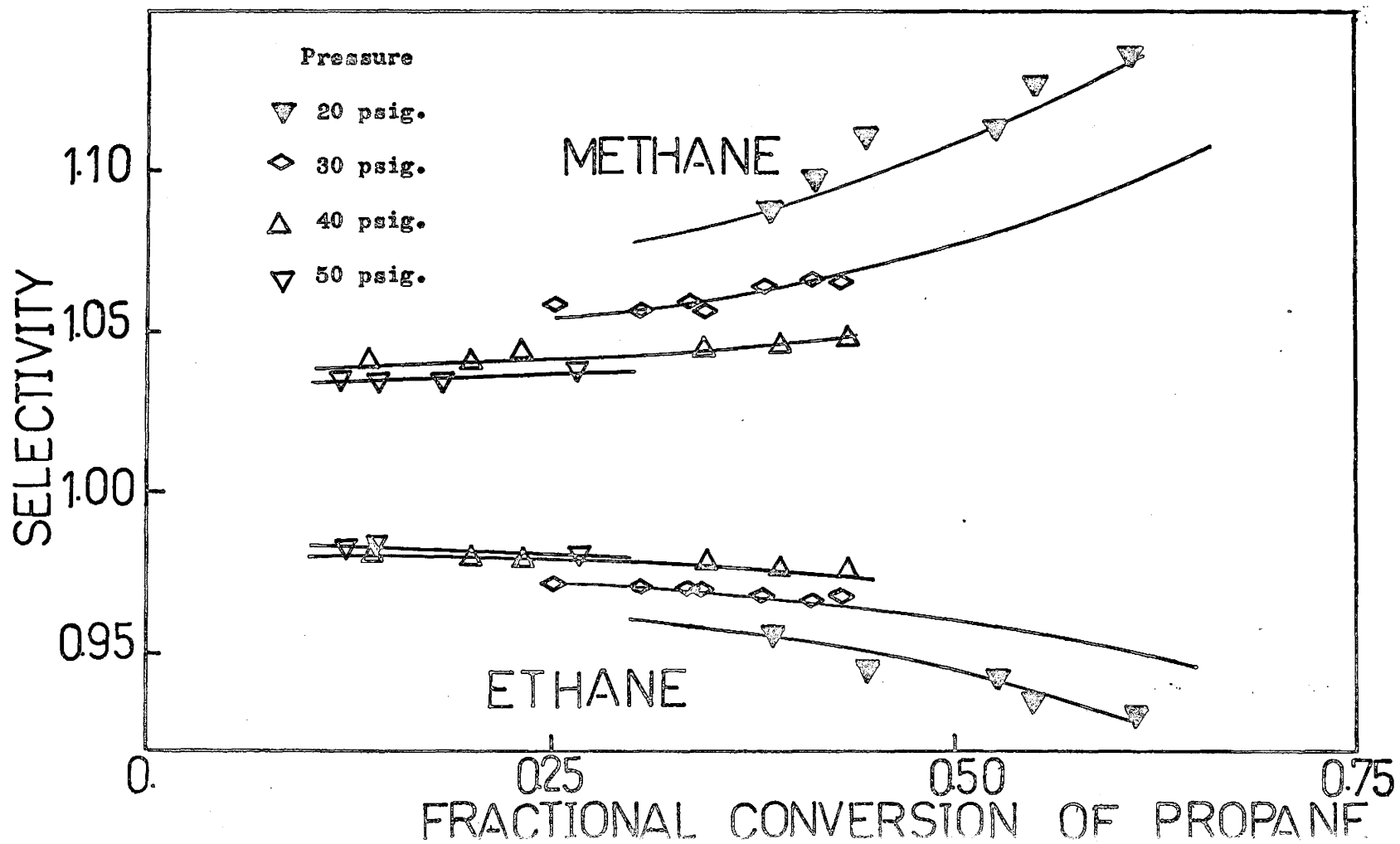


Fig. (4.19)

Product Distribution at 139°C

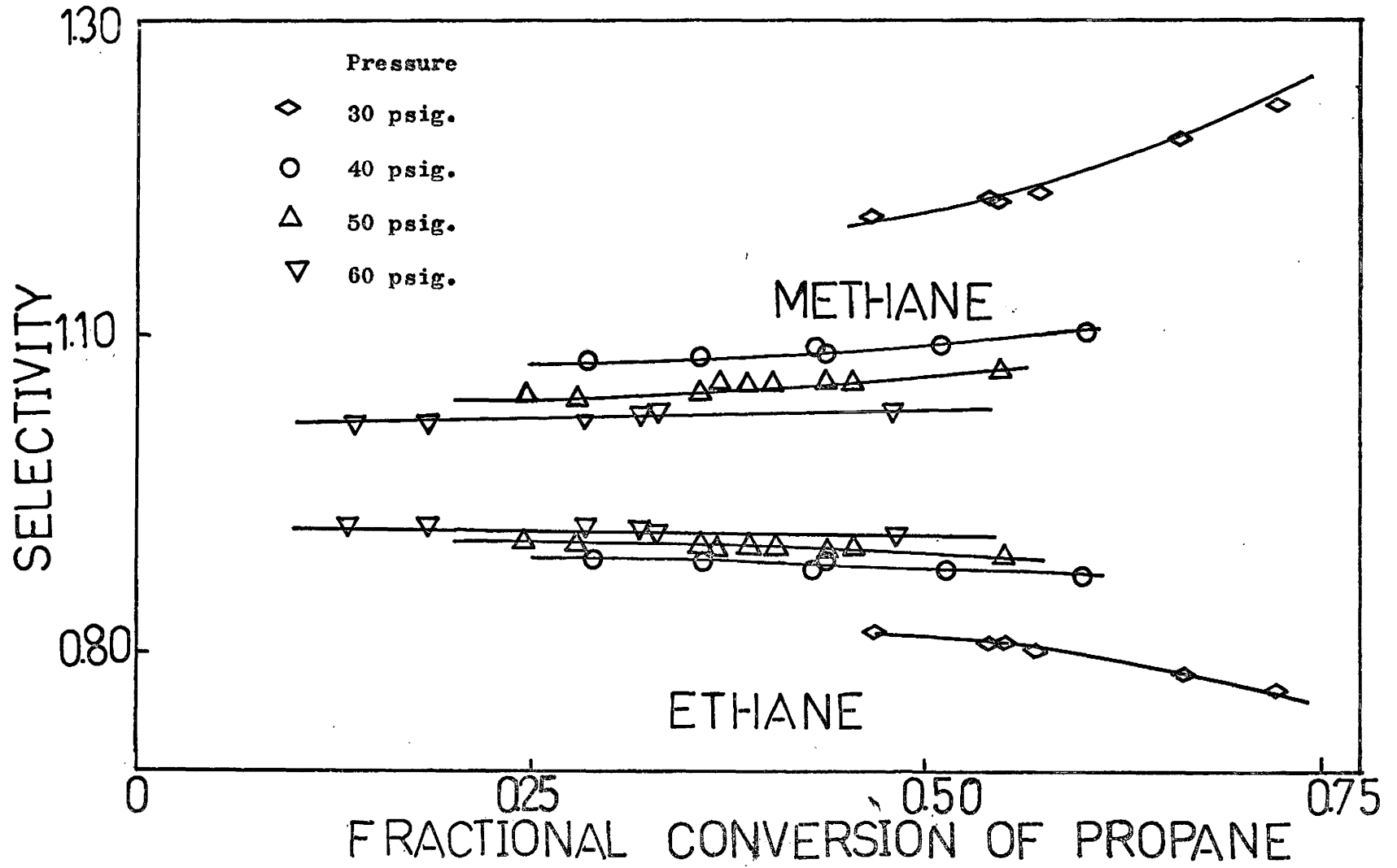


Fig.(420)

Product Distribution at 148° C

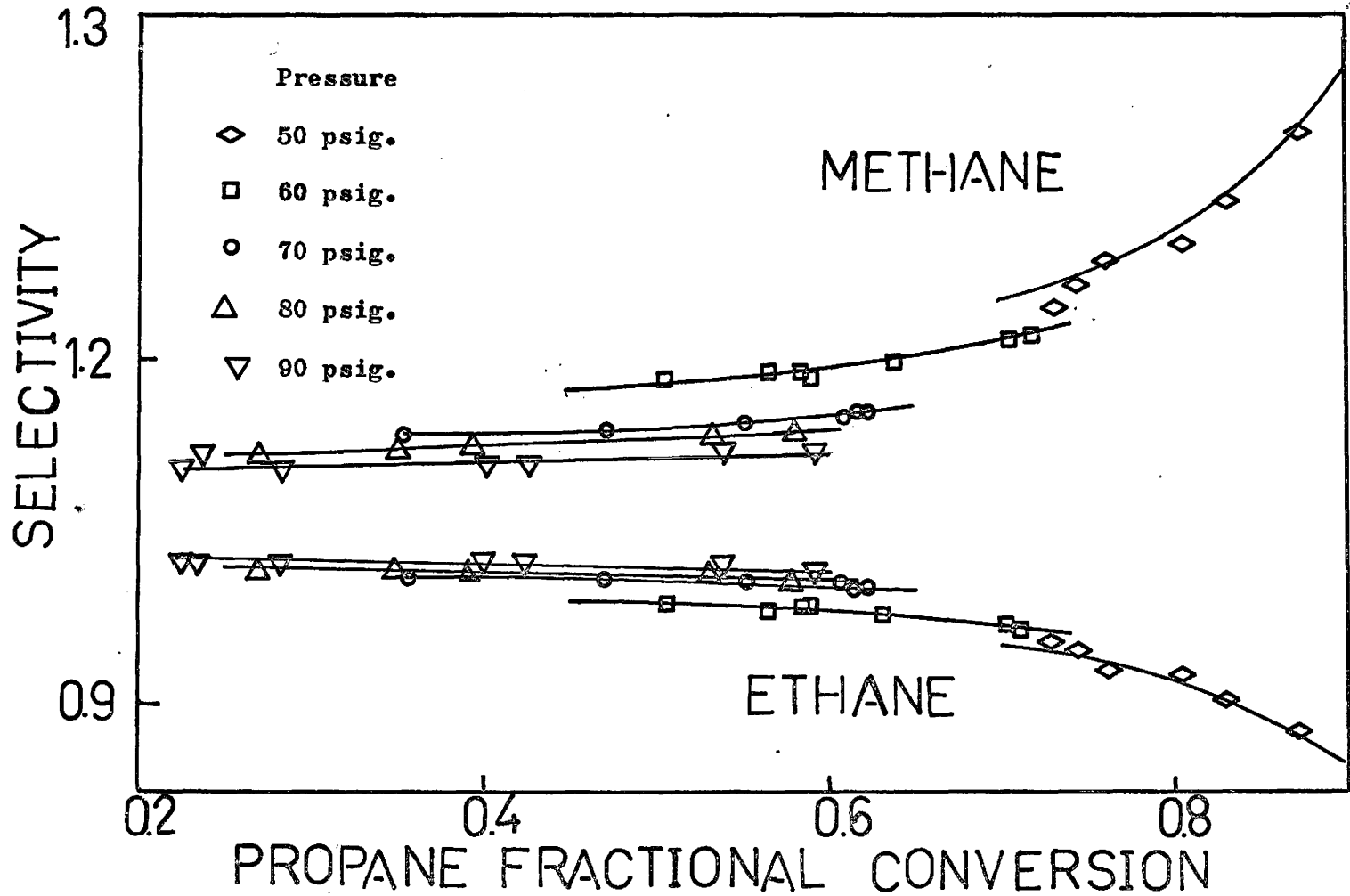


Fig.(4.21)

Product Distribution Analysis at 128°C  
( Equation 4.3 )

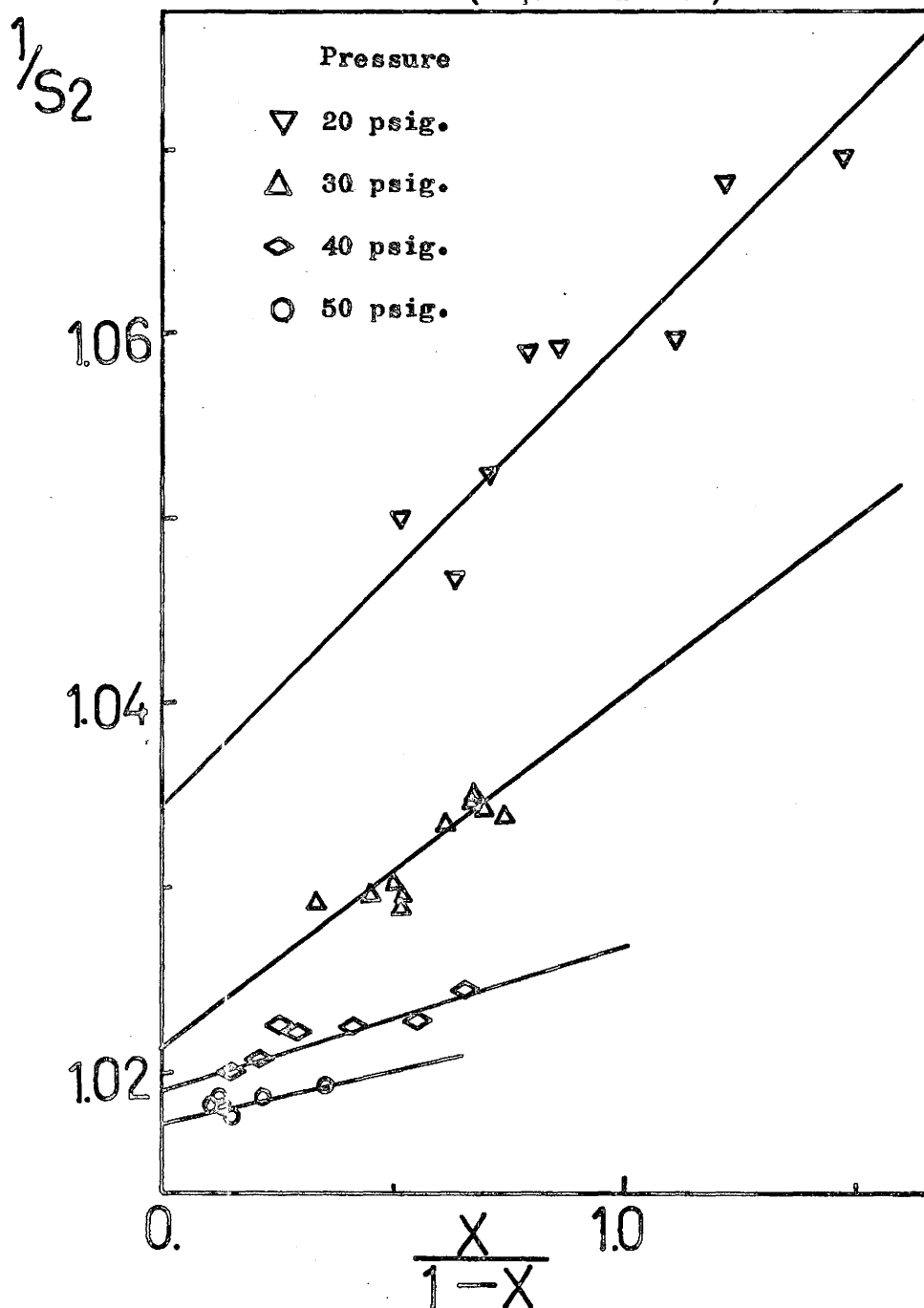


Fig.(4.22)

Product Distribution Analysis at 139°C

( Equation 4.3 )

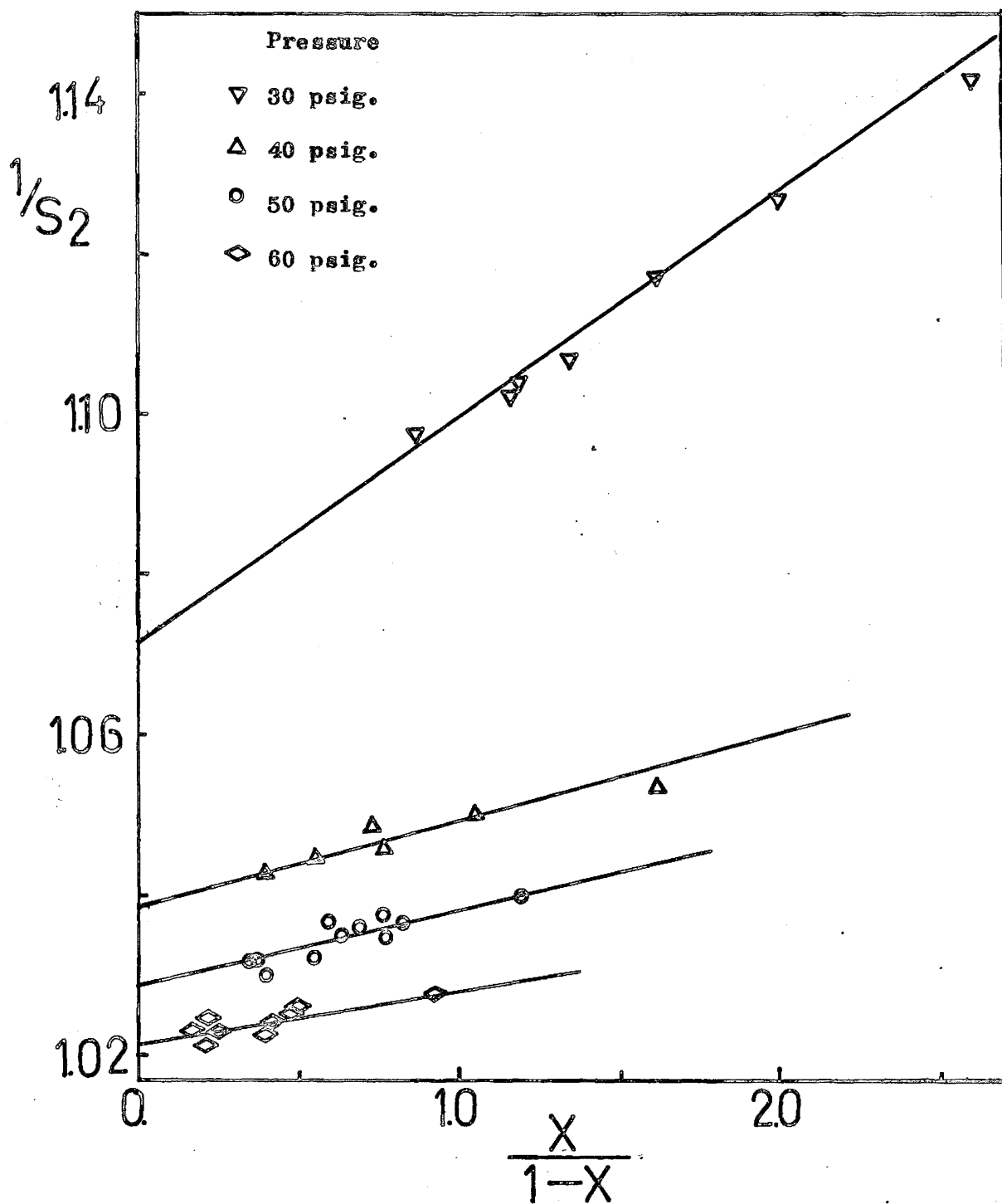


Fig.(4.23)

Product Distribution Analysis at 148 °C

( Equation 4.3 )

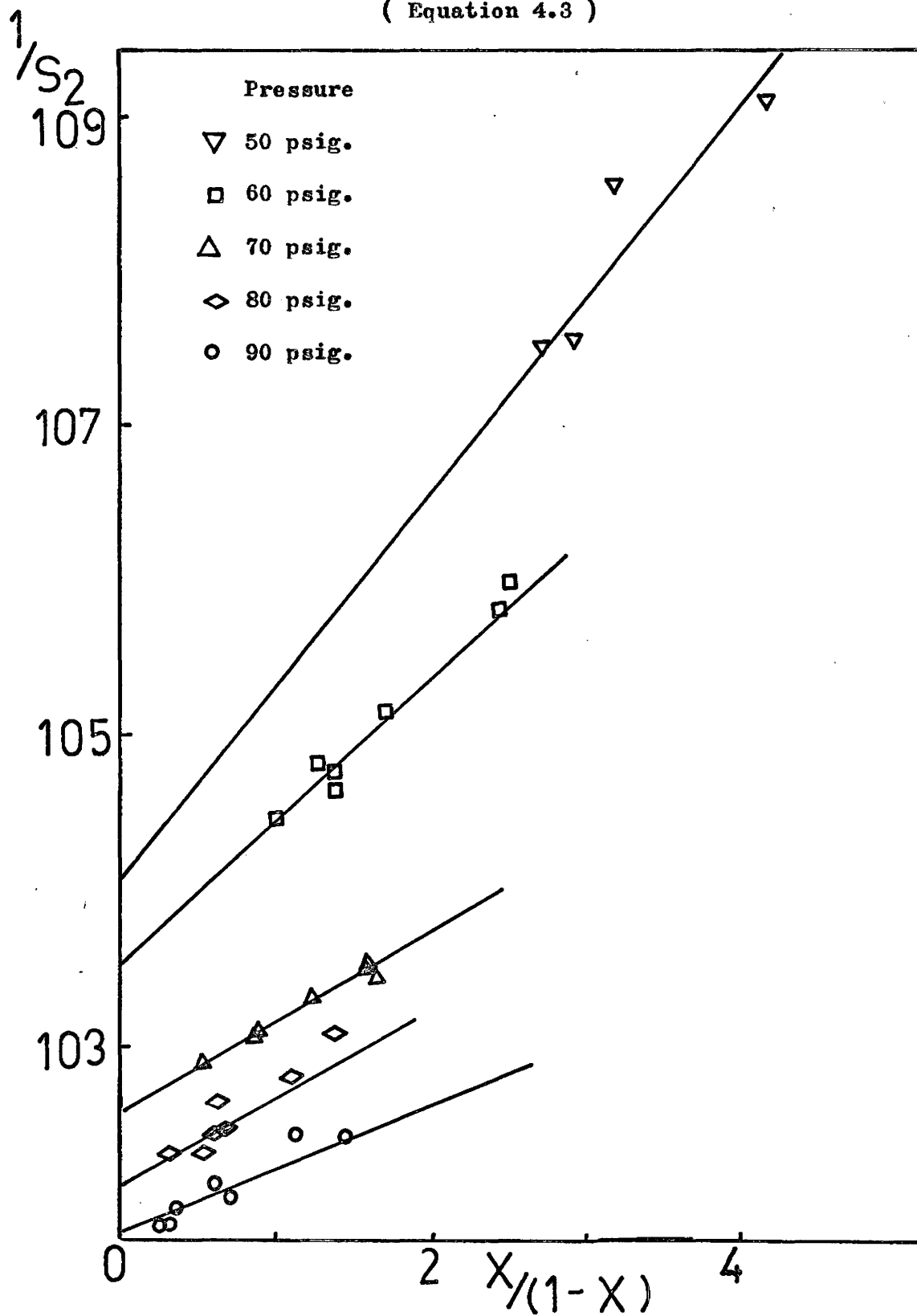


TABLE ( 4.5 )

Product Distribution Analysis ( Eqn. 4.3 )

Temp. (°C)	P <sub>T</sub> (psig)	Slope	Intercept	k <sub>2</sub> <sup>*</sup> /k <sub>2</sub> <sup>0</sup>	k <sub>2</sub> <sup>00</sup> /k <sub>3</sub> <sup>00</sup>
128	20	0.0277	1.0287	0.0287	0.0269
128	30	0.0186	1.0214	0.0214	0.0182
128	40	0.0078	1.0190	0.0190	0.0076
128	50	0.0062	1.0170	0.0170	0.0061
139	30	0.0285	1.0705	0.0705	0.0266
139	40	0.0108	1.0385	0.0385	0.0104
139	50	0.0090	1.0290	0.0290	0.0088
139	60	0.0054	1.0213	0.0213	0.0053
148	50	0.0132	1.0405	0.0405	0.0127
148	60	0.0093	1.0350	0.0350	0.0087
148	70	0.0059	1.0255	0.0255	0.0058
148	80	0.0054	1.0211	0.0211	0.0053
148	90	0.0036	1.0182	0.0182	0.0035

over the experimental ranges. The selectivity at zero conversion was obtained by extrapolation, and fig.(4.24) is the plot of zero conversion selectivity as a function of pressure. Higher temperature and lower pressure favour the formation of methane.

Both  $k_2''/k_3''$  and  $k_2^*/k_2'$  decrease with increasing pressure at a given temperature. The decreasing of  $k_2''/k_3''$  with increasing pressure indicates hydrogenolysis of ethane has a greater dependence of pressure than that of propane. A relation of  $k_2''/k_3''$  on pressure was assumed to be as :

$$\frac{k_2''}{k_3''} = A_{23} P_T^m \quad (4.9)$$

where  $P_T$  is the total pressure and  $A_{23}$  and  $m$  are constants. The values of the constant were obtained by plotting  $\log k_2''/k_3''$  against  $\log P_T$  as shown in fig. ( 4.25 ). The values of  $m$  are -1.89, -1.92 and -1.75 for temperatures of 128, 139 and 148°C. An average value of -1.85 was taken. The values of  $k_2^*/k_2'$  are subjected to large errors and it is hard to get an exact relation of  $k_2^*/k_2'$  and total pressure. However  $k_2^*/k_2'$  decreases with increasing pressure.

The pressure dependence of ethane selectivity is shown as equation (4.6). The parameters in the equation were evaluated by using the selectivity data given in Tables (C7), (C8), (C9) and (C10). Table (4.6) presents the parameters obtained from the analysis of equation (4.6) by linear least squares. The parameter,  $h_2/h_3$  is the ratio of the rate constants for adsorption of ethane to propane. It is also the ratio of rates of adsorption of ethane to propane. The values for  $h_2/h_3$  are very small. Propane adsorbs more than thirty fold faster than ethane. The parameter,  $h_2^*/h_2'$  is the ratio of rate constant of cracking of ethane

to its desorption, and  $h_3^*/h_3'$  is the ratio of rate constants of cracking of propane to its desorption. The dependence of  $h_2^*/h_2'$  and  $h_3^*/h_3'$  are represented by Arrhenius expressions :

$$\frac{h_2^*}{h_2'} = A_{22} \exp(-E_{22}/RT) \quad (4.10)$$

$$\frac{h_3^*}{h_3'} = A_{33} \exp(-E_{33}/RT) \quad (4.11)$$

where  $A_{22}$  and  $A_{33}$  are the pre-exponential factors and  $E_{22}$  and  $E_{33}$  are the activation energies for  $h_2^*/h_2'$  and  $h_3^*/h_3'$  respectively.

The Arrhenius plots for the parameters  $h_2^*/h_2'$  and  $h_3^*/h_3'$  are shown in fig.(4.26). The activation energies are 26.6 and 25.2 kcal./mole for the parameters  $h_3^*/h_3'$  and  $h_2^*/h_2'$  respectively. The activation energies are the difference between activation energies of cracking and desorption. The values are only approximate.

The ratio of the rates of cracking to desorption for ethane and propane at each pressure were calculated according to the following equations

$$\frac{R_{2,C}}{R_{2,D}} = \frac{h_2^*}{h_2'} P_{H_2}^{-2.0} \quad (4.12)$$

$$\frac{R_{3,C}}{R_{3,D}} = \frac{h_3^*}{h_3'} P_{H_2}^{-2.0} \quad (4.13)$$

where  $R_{2,C}$  and  $R_{3,C}$  represent cracking rates of ethane and propane, and  $R_{2,D}$  and  $R_{3,D}$  are the desorption rates of ethane and propane. The hydrogen pressure is assumed to be constant at each pressure because the variation of hydrogen pressures are small enough to be negligible.

Fig.(4.24)

Product Distribution at Zero Conversion at Several Temperatures

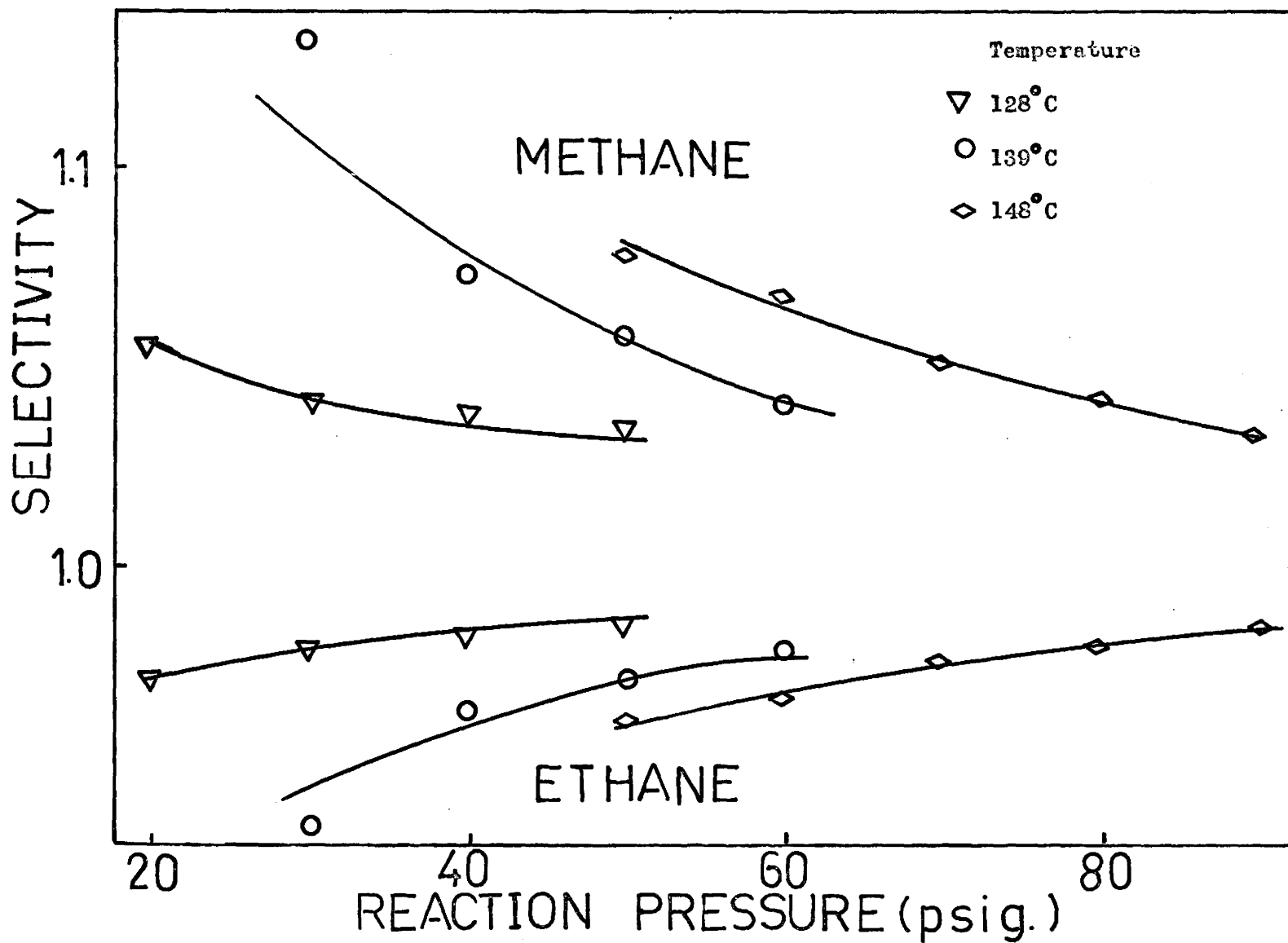


Fig.(4.25)

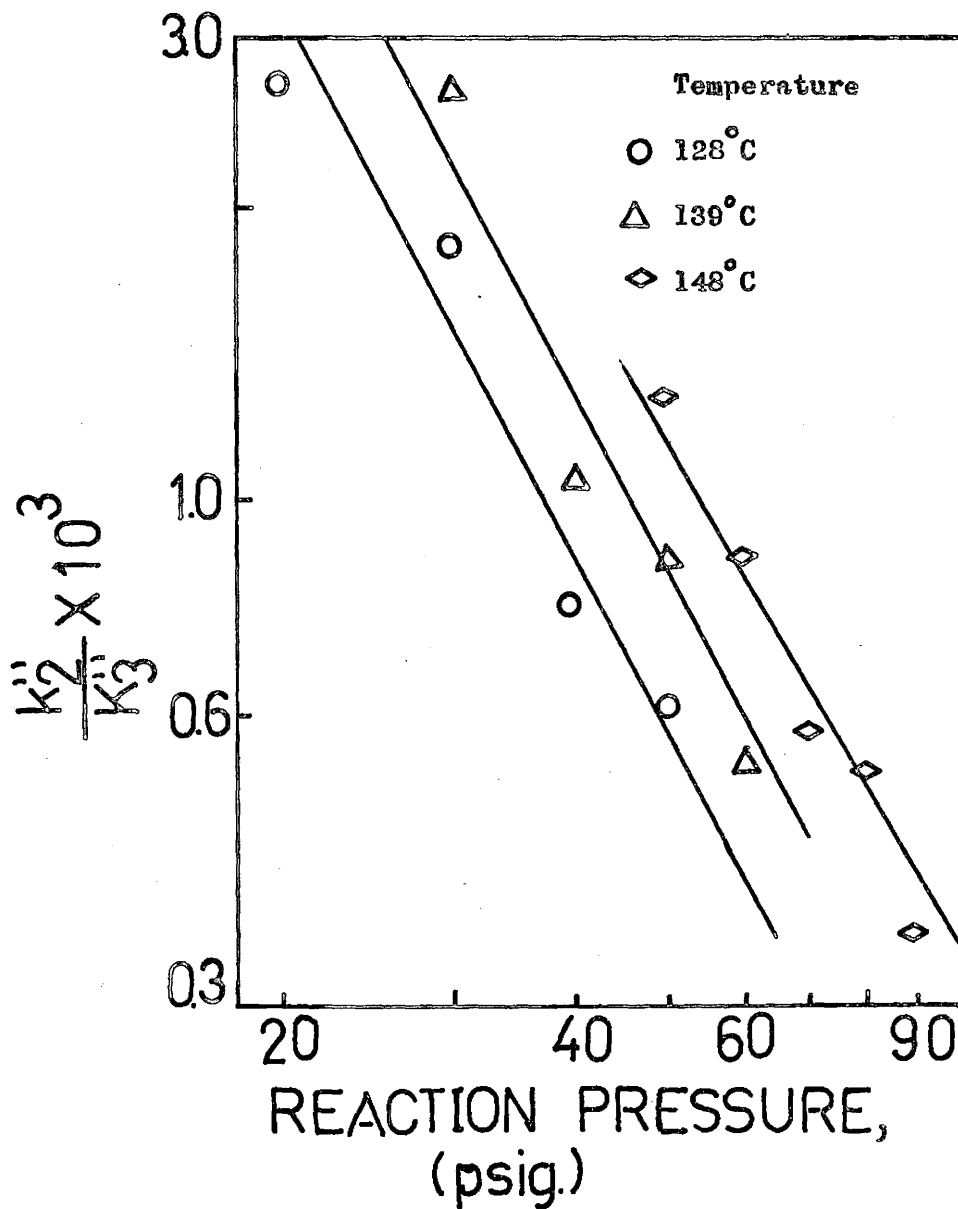
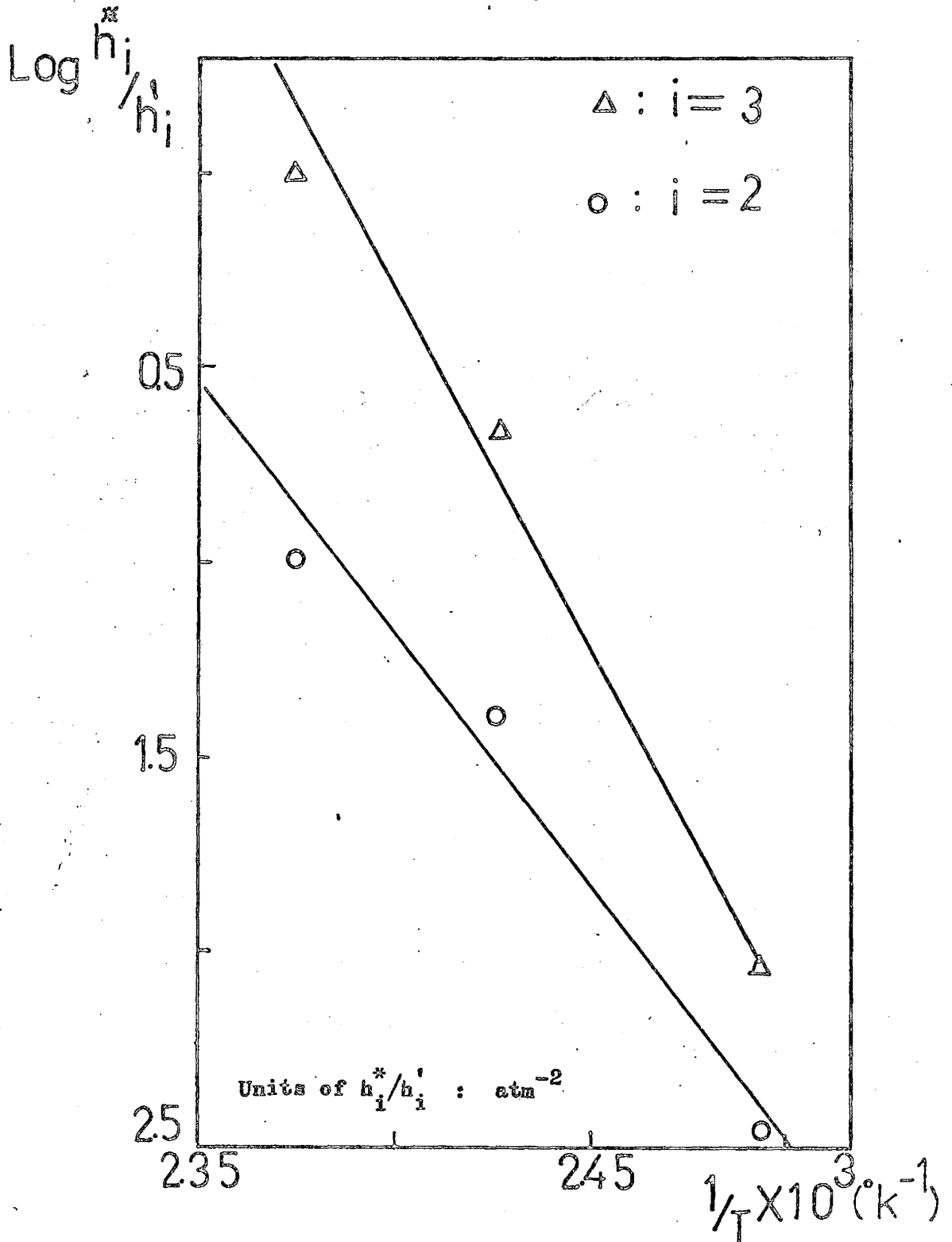
Pressure Dependence of  $k_2''/k_3''$ 

TABLE ( 4.6 )

Product Distribution Analysis ( Eqn. 4.6 )

Temp. ( °C )	Pressure Range (psig)	Residual Sum of Squares	Residual Root Mean Square	$\frac{h_2^*}{h_2}$ (atm <sup>-2</sup> )	$\frac{h_3^*}{h_3}$ (atm <sup>-2</sup> )	$\frac{h_2}{h_3}$
128	10 - 15	0.0025	0.0086	0.0838	0.1293	0.0090
139	20 - 60	0.0019	0.0076	0.2498	0.5204	0.0317
142	40 - 60	0.00042	0.0051	0.2550	0.6000	0.0224
148	40 - 90	0.00041	0.0033	0.3729	0.9739	0.0170

Fig.(4.26)

Arrhenius Plots for  $h_2^*/h_2'$  and  $h_3^*/h_3'$ 

The values for  $R_{2,C}/R_{2,D}$  and  $R_{3,C}/R_{3,D}$  are shown in Table (4.7). These values are small enough to regard adsorption-desorption as being in equilibrium. The ratio decreases with increasing pressure. The trend is similar to those obtained by equation (4.3). A comparison of the experimental and calculated selectivities by equation (4.6) for ethane appears in fig. (4.27). This figure demonstrates that the fit is reasonably good for the temperatures and pressures studied.

#### 4.3 Discussion and Summary

The product distributions for the hydrogenolysis of propane at various temperatures and pressures have been studied. It was found that high temperature, low pressure and high conversion of propane favour the formation of methane. The product distribution is useful for studying the reaction mechanism. A reaction network, similar to those proposed by Kempling, was examined. The network consists of reversible adsorption and desorption for all hydrocarbons and an irreversible rupture of the carbon-carbon bond in the adsorbed species. No single rate determining step was assumed. Two equations ( eqn.(4.3) and eqn.(4.6) ) for ethane selectivity were obtained from the network. The first assumed all reactions proportional to first power of hydrocarbon and the second proportional to first order of hydrocarbon and hydrogen with certain powers.

The parameters from equation (4.3) were evaluated. The parameter,  $k_2^*/k_2'$  is the rate of ethane cracking to its desorption. The values were

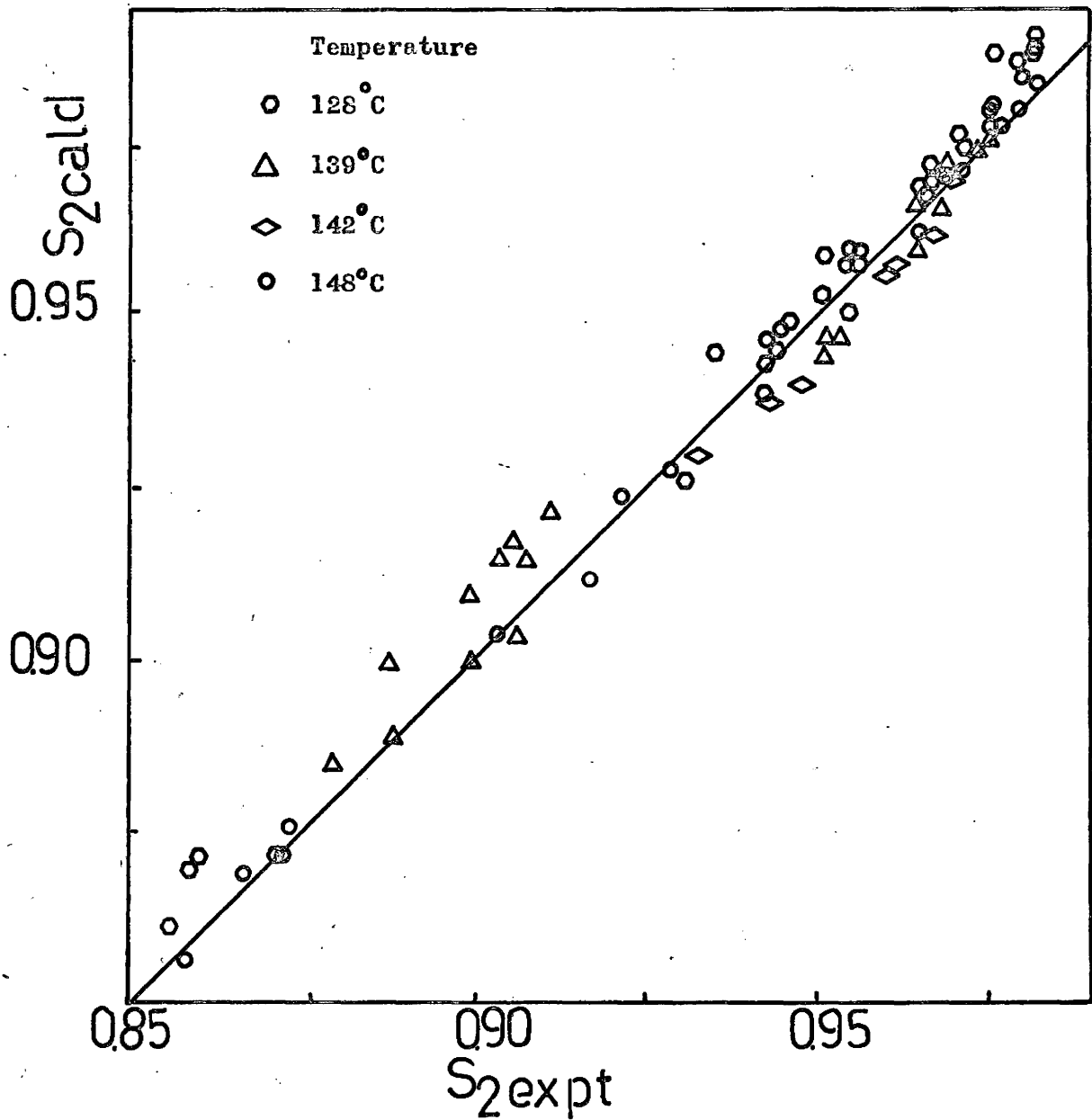
TABLE ( 4.7 )

Ratio of Cracking Rate to Desorption

Temp. (°C)	P <sub>T</sub> (psig)	Ethane from Eqn. (4.3)	Ethane from Eqn. (4.6)	Propane from Eqn. (4.6)
128	20	0.0287	0.0540	0.0827
128	30	0.0214	0.0245	0.0378
128	40	0.0190	0.0146	0.0224
128	50	0.0170	0.0093	0.0144
139	30	0.0705	0.0730	0.1360
139	40	0.0385	0.0472	0.1030
139	50	0.0290	0.0230	0.0478
139	60	0.0213	0.0198	0.0413
148	50	0.0405	0.0647	0.1690
148	60	0.0350	0.0353	0.0920
148	70	0.0255	0.0258	0.0674
148	80	0.0211	0.0211	0.0552
148	90	0.0182	0.0133	0.0360

Fig.(4.27)

Comparison of Experimental and Calculated Selectivity of Ethane



found to be small numbers far less than unity. This indicates that the rate of cracking of ethane is very much slower than its desorption. The reversible adsorption-desorption reactions in the network can, to a good approximation, be assumed to be in equilibrium. The cracking of carbon-carbon bonds is the slowest step. The parameter  $k_2^*/k_2'$  decreases with increasing pressure but increases with increasing temperature as shown in Table (4.3) and (4.4).

The parameter  $k_2''/k_3''$  is the ratio of the rates of hydrogenolysis of ethane to propane. The values for  $k_2''/k_3''$  were found to be small numbers, increasing with increasing temperature but decreasing with increasing pressure. The values for  $k_2''/k_3''$  can be found in Table (4.3). This result confirms the work by Kempling (1) that the hydrogenolysis rate for a straight chain hydrocarbon increases with number of carbon atoms in the hydrocarbon. The activation energy for  $k_2''/k_3''$  is 11.2 kcal./mole. Since the activation energy for hydrogenolysis of propane is 28.9 kcal./mole, the ethane hydrogenolysis activation energy would be 40.1 kcal./mole. This value is quite close to the activation energy of ethane hydrogenolysis obtained by Tajbl which is 42 kcal./mole (22). The dependence of  $k_2''/k_3''$  on total reaction pressure is estimated to be in the order of -1.85. As it has been shown in Chapter Three, the pressure dependence of hydrogenolysis of propane is to the order of -0.90. Thus, the dependence of total pressure of hydrogenolysis of ethane would be to the order of -2.76. Therefore, hydrogenolysis rate of ethane is decreased more by pressure than that of propane.

It was noted that  $1/S_2$  vs  $X/(1 - X)$  plots are not always very good, yet the calculated selectivity curves agree quite well with the experimental

selectivities. These was shown on fig. (4.2) to fig. (4.4), fig. (4.8) to (4.10) and fig. (4.18) to (4.20). Therefore, the network and equations were found to be consistent with the experimental observations.

The parameters from equation (4.6) were estimated. The parameters,  $h_2^*/h_2'$  and  $h_3^*/h_3'$  are the ratios of the rate constants of cracking to desorption of ethane and propane, respectively. The dependence of the parameters was represented by Arrhenius expressions. The activation energies were found to be 26.6 kcal/mole and 25.2 kcal/mole for propane and ethane respectively. These activation energies compare favourably with previous investigations. For ethane over ruthenium, the activation energy for hydrogenolysis was much greater than that for deuterium exchange (2,9).

The parameter,  $h_2/h_3$  corresponds to the ratio of the rates of adsorption of ethane to propane. The values obtained show that propane adsorbs much faster than ethane. Equation (4.6) is insensitive to the parameter  $h_2/h_3$  because their values are quite close to zero ; therefore, a temperature dependence expression for this parameter was not determined.

The ratios of the rates of cracking to desorption for ethane and propane were calculated from the parameters  $h_2^*/h_2'$  and  $h_3^*/h_3'$ . The ratios are shown in Table (4.6). The values were found to be small enough to assume that the cracking rate is much slower than the desorption rate. Comparison between the ratios for rates of ethane cracking to its desorption calculated from the parameters  $h_2^*/h_2'$  and  $k_2^*/k_2'$  appear in Table (4.6). The rate ratios calculated from both parameters show the same trend, i.e. increasing with increasing temperature but decreasing with increasing pressure. The values obtained for both parameters are of the same order of

magnitude. This result shows that both equation (4.3) and (4.6) have the ability to estimate the ratio of the rates of cracking of ethane to its desorption.

A comparison of the experimental and calculated selectivities based on equation (4.6) are shown on fig. (4.27). The figure demonstrates that the fit was good for the temperatures and pressures examined. Therefore, the assumption that reactions are proportional to first order of hydrocarbon and certain powers of hydrogen is valid.

There are two criteria for rejection of a reaction network. Either the residual sum of squares is large or an unreasonable value of one or more of the parameters is obtained. Comparison of the observed and calculated selectivities has demonstrated that the postulated reaction network is capable of fitting the experimental data. From the informations obtained, it is confirmed that the mechanism of hydrogenolysis consists of a rapid reversible adsorption-desorption process and the rupture of carbon-carbon bonds on the surface is the slowest step. Both equations derived from the network are applicable. Equation (4.3) has the ability to estimate the parameters  $k_2^*/k_2'$  and  $k_2''/k_3''$  while equation (4.6) can evaluate the parameters  $h_2^*/h_2'$ ,  $h_3^*/h_3'$  and  $h_2/h_3$ . Therefore, equation (4.3) and (4.6) should be used simultaneously to get more insight into the mechanism of hydrogenolysis.

## CHAPTER FIVE

### CONCLUSION

The hydrogenolysis of propane over supported ruthenium in a continuous stirred-tank catalytic reactor has been studied. The hydrogenolysis rate was found to be proportional to a positive power of propane partial pressure and negative power of hydrogen partial pressure. The rate decreased with increasing pressure. However, a single power rate expression failed to correlate the rate at different pressures.

A mechanism was proposed consisting of dissociative adsorption of hydrogen and propane which was in equilibrium and rupture of carbon-carbon bonds on the surface which was the rate determining step. The number of hydrogen atoms lost on adsorption to form reactive adsorbed  $C_3^{\delta}$  species was 5. The intermediate was discussed in terms of 1,2-diadsorbed species. The activation energy for the hydrogenolysis of propane was 28.9 kcal/mole. The heat of adsorption of propane was -2.19 kcal/mole and the adsorption reaction was endothermic. The heat of adsorption of hydrogen was 7.95 kcal/mole and the reaction was exothermic. The rate expression for the hydrogenolysis of propane can be represented as :

$$r = \frac{5.78 \times 10^{10} \exp(-28.9 \times 10^3/RT) P_{C_3} P_{H_2}^{-2}}{(1 + 5.18 \times 10^{-6} \exp(7.95 \times 10^3/RT) P_{H_2}^{1/2} + 13.2 \exp(-2.19 \times 10^3/RT) \frac{P_{C_3}}{P_{H_2}^{1/2}})^2}$$

where : T - Reaction temperature in absolute ( $^{\circ}K$ )

- R - Gas constant ( 1.987 cal/(g mole)-°K)
- $P_{C_3}$  - Partial pressure of propane (atm)
- $P_{H_2}$  - Partial pressure of hydrogen (atm)
- and r - Rate of hydrogenolysis of propane (mole/g. cat.- sec)

The analysis of product distributions yielded a consistent description of the mechanism. The mechanism involves a rapid reversible adsorption-desorption of propane and a surface cracking reaction which is the slowest step. The desorption of  $C_2$  and  $C_3$  adsorbed species were very much faster than cracking. The hydrogenolysis of propane was found to be faster than the hydrogenolysis of ethane. The adsorption rate of ethane was smaller than the adsorption rate of propane. The activation energy of hydrogenolysis of ethane was estimated to be 40.1 kcal/mole.

## REFERENCES

1. J. C. Kempling, PhD thesis, McMaster University, Hamilton, Ontario, Canada, 1971.
2. J. H. Sinfelt and D. J. C. Yates, *J. Catalysis* 8, 82 (1967).
3. J. J. Carberry, *Ind. Eng. Chem.* 56, 39 (1964).
4. K. Morikawa, W. S. Benedict and H. S. Taylor, *J. Am. Chem. Soc.* 58, 1795 (1936).
5. K. Morikawa, N. R. Trenner and H. S. Taylor, *J. Am. Chem. Soc.* 59, 1103 (1937).
6. A. Cimino, M. Boudart and H. S. Taylor, *J. Phys. Chem.* 58, 796 (1954).
7. J. R. Anderson and B. G. Baker, *Proc. Roy. Soc.* A271, 402 (1963).
8. A. K. Galwey, *Proc. Roy. Soc.* A271, 218 (1963).
9. J. R. Anderson and C. Kemball, *Proc. Roy. Soc.* A223, 361 (1954).
10. C. Kemball, *Proc. Roy. Soc.* A223, 377 (1954).
11. L. Guzzi, B. S. Gudkov and P. Teyenyi, *J. Catalysis* 24, 187 (1972).
12. L. Cuczi, A. Sarkamy and P. Teyenyi, *Proc. of the 5th international Congress on Catalysis, U.S.A.*, (1972)
13. C. Kemball, *Disc. Faraday Soc.* 41, 190 (1966).
14. J. H. Sinfelt and W. F. Taylor, *Trans. Faraday Soc.* 64, 3086 (1968).
15. J. H. Sinfelt and D. J. C. Yates, *J. Catalysis* 10, 362 (1968).
16. R. S. Dowie, M. C. Gray, D. A. Whan and C. Kemball, *Chem. Com.* (1971).
17. D. J. C. Yates, J. H. Sinfelt and W. F. Taylor, *Trans. Faraday Soc.* 61, 2046 (1965).

18. J. H. Sinfelt, W. F. Taylor and D. J. C. Yates, *J. Phys. Chem.* 69, 95 (1965).
19. D. J. C. Yates and J. H. Sinfelt, *J. Catalysis* 14, 182 (1969).
20. J. H. Sinfelt, *Catalysis Review*, 3(2), 175 (1969).
21. D. G. Tajbl, *Can. J. Chem. Eng.* 47, 154 (1969).
22. D. G. Tajbl, *Ind. Eng. Chem. Proc. Des. Dev.* 8, 364 (1969).
23. J. C. Kempling and R. B. Anderson, *Ind. Eng. Chem., Process Des. Develop.* 9, 116 (1970).
24. J. C. Kempling and R. B. Anderson, *Ind. Eng. Chem., Process Des. Develop.* 11, 146 (1972).
25. F. E. Shephard, *J. Catalysis* 14, 148 (1969).
26. E. Kikuchi and Y. Morita, *J. Catalysis* 15, 217 (1969).
27. J. M. Smith, *Can. J. Chem. Eng.* 48, 142 (1970).
28. R. B. Anderson, "Experimental Method in Catalysis Research", Academic Press, N. Y. (1968).
29. J. J. Carberry, *Catalysis Review*, 3(1), 61 (1969).
30. D. G. Tajbl, J. B. Simon and J. J. Carberry, *Ind. Eng. Chem., Fund.* 5, 171 (1966).
31. J. R. Kittrell and R. Mezaki, *Ind. Eng. Chem.* 59, 28 (1967).
32. M. Boudart, *A. I. Ch. E. J.* 18, 465 (1972).
33. S. Weller, *A. I. Ch. E. J.* 2, 59 (1956).
34. O. A. Hougen and K. M. Watson, "Chemical Process Principle, Part 3", Wiley, N. Y. (1947).
35. J. R. Kittrell, R. Mezaki and C. C. Watson, *Brit. Chem. Eng.* 11, 1 (1966).

36. J. R. Kittrell, R. Mezaki and C. C. Watson, Brit. Chem. Eng. 10, 291 (1965).
37. O. Levenspiel, N. J. Weinstein and J. C. R. Li, Ind. Eng. Chem. 48, 324 (1956).
38. J. R. Kittrell, W.G. Hunter and C. C. Watson, A. I. Ch. E. J. 11, 1051 (1965).
39. N. R. Draper and H. Smith, "Applied Regression Analysis", J. Wiley and Sons, N.Y. (1966).
40. M. R. Spiegel, "Statistics", Schaum Publishing Co., N.Y. (1961) pp. 217-283.
41. J. M. Thomas and W. J. Thomas, "Introduction of the Principle of Heterogenous Catalysis", Academic Press. (1967), pp. 67-239.
42. P. H. Emmett, "Catalysis ", vol. I, Reinhold Publishing Corp. N. Y. (1954), pp. 31-119.
43. J. H. Sinfelt, Ind. Eng. Chem. 58, 18 (1966).

## A P P E N D I X A

### Measurement of Pore Size Distribution and Specific Area

#### By Mercury Porosimeter

The pore size distribution and the specific surface area of the catalyst, 0.5 weight percent ruthenium impregnated on  $\gamma$ -alumina were measured by a mercury porosimeter ( Micrometrics Instrument Corporation, Model 900/910 Series ). The instrument operates on the principle that mercury exhibits an angle of contact with the catalyst greater than  $90^\circ$ ; the mercury does not wet the catalyst. Thus an external force is required to force the mercury into the pores. The mercury surface tension ( 474 dynes/cm. at  $25^\circ\text{C}$  ) is the measure of this resistance. If pressure  $P$  is imparted to the mercury, the force which tends to drive mercury into the cylindrical pore is  $\pi r^2 P$  and the force due to surface tension is  $2\pi r \sigma \cos \theta$ . Equating these two forces, gives

$$P = \frac{-2\sigma \cos \theta}{r} \quad ( A1 )$$

where :  $r$  - the cylindrical pore radius

$\theta$  - the angle of contact

$\sigma$  - the surface tension

The sample was dried before placing into the sample cell. The pressure chamber was then evacuated and the mercury was allowed to enter the cell. The pressure below atmospheric was obtained by slowly opening the valve to the atmosphere. Higher pressure was generated with a hydraulic pump. The amount of mercury penetrating the pores was measured by following the mercury level in the constant diameter tube of the

porosimeter cell by a movable electrical contact mechanism.

The pore size distribution for cylindrical pores can be represented as (41)

$$D(r) = - \frac{P}{r} \frac{dV}{dP} \quad (A2)$$

where  $D(r)$  is the pore size distribution function. The right hand side is plotted as a function of  $r$  from the data shown in Table (D1). The distribution curve gives the volume of pores which have a given radius, and

$$dS = - \frac{P}{\sigma \cos \theta} \frac{dV}{dr} \quad (A3)$$

For mercury  $\theta$  is  $130^\circ$  and  $\sigma$  is 474 dynes/cm. at  $25^\circ\text{C}$ . Then

$$S = 0.0225 \int_0^{V_{\max}} P dV \quad (A4)$$

where :  $P$  - pressure in psia.

$V$  - volume in cc./gm.

and  $S$  - specific surface area in  $\text{m}^2/\text{gm}$ .

The integration is obtained graphically from Fig. (A1)

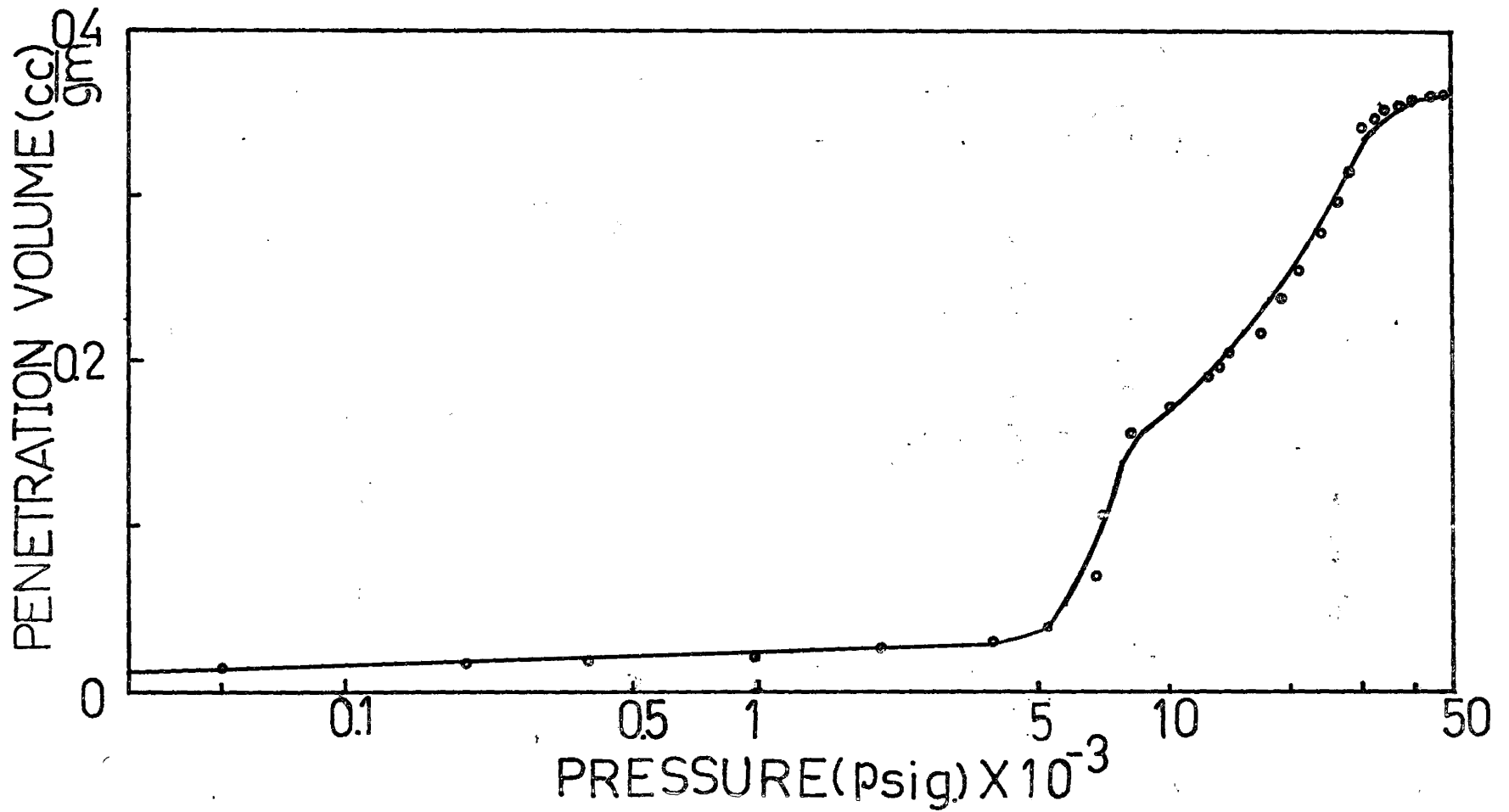
The average pore radius was evaluated from (42)

$$\bar{r} = \frac{2 V_{\max}}{S} \quad (A5)$$

where  $V_{\max}$  is the pore volume of the sample.

Fig.(A1)

Penetration Volume vs External Pressure Plot

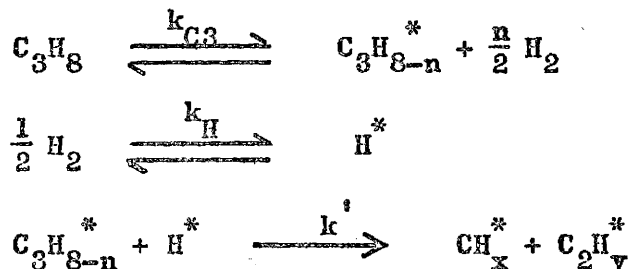


A P P E N D I X B

Various Possible Mechanisms for the Hydrogenolysis  
of Propane

Various mechanisms were proposed for the hydrogenolysis of propane, and the Hougen-Watson type of rate expressions were derived from the proposed mechanisms. The parameters in the rate expressions were obtained by linear least squares. The appropriate mechanism will be the one that gives the smallest residual sum of squares and acceptable parameters. The following is the derivation of the equations from the proposed mechanisms.

( 1 ) The proposed mechanism involves a dissociative adsorption of both hydrogen and propane in equilibrium and a surface cracking reaction of adsorbed hydrogen and C<sub>3</sub> species which is the rate determining step.



The fractional coverage of adsorbed hydrogen and C<sub>3</sub> species can be represented as

$$\theta_{\text{H}} = \frac{k_{\text{H}} P_{\text{H}}^{1/2}}{\left( 1 + k_{\text{H}} P_{\text{H}}^{1/2} + k_{\text{C3}} \frac{P_{\text{C3}}}{P_{\text{H}}^{n/2}} \right)} \quad ( \text{B1} )$$

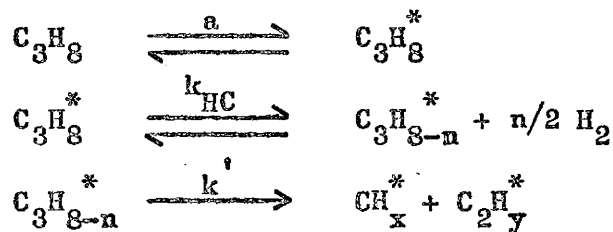
$$\text{and } \theta_{C_3} = \frac{k_{C_3} P_{C_3} P_H^{-n/2}}{\left(1 + k_H P_H^{1/2} + k_{C_3} \frac{P_{C_3}}{P_H^{n/2}}\right)} \quad (\text{B2})$$

If the rate determining step is assumed to be the surface cracking reaction, then

$$r = k' \theta_{C_3} \theta_H \quad (\text{B3})$$

$$\text{or } r = \frac{k P_{C_3} P_H^{(1-n)/2}}{\left(1 + k_H P_H^{1/2} + k_{C_3} \frac{P_{C_3}}{P_H^{n/2}}\right)^2} \quad (\text{B4})$$

( 2 ) The proposed mechanism involves an initial adsorption of gaseous propane. The adsorbed  $C_3$  species gives off  $n/2$  molecule of hydrogen on the surface to form the reactive  $C_3$  species which cracks into adsorbed  $C_2$  and  $C_1$  species.



The surface coverage of  $C_3H_8^*$  is

$$\theta_{C_3} = \frac{a P_{C_3}}{1 + a P_{C_3}} \quad (\text{B5})$$

If the surface cracking reaction is assumed to be the rate determining step, then

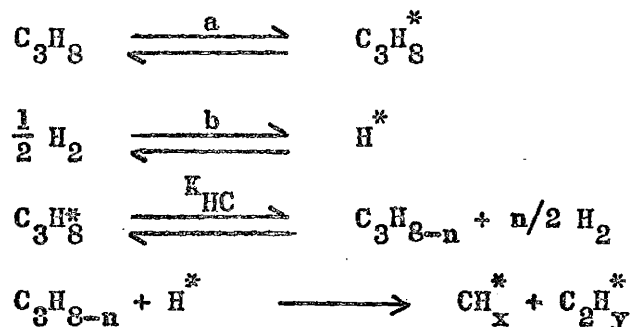
$$r = k' \theta_C \quad (B6)$$

$$\text{where } \theta_C = k_{HC} \theta_{C3} P_H^{-n/2} \quad (B7)$$

Substituting equation (B7) and (B5) into (B6) obtains

$$r = k \frac{P_{C3}}{(1 + a P_{C3})} P_H^{-n/2} \quad (B8)$$

(3) The proposed mechanism involves adsorption of hydrogen and propane on different sites. The initial adsorbed  $C_3$  species gives off  $n/2$  molecules of hydrogen to form the reactive  $C_3$  species. The final  $C_3$  species reacts with adsorbed hydrogen to form  $C_1$  and  $C_2$  species.



The surface coverage for hydrogen and  $C_3H_8^*$  are :

$$\theta_H = \frac{b P_H^{1/2}}{1 + b P_H^{1/2}} \quad (B9)$$

$$\theta_{C3} = \frac{a P_{C3}}{1 + a P_{C3}} \quad (B10)$$

If the surface reaction of adsorbed hydrogen and  $C_3$  species is assumed to

be the rate determining step, then

$$r = k' \theta_H \theta_C \quad (B11)$$

$$\text{where } \theta_C = \frac{k_{HC} \theta_{C3} P_H^{-n/2}}{1 + k_{HC} \theta_{C3} P_H^{-n/2}} \quad (B12)$$

Substituting equations (B12), (B9) and (B10) into equation (B11) yields

$$r = \frac{k}{(1 + a P_{C3})} \frac{1}{(1 + b P_H^{1/2})} P_{C3} P_H^{(1-n)/2} \quad (B13)$$

( 4 ) The proposed mechanism that has been tried is exactly identical to that proposed by Cimino et al., and it has been described in full length in Chapter One. The rate is expressed as

$$r = \frac{k}{1 + \frac{k_{HC} P_{C3}}{P_H^{n/2}}} P_{C3} P_H^{-n/2} \quad (B14)$$

Equation (B4) is rejected because the heat of adsorption for both hydrogen and propane are endothermic. Equations (B8) and (B14) are rejected because the residual sum of squares ( in the order of  $10^{-12}$  ) is large. Equation (B13) is unacceptable because the rate of adsorption constants evaluated are negative.

## A P P E N D I X C

### Product Distribution Network

The reaction network proposed for the hydrogenolysis of propane is shown in Fig. ( C1 ). Each of the hydrocarbons was assumed to adsorb and desorb reversibly to produce reactive species on the metal surface. The adsorbed species were assumed to react irreversibly via the rupture of one carbon-carbon bond to produce smaller adsorbed fragments. This assumption is proper, because the hydrogenolysis reaction is so highly favoured thermodynamically (44) that the reversed reaction does not occur. Each reaction was assumed to be first order in the concentration of the hydrocarbon involved. The effect of hydrogen pressure was assumed to be nearly constant at a given pressure and incorporated into the rate constant. The corresponding rate constants are shown in Fig. ( C1 ).

From the reaction network, the overall rate of formation of propane is

$$r_3 = -k_3 C_3 + k_3' A_3 \quad ( C1 )$$

$$r_3 = -k_3^* A_3 \quad ( C2 )$$

where  $r_3$  is the overall rate of formation of propane,  $C_3$  and  $A_3$  are the concentration of gaseous propane and fractional coverage of  $C_3$  species.

The combination of equation ( C1 ) and ( C2 ) yields

$$-r_3 = k_3'' C_3 \quad ( C3 )$$

$$\text{where : } k_3'' = k_3 k_3^* / (k_3^* + k_3')$$

Since the hydrogenolysis reactions are equimolar, there is no change in volume and flow-rate between inlet and outlet. A propane mass balance over the reactor yields :

$$FC_3^0 = FC_3 + Vk_3''C_3 \quad (C4)$$

$$\text{or } C_3^0 = C_3 + tk_3''C_3 \quad (C5)$$

where :  $C_3^0$  - concentration of propane in inlet

$C_3$  - concentration of propane in effluent

$F$  - flow rate

$V$  - reactor volume

$t$  - reactor residence time (  $V/F$  )

From the definition of conversion

$$X_3 = 1 - (C_3/C_3^0) \quad (C6)$$

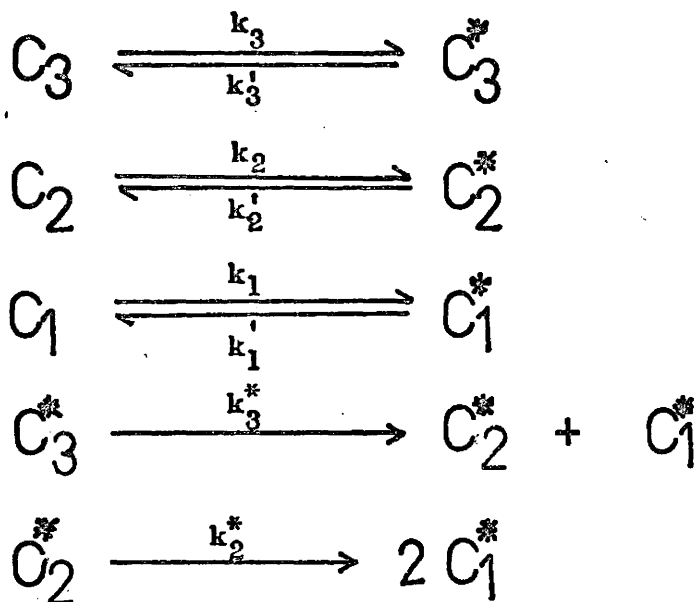
Rearranging equation ( C5 ) obtains

$$X_3 = \frac{k_3''t}{1 + k_3''t} \quad (C7)$$

$$\text{or } t = \frac{X_3}{k_3''(1 - X_3)} \quad (C8)$$

The overall rate of formation of ethane is

$$r_2 = -k_2C_3 + k_2'A_2 \quad (C9)$$



$C_3, C_2, C_1$  - gaseous propane, ethane and methane

$C_3^*, C_2^*, C_1^*$  - adsorbed hydrocarbon species

$k_i$  - adsorption rate constant

$k_i'$  - desorption rate constant

$k_i^*$  - cracking rate constant

Fig. ( C 1 )

## Propane Hydrogenolysis Mechanism

$$r_2 = -k_2^* A_2 + k_3^* A_3 \quad (C10)$$

where :  $r_2$  - the rate of formation of ethane

$C_2$  - the concentration of gaseous ethane

$A_2$  - the concentration of adsorbed  $C_2$  species

Substituting equations ( C2 ) and ( C3 ) into equations ( C9 ) and ( C10 ) yields

$$-r_2 = k_2'' C_2 - \frac{k_3' k_2''}{k_2 + k_2'} C_3 \quad (C11)$$

where :

$$k_2'' = \frac{k_2 k_2^*}{k_2^* + k_2'}$$

A mass balance of ethane over the reactor yields

$$0 = C_2 + \tau \left( k_2'' C_2 - \frac{k_3' k_2''}{k_2 + k_2'} C_3 \right) \quad (C12)$$

Substitution of equations ( C6 ), ( C7 ) and ( C8 ) yields

$$\frac{C_2}{C_3} = \frac{\frac{k_2''}{k_2 + k_2'} X_3}{1 + \frac{k_2''}{k_3''} \frac{X_3}{1 - X_3}} \quad (C13)$$

If the selectivity of ethane is defined as

$$S_2 = \frac{C_2}{C_3 X_3} \quad (C14)$$

Then

$$S_2 = \frac{\frac{k_2'}{k_2^* + k_2'}}{1 + \frac{k_2''}{k_3} \frac{X_3}{1 - X_3}} \quad (C15)$$

The parameter,  $k_2'/(k_2^* + k_2')$  corresponds to relative rates of desorption and cracking of adsorbed  $C_2$  species and  $k_2''/k_3$  is the ratio of rate constants of hydrogenolysis of ethane to propane. Since all the reactions are assumed to be first order in the concentration of the hydrocarbon involved. Then  $k_2''/k_3$  represents the relative hydrogenolysis rates of ethane to propane.

The methane selectivity can be obtained from a carbon balance according to

$$2S_2 + S_1 = 3 \quad (C16)$$

In the previous development of equations, the hydrogen partial pressures were assumed to be constant and incorporated into the rate constant. Another reaction network was proposed and is shown in fig. (C2). All the surface reactions were assumed to involve an adsorbed hydrocarbon species and an adsorbed hydrogen species. The desorption reactions were assumed to be  $n/2$  order in hydrogen for propane and  $m/2$  order in hydrogen for ethane.  $n$  and  $m$  represents the number of hydrogen

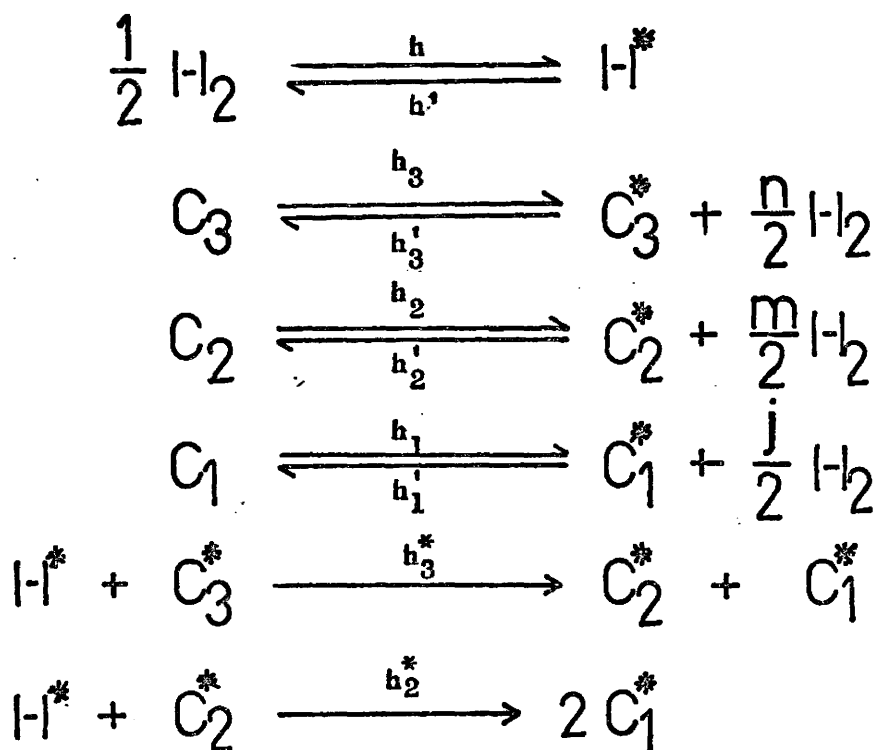
atoms acquired by the adsorbed species on desorption. The adsorption rate was assumed to be independent of hydrogen. The adsorbed hydrogen species was assumed to be proportional to  $1/2$  order of hydrogen partial pressure.

Similar derivation to the previous network leads to the selectivity of ethane as

$$S_2 = \frac{\frac{h_2' P_{H_2}^{m/2}}{1 + \frac{h_2 h_2^* P_{H_2}^{1/2}}{h_2' P_{H_2}^{m/2} + h_2^* P_{H_2}^{1/2}}}}{\frac{h_2 h_2^* P_{H_2}^{1/2}}{h_2' P_{H_2}^{m/2} + h_2^* P_{H_2}^{1/2}} + \frac{h_3 h_3^* P_{H_2}^{1/2}}{h_3' P_{H_2}^{n/2} + h_3^* P_{H_2}^{1/2}}} \cdot \frac{X_3}{1 - X_3}} \quad (C17)$$

which simplifies to

$$S_2 = \frac{1}{1 + \frac{h_2^*}{h_2} P_{H_2}^{\frac{1}{2} - \frac{m}{2}} + \frac{h_2 h_2^*}{h_3 h_3^*} \left\{ \frac{h_3^*}{h_2'} P_{H_2}^{\frac{1}{2} - \frac{m}{2}} + \frac{h_3'}{h_2} P_{H_2}^{\frac{n}{2} - \frac{m}{2}} \right\} \frac{X_3}{1 - X_3}} \quad (C18)$$



$\text{C}_3, \text{C}_2, \text{C}_1$  - gaseous propane, ethane and methane

$\text{C}_3^*, \text{C}_2^*, \text{C}_1^*$  - adsorbed hydrocarbon species

$h_i$  - adsorption rate constant

$h_i'$  - desorption rate constant

$h_i^*$  - cracking rate constant

$\text{H}_2$  and  $\text{H}^*$  - gaseous and adsorbed hydrogen

Fig. (C2)

## Propane Hydrogenolysis Mechanism

TABLE ( A1 )

Hydrogenolysis Data at 2psig. and 120°C

Methane	Partial Pressure ( atm. )			Hydrogen	Rate ( X 10 <sup>7</sup> ) moles g. catalyst - sec.
	Ethane	Propane			
.2686	.1857	.0794		.6022	4.150
.2476	.1724	.0628		.6532	3.545
.0412	.0358	.0319		1.027	1.110
.1026	.0779	.0668		.8886	2.875
.2277	.1628	.0782		.6673	3.600
.3188	.2080	.0668		.5425	4.310
.2190	.1580	.0672		.6919	3.204
.2694	.1851	.0626		.6190	3.620
.2380	.1638	.0472		.6877	2.760
.1673	.1220	.0447		.8019	2.270
.1478	.1152	.1165		.7566	4.200
.2078	.1563	.1550		.6170	6.830
.2892	.2029	.1271		.5169	7.600
.2391	.1701	.0627		.6640	3.430
.2231	.1592	.0573		.6964	3.170
.4172	.2104	.0239		.4846	2.340
.3092	.1884	.0273		.6113	1.661
.1554	.1127	.0332		.8347	1.270
.2202	.1563	.0490		.7105	2.130
.1446	.1084	.0483		.8347	1.770

TABLE ( A2 )

Hydrogenolysis Data at 15psig. and 114.5°C

Methane	Partial Pressure ( atm. )			Hydrogen	Rate (X 10 <sup>7</sup> ) moles g. catalyst - sec.
	Ethane	Propane			
.1406	.1277	.2536		1.499	1.360
.1615	.1455	.2439		1.469	1.580
.1956	.1782	.4562		1.109	2.588
.2835	.2521	.5374		.9474	4.440
.1562	.1418	.1727		1.550	.9510
.2008	.1810	.1172		1.522	.7890
.2592	.2342	.2752		1.252	1.791
.2386	.2134	.1158		1.453	.8540
.0978	.0873	.0709		1.764	.5070
.1212	.1441	.1606		1.595	.9070
.0879	.0756	.1085		1.749	.7612
.2639	.2390	.3788		1.140	2.510
.0950	.0861	.4392		1.400	1.794
.1853	.1687	.2841		1.382	1.531
.1180	.1055	.1855		1.608	1.118
.0776	.0653	.1164		1.761	.8050
.1200	.1087	.3966		1.395	2.195
.1624	.1523	.5572		1.148	3.510
.1657	.1493	.2544		1.451	1.518
.1760	.1568	.2594		1.428	1.662
.1932	.1750	.4120		1.241	2.675
.1368	.1253	.2519		1.506	1.194
.3326	.3014	.4518		.9346	3.399
.2431	.2220	.4310		1.124	2.606

TABLE ( A2 )

Hydrogenolysis Data at 20psig. and 126°C

Methane	Partial Pressure ( atm. )			Rate ( X 10 <sup>7</sup> ) <u>moles</u> g. catalyst - sec.
	Ethane	Propane	Hydrogen	
.2287	.2009	.2309	1.702	2.066
.1575	.1395	.2219	1.842	1.940
.1267	.1114	.1416	1.981	1.490
.1152	.1022	.1253	2.018	1.180
.2658	.2318	.1983	1.665	2.496
.1787	.1572	.2106	1.732	2.214
.1480	.1006	.1589	1.953	1.403
.2606	.2286	.2070	1.664	2.477
.2703	.2453	.2217	1.663	2.674
.1419	.1268	.1924	1.900	1.698
.1973	.1747	.2453	1.743	2.370
.1135	.1013	.1657	1.980	1.450
.1452	.1291	.2007	1.886	2.005
.0994	.0881	.1295	2.044	1.320
.0250	.0214	.0210	2.293	.2943
.3823	.2460	.1997	1.633	2.670
.1487	.1265	.0442	2.241	.5606
.1327	.1133	.0534	2.063	.6480
.0878	.0763	.0538	2.143	.6083
.2932	.2545	.1960	1.617	2.714
.0368	.0314	.0108	2.282	.2366
.3182	.2788	.1886	1.575	3.040
.2453	.2179	.2172	1.680	2.810
.2842	.2531	.2828	1.541	3.68

TABLE ( A3 ) (Continued)

Methane	Partial Pressure ( atm. )			Rate (X 10 <sup>7</sup> ) moles g. catalyst - sec.
	Ethane	Propane	Hydrogen	
.2571	.2299	.3583	1.515	4.240
.4181	.3368	.2870	1.289	4.502
.1723	.1546	.2623	1.771	2.840
.4065	.3539	.2363	1.365	4.096
.3763	.3350	.2096	1.440	3.800
.3295	.2887	.2273	1.515	3.145
.0609	.0548	.1452	2.099	1.190
.1258	.1119	.2863	1.837	2.566
.1685	.1511	.3966	1.645	3.810
.2899	.2561	.3227	1.492	4.260
.2500	.2226	.3314	1.556	4.072
.2231	.1981	.2627	1.677	2.470
.3527	.3078	.2462	1.454	3.520
.2474	.2169	.2091	1.687	2.290
.1970	.1759	.6643	1.324	6.540
.3281	.2870	.6267	1.119	8.690
.3524	.3085	.5736	1.145	7.790

TABLE ( A4 )

Hydrogenolysis Data at 40psig. and 144.5° C

Methane	Partial Pressure ( atm. )			Hydrogen	Rate (X 10 <sup>7</sup> ) moles g. catalyst - sec.
	Ethane	Propane			
.4875	.4134	.1260		2.694	3.897
.4778	.3929	.1113		2.739	3.878
.6318	.5165	.2532		2.319	8.960
.8118	.6385	.3335		1.937	13.88
.6538	.5295	.2009		2.337	7.230
.8287	.6385	.1046		2.149	4.661
.4756	.3952	.1150		2.735	3.890
.2891	.2460	.1273		3.059	2.856
.3412	.2932	.2061		2.880	4.415
.5425	.4525	.1965		2.530	5.075
.2995	.2527	.1206		3.048	3.184
.4603	.3836	.1786		2.700	4.871
.7613	.5757	.1005		2.283	3.825
.4402	.3721	.2471		2.6617	6.853
.4986	.4110	.1708		2.632	4.190
.8905	.6858	.4242		1.721	19.65
.9954	.7474	.3483		1.631	17.74
.8893	.6702	.3222		1.839	13.63
.7792	.6218	.2549		2.065	9.250
.8090	.6282	.2151		2.060	7.798
.6605	.5336	.1894		2.338	6.350
.5157	.4231	.1674		2.615	4.990
.6449	.4930	.0893		2.493	3.025
.5310	.4287	.1399		2.622	4.250
.3721	.3103	.1630		2.876	4.638
.4968	.4283	.1440		2.652	4.157
.4283	.3632	.1176		2.812	3.550
.7520	.5559	.3170		2.096	11.67
.9545	.7383	.2047		1.824	10.06

TABLE ( A5 )

Hydrogenolysis Data at 60 psig. and 147.5°C

Methane	Partial Pressure ( atm. )			Hydrogen	Rate (X 10 <sup>7</sup> )
	Ethane	Propane			<u>moles</u> g. catalyst - sec.
.6922	.6250	.3163		3.448	4.265
.4131	.3791	.2973		3.992	3.578
.3979	.3654	.3511		3.967	4.676
.6189	.5463	.1692		3.747	2.736
.4402	.4111	.5183		3.707	7.441
.9004	.8084	.4360		2.940	8.428
.7440	.6713	.3425		3.324	5.587
.4787	.4385	.4477		3.717	6.666
.5153	.4721	.3593		3.735	4.201
.4619	.4243	.3440		3.851	4.049
.4101	.3791	.4335		3.860	4.793
.4670	.4304	.4579		3.726	5.351
.4847	.4467	.5864		3.563	7.412
.8649	.7694	.3080		3.139	5.011
.3750	.3481	.5630		3.796	6.659
.4314	.3989	.7160		3.535	9.281
.5127	.4711	.4675		3.630	6.210
.8019	.7331	.6489		2.968	12.26
.7943	.7191	.5793		2.989	9.723

TABLE ( A6 )

Hydrogenolysis Data at 80 psig. and 150°C

Methane	Partial Pressure ( atm. )			Hydrogen	Rate (X 10 <sup>7</sup> ) moles g. catalyst = sec.
	Ethane	Propane			
.8665	.7666	.4155		4.394	2.756
.5064	.4555	.3505		5.130	2.006
2.674	1.730	.1643		1.873	8.240
1.276	1.126	.5328		3.529	4.664
1.703	1.401	.4072		2.931	6.021
1.191	1.011	.3163		3.931	3.243
.9257	.8040	.2757		4.437	3.009
1.161	1.007	.2577		4.017	2.677
1.625	1.371	.3305		3.090	5.371
1.928	1.533	.3002		2.681	5.258
1.808	1.454	.2809		2.899	4.988
.9831	.7834	.1623		4.514	2.234
2.893	1.602	.1134		1.836	6.448
1.785	1.478	.3968		2.783	6.975
1.488	1.304	.5366		3.114	6.665
1.699	1.450	.4387		2.855	6.828

TABLE ( A7 )

Hydrogenolysis Data at 20 psig.

TEMPERATURE = 122.5°C				
Methane	Partial Pressure ( atm. )			Rate (X 10 <sup>7</sup> ) moles g. catalyst - sec.
	Ethane	Propane	Hydrogen	
.1402	.1249	.2472	1.848	1.320
.1036	.0921	.2762	1.889	1.380
.1331	.1185	.2653	1.844	1.440
.1320	.1173	.3092	1.802	1.710
.1435	.1282	.3048	1.784	1.810
.0956	.0843	.2290	1.952	1.300

TEMPERATURE = 131°C				
.1362	.1135	.0754	2.035	1.210
.3217	.2705	.2120	1.556	4.340
.3753	.3163	.3052	1.364	7.050
.3989	.3340	.2564	1.372	5.550
.3612	.3012	.2106	1.487	4.860
.4509	.3678	.1721	1.358	4.940
.1759	.1504	.1966	1.837	3.480
.4372	.3583	.1848	1.380	4.910
.4065	.3352	.1846	1.434	4.630
.4126	.3404	.2710	1.343	6.960

TABLE ( A8 )

Hydrogenolysis Data at 40 psig.

Temperature = 126.5°C					
Methane	Partial Pressure ( atm. )			Hydrogen	Rate (X 10 <sup>7</sup> ) moles g. catalyst - sec.
	Ethane	Propane			
.1105	.1008	.3807		3.012	.0923
.0722	.0655	.5035		3.202	.7470
.0796	.0722	.8283		3.066	1.000
.2556	.2370	.9972		2.230	2.410
Temperature = 128°C					
.0790	.0733	.3903		3.179	.8590
.1157	.1075	.6129		2.885	1.422
.1474	.1366	.6103		2.808	1.540
.1291	.1206	.5563		2.915	1.360
.1548	.1447	.7118		2.709	1.790
Temperature = 139°C					
.6679	.5786	.3993		2.075	6.440
.5924	.5087	.2984		2.322	4.610
.3628	.3241	.3862		2.648	4.634
.6341	.5496	.3859		2.152	6.090
.5098	.4443	.4313		2.331	6.676
.2486	.2199	.3081		2.945	3.607
.7167	.6129	.3446		2.047	6.680
.6229	.5399	.3237		2.234	5.500
.3438	.3051	.5050		2.567	5.530
.6084	.5206	.6936		1.899	11.78
.5295	.4564	.6069		2.126	8.910
.7669	.6397	.3948		1.920	7.156

TABLE ( A8 ) (Continued)

Temperature = 139°C

Methane	Partial Pressure ( atm. )			Hydrogen	Rate ( X 10 <sup>7</sup> ) <u>moles</u> g. catalyst - sec.
	Ethane	Propane			
.4982	.4298	.3639		2.429	4.900
.3602	.3155	.4000		2.645	4.825

Temperature = 137°C

.7308	.6043	.2523		2.134	3.526
.4130	.3598	.4752		2.473	4.658
.3394	.2984	.5299		2.553	4.883
.2687	.2359	.4670		2.749	4.250
.3557	.3100	.4484		2.607	4.432
.5597	.4778	.4432		2.241	5.084

TABLE ( A9 )

Hydrogenolysis Data at 60 psig.

Temperature = 152.5°C

Methane	Partial Pressure ( atm. )			Hydrogen	Rate ( X 10 <sup>7</sup> ) moles g. catalyst - sec.
	Ethane	Propane			
.5336	.4558	.1276		3.965	3.168
.5905	.5112	.1997		3.781	4.948
.6144	.5262	.1753		3.766	4.376
.3374	.2804	.0483		4.417	1.553
.2714	.2383	.1016		4.470	2.861
.7831	.6845	.2307		3.383	6.010
.7638	.6693	.2734		3.375	7.100
.6215	.5326	.1265		3.770	3.107
.3938	.3450	.1321		4.217	3.293
.7775	.6819	.4064		3.217	12.01
.9680	.8080	.2022		3.1033	6.850

Temperature = 132°C

.1453	.1352	.8136		3.988	1.183
.1626	.1519	.5900		4.177	.8380
.1408	.1311	.4182		4.392	.6197
.1616	.1514	.7739		3.995	1.158
.0416	.0371	.3135		4.688	.4724
.1021	.0945	.9106		3.974	1.320
.1306	.1230	.8710		3.957	1.301

Temperature = 130°C

.1011	.0935	1.213		3.674	1.500
-------	-------	-------	--	-------	-------

TABLE ( A9 ) (Continued)

Temperature = 130°C

Methane	Partial Pressure ( atm. )			Hydrogen	Rate ( X 10 <sup>7</sup> ) moles g. catalyst - sec.
	Ethane	Propane			
.1199	.1123	1.079		3.771	1.251
.1814	.1692	1.101		3.621	1.390
.1865	.1743	1.060		3.661	1.400
.2343	.2297	1.083		3.535	1.494
.2764	.2002	.9584		3.587	1.329

Temperature = 138 °C

.3776	.3526	.8949		3.547	3.287
.5473	.5092	.6774		3.348	2.498
.6798	.6210	.5925		3.198	2.245
.8385	.7602	.4751		3.001	2.510
1.033	.9264	.3725		2.749	2.380
.2973	.2749	.4004		4.109	1.415
.5661	.5183	.3135		3.684	1.199
.1763	.1621	.2830		4.460	.8600
.0798	.0727	.2343		4.691	.7020
.2216	.2058	.3344		4.320	1.050

TABLE ( A10 )

Hydrogenolysis Data at 80 psig.

Temperature = 147°C

Methane	Partial Pressure ( atm. )			Hydrogen	Rate (X 10 <sup>7</sup> ) moles g. catalyst - sec.
	Ethane	Propane			
.8149	.7628	.8658		3.999	4.088
.6081	.5721	.6565		4.655	2.950
.6391	.6062	.9232		4.274	3.876
.5482	.5199	.8987		4.475	3.453
.3827	.3633	1.032		4.664	3.465
.4214	.3981	.7814		4.841	2.635
.4909	.4658	1.708		3.778	6.720
1.042	.9702	1.024		3.420	5.286
.2841	.2667	1.172		4.719	3.541
.4374	.4142	1.078		4.512	3.990
.1630	.1450	.5740		5.561	2.244
.3550	.3376	.9296		4.819	2.830
.5605	.5302	1.067		4.285	3.548
.4980	.4677	1.006		4.471	3.160

Temperature = 131°C

.2016	.1933	1.488		4.560	.6550
.2036	.1933	1.549		4.496	.5890
.1862	.1754	1.887		4.194	.7590

TABLE ( B1 )

Hydrogenolysis Data at 128°C

Total Pressure ( psig. )	Partial Pressure ( atm. )				Rate ( X 10 <sup>7</sup> ) <u>moles</u> g. cat.-sec.
	Methane	Ethane	Propane	Hydrogen	
10	.4743	.3156	.1143	.7760	5.564
10	.4481	.2998	.1233	.8092	6.678
10	.4226	.2830	.1776	.7971	9.593
10	.5442	.2952	.1648	.6758	12.72
20	.3697	.3168	.3090	1.365	4.745
20	.4395	.3727	.3524	1.196	5.645
20	.4100	.3491	.2653	1.306	4.365
20	.5307	.4351	.2952	1.098	5.768
20	.3706	.3149	.4133	1.262	6.322
20	.4159	.3451	.3017	1.298	5.103
20	.3114	.2731	.4537	1.323	6.422
20	.3742	.3177	.3970	1.271	5.907
20	.2370	.2061	.4580	1.460	5.608
30	.3166	.2913	.5662	1.867	3.433
30	.4087	.3719	.5078	1.752	3.593
30	.2877	.2643	.6146	1.874	3.425
30	.3220	.2956	.5945	1.830	3.761
30	.4029	.3661	.5331	1.739	4.036
30	.2262	.2080	.6310	1.976	3.598
30	.3923	.3555	.5434	1.749	3.502
30	.2968	.2728	.6295	1.842	3.759
30	.4019	.3634	.5641	1.712	3.835
30	.3485	.3169	.5255	1.850	3.472

TABLE ( B1 ) (Continued)

Total Pressure ( psig. )	Partial Pressure ( atm. )				Rate ( X 10 <sup>7</sup> ) <u>moles</u> g. cat.-sec.
	Methane	Ethane	Propane	Hydrogen	
40	.1723	.1604	.7785	2.610	1.942
40	.1663	.1567	.7345	2.664	1.645
40	.1388	.1273	.8525	2.603	2.073
40	.4227	.3918	.8841	2.023	2.505
40	.2504	.2348	.7896	2.446	2.070
40	.2021	.1890	.8551	2.475	2.150
50	.1734	.1408	.8886	3.199	1.110
50	.1131	.1078	.9040	3.277	.9250
50	.2359	.2236	1.005	2.937	1.225
50	.1202	.1140	.8820	3.285	1.011
50	.1743	.1655	1.010	3.052	1.224
50	.1272	.1206	.9084	3.245	1.038

TABLE ( B2 )

Hydrogenolysis Data at 139°C

Total Pressure ( psig. )	Partial Pressure ( atm. )				Rate ( X 10 <sup>7</sup> ) <u>moles</u> g. cat.-sec.
	Methane	Ethane	Propane	Hydrogen	
20	.7894	.3956	.0753	1.100	6.334
20	.5800	.3609	.1839	1.236	10.23
20	.5776	.3508	.2049	1.227	12.16
30	.5224	.3980	.1855	1.934	4.015
30	.5410	.4032	.1983	1.891	4.694
30	.7622	.4941	.1350	1.649	4.070
30	.6374	.4516	.1803	1.771	4.631
30	.5680	.4129	.2348	1.825	5.808
30	.4516	.3445	.3208	1.924	7.001
30	.6279	.4412	.1937	1.778	5.428
30	.6091	.4443	.1872	1.800	5.340
30	.4741	.3628	.3363	1.868	7.600
30	.4725	.3585	.2947	1.915	4.853
30	.5972	.4324	.2475	1.764	5.350
30	.5023	.3749	.3424	1.821	7.050
30	.4105	.3178	.3971	1.915	7.534
40	.4331	.3807	.5120	2.395	4.716
40	.4666	.4071	.5623	2.285	5.760
40	.5120	.4462	.4469	2.316	4.026
40	.3714	.3278	.6162	2.406	5.209
40	.7688	.6240	.4060	1.922	6.057
40	.3844	.3353	.6776	2.324	6.656
50	.4102	.3710	.6065	3.014	2.777
50	.2522	.2320	.6193	3.298	2.646
50	.2223	.2047	.4569	3.518	2.219
50	.2324	.2122	.6655	3.292	2.730

TABLE ( B2 ) (Continued)

Total Pressure ( psig. )	Partial Pressure ( atm. )				Rate (X 10 <sup>7</sup> ) <u>moles</u> g. cat.-sec.
	Methane	Ethane	Propane	Hydrogen	
50	.1989	.1831	.6312	3.386	2.484
50	.3680	.3358	.6215	3.077	2.515
50	.4745	.4296	.5678	2.930	2.913
50	.4679	.4217	.5229	2.989	2.393
50	.2903	.2667	.7086	3.135	2.870
50	.2729	.2491	.7430	3.136	3.122
50	.4476	.4032	.7209	2.830	3.616
50	.4309	.3886	.5902	2.992	2.900
60	.4294	.4040	.9579	3.290	2.932
60	.2200	.2068	.9223	3.732	2.040
60	.3638	.3405	.8674	3.511	2.179
60	.2327	.2180	.9040	3.717	2.203
60	.1840	.1723	1.107	3.617	2.757
60	.2876	.2678	1.173	3.353	3.301
60	.4055	.3760	.8136	3.486	2.223
60	.3659	.3415	.8319	3.542	2.162

TABLE ( B3 )

Hydrogenolysis Data at 143.5°C

Total Pressure ( psig. )	Partial Pressure ( atm. )				Rate (X 10 <sup>7</sup> ) <u>moles</u> g. cat.-sec.
	Methane	Ethane	Propane	Hydrogen	
40	.5984	.5072	.2605	2.355	5.640
40	.5731	.4927	.3576	2.298	7.230
40	.6862	.5753	.3044	2.155	7.271
40	.7148	.5969	.3029	2.107	6.959
40	.5258	.4521	.3297	2.414	5.894
40	.5642	.4957	.4768	2.164	9.694
40	.6802	.5608	.4369	2.043	9.177
50	.5907	.5308	.5458	2.734	5.880
50	.7201	.6382	.4974	2.546	7.292
50	.4996	.4546	.6840	2.766	6.763
50	.6313	.5651	.5277	2.697	5.843
50	.6686	.5951	.5070	2.631	5.935
50	.4798	.4344	.7133	2.774	7.130
60	.5072	.4685	.6317	3.473	4.132
60	.4889	.4523	.7419	3.398	4.760
60	.4380	.4050	.5371	3.702	3.228
60	.5346	.4946	.6601	3.395	4.346
60	.3425	.3181	.7714	3.650	4.412
60	.3776	.3511	.7180	3.634	4.347

TABLE ( B4 )

Hydrogenolysis Data at 148°C

Total Pressure ( psig. )	Partial Pressure ( atm. )				Rate (X 10 <sup>7</sup> ) <u>moles</u> g. cat.-sec.
	Methane	Ethane	Propane	Hydrogen	
40	.9173	.6397	.1124	2.051	6.283
40	1.085	.7252	.1574	1.754	10.60
40	1.243	.7059	.0852	1.688	7.513
50	.9045	.7196	.2434	2.536	7.884
50	1.020	.8015	.2086	2.371	6.449
50	.8662	.7051	.2579	2.572	8.399
50	1.251	.8688	.1184	1.163	5.050
50	1.086	.6307	.3037	2.381	10.96
50	1.345	.9234	.1580	1.971	7.736
50	1.067	.8085	.1791	2.347	6.551
60	.7048	.6189	.4502	3.307	6.135
60	.7912	.6855	.4110	3.194	6.045
60	.8857	.7511	.3146	3.135	4.764
60	.6459	.5691	.5778	3.289	7.699
60	.8700	.7404	.3222	3.149	5.025
60	.6728	.5874	.4741	3.347	6.544
60	.6820	.5966	.4426	3.361	6.279
70	.9174	.8291	.5382	3.477	5.340
70	.8931	.8101	.5289	3.530	4.718
70	.6315	.5785	.6638	3.889	5.324
70	.8182	.7421	.4650	3.737	4.312
70	.5566	.5186	.6960	3.991	4.869
70	.7571	.6937	.8080	3.502	6.876
70	.9317	.8401	.7070	3.283	7.856

TABLE ( B4 ) (Continued)

Total Pressure ( psig. )	Partial Pressure ( atm. )				Rate ( X 10 <sup>7</sup> ) <u>moles</u> g. cat.-sec.
	Methane	Ethane	Propane	Hydrogen	
70	.4656	.4281	.7975	4.071	5.932
80	.5573	.5192	.7467	4.555	3.573
80	.4419	.4123	.6848	4.903	3.215
80	.7369	.6784	.6036	4.423	3.394
80	.7177	.6578	.4903	4.576	2.580
80	.5476	.5122	.9361	4.446	4.621
80	.5341	.4986	1.370	4.039	6.986
80	.5991	.5553	.8794	4.408	4.044
80	.8310	.7660	.6887	4.157	3.887
90	.3868	.3682	1.105	5.261	2.590
90	.4088	.3875	1.363	4.962	3.428
90	.6966	.6567	.8996	4.870	3.054
90	.4943	.4601	.4001	5.767	1.366
90	.3433	.3319	.7158	5.731	2.361
90	.3490	.3298	.8511	5.593	2.677
90	.4252	.3996	.6211	5.677	2.090
90	.4444	.4209	1.376	4.881	4.773

TABLE ( B5 )

Data for Pressure Dependence of RateFlow Rate =  $3.041 \pm 0.05$  ml/sec.Flow Ratio =  $0.22 \pm 0.01$  (  $C_3H_8/H_2$  )Temperature =  $128^\circ C$ 

Total Pressure ( psig. )	Partial Pressure ( atm. )				Rate ( $\times 10^7$ ) moles g. cat.-sec.
	Methane	Ethane	Propane	Hydrogen	
10	.3134	.2429	.1183	1.006	5.020
20	.2212	.1959	.2970	1.646	2.686
30	.2247	.2047	.4546	2.157	2.195
40	.1667	.2244	.6738	2.686	1.510
50	.1624	.1505	.8319	3.257	1.020
60	.0976	.0879	.7932	4.103	.5470

Temperature =  $138^\circ C$ 

20	.6307	.3819	.1142	1.237	6.284
30	.5410	.4032	.1983	1.898	4.694
40	.5120	.4462	.4469	2.316	4.026
50	.4309	.3886	.5902	2.993	2.900
60	.3659	.3415	.8317	3.542	2.162

Temperature =  $148^\circ C$ 

40	.9173	.6397	.1124	2.051	7.404
50	1.020	.8015	.2086	2.371	6.450
60	.8699	.7404	.3222	3.149	5.02
70	.8182	.7421	.4650	3.737	4.312
80	.7810	.6784	.6036	4.423	3.894
90	.6966	.6567	.8996	4.870	3.054

TABLE ( C1 )

Product Distribution Data at 2 psig. and 120°C

Fractional Conversion of Propane	Selectivity	
	Methane	Ethane
0.6226	1.168	0.9162
0.6064	1.178	0.9109
0.7654	1.3197	0.8401
0.7287	1.259	0.8705
0.7587	1.254	0.8731
0.5411	1.057	0.9521
0.7641	1.338	0.8311
0.7023	1.235	0.8827
0.7558	1.302	0.8492
0.7263	1.228	0.8860
0.7730	1.264	0.8682
0.3520	1.065	0.9680
0.2300	1.054	0.9730
0.6457	1.248	0.8758
0.4531	1.105	0.9451

TABLE ( C2 )

Product Distribution Data at 30 psig. and 130°C

Fractional Conversion of Propane	Selectivity	
	Methane	Ethane
0.4916	1.078	0.9611
0.4408	1.075	0.9628
0.4400	1.071	0.9645
0.3413	1.070	0.9652
0.3355	1.072	0.9639
0.7047	1.104	0.9479
0.6226	1.092	0.9541
0.5763	1.085	0.9573
0.5132	1.097	0.9517
0.4714	1.081	0.9593
0.4608	1.074	0.9300
0.5052	1.077	0.9617
0.5318	1.081	0.9597
0.4703	1.079	0.9606
0.5555	1.095	0.9530
0.5287	1.087	0.9563
0.7141	1.131	0.9361

TABLE ( C3 )

Product Distribution Data at 80 psig. and 150°C

Fractional Conversion of Propane	Selectivity	
	Methane	Ethane
0.6581	1.083	0.9584
0.5741	1.072	0.9641
0.9256	1.308	0.8462
0.4609	1.069	0.9656
0.6882	1.085	0.9576
0.7784	1.108	0.9460
0.7721	1.112	0.9441
0.7539	1.096	0.9519
0.8150	1.116	0.9419
0.8472	1.158	0.9209
0.8484	1.150	0.9250
0.8397	1.157	0.9217
0.5028	1.072	0.9638
0.7993	1.129	0.9353
0.7179	1.090	0.9550
0.7775	1.108	0.9459
0.5572	1.077	0.9680
0.8228	1.127	0.9360

TABLE ( C4 )

Product Distribution Data at 40 psig.

Reaction Temperature ( C°)	Fractional Conversion of Propane	Selectivity	
		Methane	Ethane
139	0.8170	1.162	0.9193
139	0.6037	1.098	0.9511
139	0.6426	1.104	0.9480
139	0.4660	1.077	0.9617
139	0.5996	1.098	0.9513
139	0.5194	1.094	0.9532
139	0.6527	1.107	0.9466
139	0.5377	1.089	0.9555
139	0.6368	1.098	0.9513
139	0.4285	1.084	0.9581
139	0.3864	1.081	0.9594
139	0.6334	1.124	0.9378
139	0.5543	1.108	0.9496
139	0.4524	1.090	0.9549
139	0.4159	1.097	0.9514
139	0.7193	1.130	0.9348
139	0.4427	1.094	0.9530
139	0.3706	1.088	0.9562
139	0.3460	1.089	0.9557
139	0.4204	1.094	0.9532
139	0.5326	1.108	0.9460
139	0.8638	1.194	0.9030
139	0.7525	1.147	0.9265
139	0.3005	1.082	0.9605
144.5	0.5326	1.108	0.9460
144.5	0.6867	1.139	0.9307

TABLE ( C4 ) (Continued)

Reaction Temperature ( C°)	Fractional Conversion of Propane	Selectivity	
		Methane	Ethane
144.5	0.5751	1.126	0.9370
144.5	0.7397	1.145	0.9274
144.5	0.7619	1.175	0.9125
144.5	0.7525	1.167	0.9165
144.5	0.6036	1.142	0.9291
144.5	0.7157	1.149	0.9254
144.5	0.6151	1.115	0.9425
144.5	0.7257	1.156	0.9222
144.5	0.5010	1.118	0.9413
144.5	0.6500	1.141	0.9311
128	0.1379	1.039	0.9807
128	0.3446	1.044	0.9779
128	0.1788	1.040	0.9798
128	0.2331	1.043	0.9783
128	0.1841	1.045	0.9776
128	0.3943	1.045	0.9777
128	0.4554	1.047	0.9763
133	0.3548	1.062	0.9692
133	0.4286	1.061	0.9693
133	0.5556	1.072	0.9640
133	0.6377	1.072	0.9638
133	0.6845	1.087	0.9565
133	0.7183	1.094	0.9531

TABLE ( C5 )

Product Distribution at 30 and 50 psig.

Pressure = 30 psig.

Reaction Temperature ( C° )	Fractional Conversion of Propane	Selectivity	
		Methane	Ethane
135	0.363	1.106	0.9471
135	0.5556	1.138	0.9310
135	0.6364	1.153	0.9232
135	0.6875	1.180	0.9111
135	0.5885	1.104	0.9460
128	0.3461	1.056	0.9719
128	0.4307	1.064	0.9681
128	0.3069	1.057	0.9713
128	0.3386	1.058	0.9710
128	0.4151	1.065	0.9676
128	0.2533	1.057	0.9716
128	0.6529	1.107	0.9467
128	0.4036	1.067	0.9666
128	0.3085	1.057	0.9713
128	0.4001	1.068	0.9661
128	0.3839	1.064	0.9678
139	0.5424	1.188	0.9062
139	0.7222	1.247	0.8764
139	0.5432	1.186	0.9072
139	0.5737	1.192	0.9041
139	0.6632	1.226	0.8873
139	0.4675	1.177	0.9113
139	0.6150	1.208	0.8961

TABLE ( B5 ) (Continued)

Pressure = 50 psig.

Reaction Temperature ( C°)	Fractional Conversion of Propane	Selectivity	
		Methane	Ethane
128	0.1195	1.036	0.9819
128	0.1847	1.036	0.9820
128	0.1163	1.035	0.9823
128	0.1191	1.036	0.9821
128	0.2671	1.038	0.9813
128	0.1430	1.035	0.9826
139	0.4364	1.073	0.9636
139	0.3877	1.068	0.9660
139	0.2475	1.062	0.9692
139	0.3580	1.062	0.9691
139	0.4391	1.067	0.9663
139	0.4553	1.071	0.9648
139	0.2794	1.059	0.9706
139	0.2570	1.062	0.9692
139	0.3670	1.071	0.9645
139	0.4059	1.070	0.9650
139	0.5459	1.077	0.9610
148	0.7624	1.158	0.9211
148	0.8074	1.167	0.9168
148	0.7463	1.142	0.9292
148	0.8332	1.193	0.9036
148	0.8709	1.230	0.8850
148	0.7333	1.131	0.9346

TABLE ( C6 )

Product Distribution Data at 60 psig.

Reaction Temperature ( C°)	Fractional Conversion of Propane	Selectivity	
		Methane	Ethane
141.5	0.1455	1.049	0.9756
141.5	0.2086	1.046	0.9771
141.5	0.2431	1.048	0.9761
141.5	0.1667	1.044	0.9781
141.5	0.1260	1.041	0.9797
141.5	0.0645	1.049	0.9754
141.5	0.0962	1.044	0.9779
141.5	0.1350	1.047	0.9765
141.5	0.1440	1.046	0.9772
141.5	0.4352	1.049	0.9757
141.5	0.5182	1.051	0.9745
141.5	0.6234	1.066	0.9668
141.5	0.7208	1.074	0.9632
141.5	0.4136	1.053	0.9736
141.5	0.6302	1.060	0.9702
141.5	0.3702	1.057	0.9716
141.5	0.6156	1.062	0.9690
141.5	0.4674	1.047	0.9765
141.5	0.3869	1.050	0.9751
147.5	0.6719	1.069	0.9655
147.5	0.5172	1.058	0.9712
147.5	0.7712	1.085	0.9575
147.5	0.6581	1.073	0.9635
147.5	0.6700	1.070	0.9652
147.5	0.5752	1.060	0.9704
147.5	0.4732	1.053	0.9735
147.5	0.4915	1.055	0.9724
147.5	0.4393	1.055	0.9724

TABLE ( C6 ) (Continued)

Reaction Temperature ( °C )	Fractional Conversion of Propane	Selectivity	
		Methane	Ethane
144.5	0.7224	1.080	0.9603
144.5	0.3640	1.053	0.9736
144.5	0.5092	1.057	0.9714
144.5	0.5623	1.067	0.9663
152.5	0.7907	1.108	0.9462
152.5	0.7292	1.098	0.9509
152.5	0.7602	1.106	0.9471
152.5	0.8611	1.127	0.9365
152.5	0.7104	1.088	0.9558
152.5	0.7566	1.092	0.9542
152.5	0.7194	1.090	0.9551
152.5	0.8163	1.105	0.9473
152.5	0.7323	1.090	0.9550
152.5	0.6377	1.089	0.9554
152.5	0.8099	1.124	0.9381
137	0.2250	1.042	0.9790
137	0.3751	1.049	0.9761
137	0.3865	1.058	0.9709
137	0.4152	1.055	0.9732
137	0.4413	1.068	0.9661

TABLE ( C7 )

Product Distribution Data at 128°C

Reaction Pressure ( psig. )	Fractional Conversion of Propane	Selectivity	
		Methane	Ethane
20	0.5285	1.113	0.9436
20	0.6127	1.137	0.9318
20	0.4465	1.111	0.9443
20	0.5500	1.128	0.9360
20	0.3865	1.089	0.9554
20	0.4589	1.113	0.9437
20	0.3209	1.095	0.9524
20	0.4152	1.099	0.9505
20	0.5943	1.130	0.9352
40	0.1379	1.039	0.9807
40	0.3446	1.044	0.9779
40	0.1788	1.040	0.9798
40	0.2331	1.043	0.9783
40	0.1844	1.045	0.9715
40	0.3943	1.045	0.9777
40	0.4354	1.0474	0.9763

\*\*\* Data at 30 and 50 psig. can be found in Table ( C5 ) \*\*\*

TABLE ( C8 )

Product Distribution Data at 139° C

Reaction Pressure ( psig. )	Fractional Conversion of Propane	Selectivity	
		Methane	Ethane
40	0.6039	1.100	0.9499
40	0.4375	1.088	0.9561
40	0.4316	1.093	0.9535
40	0.5116	1.094	0.9531
40	0.3571	1.085	0.9576
40	0.2871	1.085	0.9571
60	0.1863	1.042	0.9792
60	0.2865	1.045	0.9776
60	0.1978	1.044	0.9780
60	0.1373	1.044	0.9779
60	0.1896	1.048	0.9759
60	0.3217	1.051	0.9745
60	0.2960	1.0465	0.9767
60	0.3310	1.052	0.9740
60	0.4811	1.053	0.9749

\*\*\*\* Data at 30 and 50 psig. can be found in Table ( C5 ). \*\*\*\*

TABLE ( C9 )

Product Distribution at 142°C

Reaction Pressure ( psig. )	Fractional Conversion of Propane	Selectivity	
		Methane	Ethane
40	0.6736	1.113	0.9435
40	0.5923	1.103	0.9484
40	0.5911	1.103	0.9485
40	0.5242	1.112	0.9438
40	0.5789	1.133	0.9337
50	0.5023	1.073	0.9638
50	0.4071	1.064	0.9618
50	0.5268	1.075	0.9624
50	0.5500	1.079	0.9604
50	0.3866	1.067	0.9663
60	0.2973	1.050	0.9751
60	0.3339	1.048	0.9755
60	0.4325	1.054	0.9733
60	0.3850	1.053	0.9737
60	0.4365	1.053	0.9735
60	0.4349	1.053	0.9737

TABLE ( C10 )

Product Distribution Data at 148°C

Reaction Pressure ( psig. )	Fractional Conversion of Propane	Selectivity	
		Methane	Ethane
60	0.5899	1.089	0.9558
60	0.6368	1.098	0.9511
60	0.7168	1.113	0.9436
60	0.5072	1.086	0.9570
60	0.7086	1.110	0.9445
60	0.5650	1.092	0.9538
60	0.5854	1.091	0.9545
70	0.6147	1.069	0.9658
70	0.6130	1.066	0.9670
70	0.4732	1.059	0.9704
70	0.6227	1.066	0.9670
70	0.4693	1.059	0.9705
70	0.5519	1.059	0.9711
70	0.3559	1.058	0.9717
80	0.4160	1.091	0.9545
80	0.3814	1.047	0.9766
80	0.5803	1.089	0.9705
80	0.3589	1.045	0.9775
80	0.2714	1.046	0.9769
80	0.3932	1.051	0.9744
80	0.5335	1.055	0.9725
90	0.2245	1.036	0.9820
90	0.4269	1.040	0.9802
90	0.5404	1.048	0.9758
90	0.2831	1.038	0.9809
90	0.3965	1.041	0.9791
90	0.2370	1.034	0.9817
90	0.5913	1.046	0.9770

\*\*\* Data at 50 psig. can be found in Table ( C5 ) . \*\*\*

TABLE ( D1 )

Porosimeter Data

Applied Pressure (psia)	Pore Diameter (microns)	Volume of Pores (cc/gm)
0.5	176.76	0
1.0	88.38	0.00659
7.3	12.10	0.00934
4000	$22.10 \times 10^{-3}$	0.0335
5800	$15.24 \times 10^{-3}$	0.0412
6500	$13.60 \times 10^{-3}$	0.0544
7000	$12.60 \times 10^{-3}$	0.0654
8000	$11.05 \times 10^{-3}$	0.1555
9000	$9.82 \times 10^{-3}$	0.1620
10000	$8.88 \times 10^{-3}$	0.1686
11000	$8.03 \times 10^{-3}$	0.1747
12000	$7.40 \times 10^{-3}$	0.1813
14000	$6.30 \times 10^{-3}$	0.1928
16000	$5.52 \times 10^{-3}$	0.2049
18000	$4.91 \times 10^{-3}$	0.2186
20000	$4.42 \times 10^{-3}$	0.2346
22000	$4.02 \times 10^{-3}$	0.2516
24000	$3.68 \times 10^{-3}$	0.2834
26000	$3.40 \times 10^{-3}$	0.3054
28000	$3.16 \times 10^{-3}$	0.3279
30000	$2.95 \times 10^{-3}$	0.3411
32000	$2.76 \times 10^{-3}$	0.3483
34000	$2.60 \times 10^{-3}$	0.3537
36000	$2.46 \times 10^{-3}$	0.3559
38000	$2.33 \times 10^{-3}$	0.3587
40000	$2.21 \times 10^{-3}$	0.3598